

NASA Contractor Report 3711

**Critical Composite Joint Subcomponents
Analysis and Test Results**

B. L. Bunin

**CONTRACT NAS1-16857
SEPTEMBER 1983**



25th Anniversary
1958-1983

NASA

NASA Contractor Report 3711

**Critical Composite Joint Subcomponents
Analysis and Test Results**

B. L. Bunin
Douglas Aircraft Company
McDonnell Douglas Corporation
Long Beach, California

Prepared for
Langley Research Center
under Contract NAS1-16857



National Aeronautics
and Space Administration

**Scientific and Technical
Information Branch**

1983

SUMMARY

A program has been conducted at the Douglas Aircraft Company of the McDonnell Douglas Corporation, under NASA Langley Contract NAS1-16857, to develop the technology for critical structural joints of a composite wing structure meeting design requirements for a 1990 commercial transport aircraft. The prime objective of the program was to demonstrate the ability to reliably predict the strength of large bolted composite joints. To this end, the experiments fell into one of two classes. The ancillary test program, of 180 specimens, generated data on strength and load-deflection characteristics which provided the input to the joint analysis. The load sharing between the fasteners in multirow bolted joints was computed by the nonlinear analysis program A4EJ. That program was used both to assess the efficiency of different joint design concepts and to predict the strengths of 20 additional large structural joints. In most cases, the predictions were accurate to within a few percent of the test results. In a few cases, the observed mode of failure was different than that anticipated - almost all such instances involved delaminations of the splice plates rather than the stronger net-section or bearing failures. After-the-fact reanalysis of these cases was also found to be accurate enough for design purposes. The real highlight of the testing of these large structural joints (representing a strip from a wing root chord-wise splice) was the consistent ability to achieve gross-section failure strains on the order of 0.005. That represents a considerable improvement over the prior state of the art. The improvement was attained largely as the result of the better understanding of the load sharing in multirow joints provided by the program A4EJ (developed under U.S. Air Force Contract F33615-79-C-3212), building upon the knowledge acquired during the earlier NASA Langley contract, NAS1-13172, on bolted joints in fibrous composite structures. Both tensile and compressive loads were tested and the bolt diameters were 1/4 inch, 1/2 inch, and 3/4 inch. The typical load intensity on the structural joints was about 40 to 45 thousand pounds per inch (with a 37 1/2 percent 0-degree plies, 50 percent ± 45 -degrees and 12 1/2 percent 90-degrees, all thoroughly interspersed and not bunched together. The composite materials are Toray 300 fiber and Ciba-Geigy 914 resin, in the form of 0.010 inch unidirectional tape.

NOMENCLATURE

C	reduction factor and compliance coefficient
d	bolt or hole diameter
d/t	diameter-to-thickness ratio
d/w	diameter-to-width ratio
E	Young's modulus
EI	bending stiffness
e	edge distance
e/d	edge distance-to-diameter ratio
F	allowable stress
f	operating stress
G	shear modulus
K	elastic spring rate
K_{tc}	composite stress concentration factor
K_{te}	elastic stress concentration factor
N_x	load intensity
P	bolt or joint load
t	thickness
w	width
w/d	width-to-diameter ratio
β	coefficient
δ	displacement

SUBSCRIPTS

bb	bolt bending
bbr	bolt bearing
brg	bearing
bru	bearing ultimate
bry	bearing yield
bs	bolt shear
cu	compression ultimate
p	plate
pbr	plate bearing
tu	tension ultimate
ult	ultimate

TABLE OF CONTENTS

<u>Section</u>		<u>Page</u>
1.0	INTRODUCTION	1
2.0	TEST SPECIMENS	4
2.1	MATERIALS	4
2.2	LAMINATE PATTERN SELECTION	4
2.3	FABRICATION	5
2.4	CONFIGURATIONS	6
2.4.1	4-Bolt Joint	8
2.4.2	8-Bolt Tapered Joint	8
2.4.3	12-Bolt Joint	12
2.4.4	24-Bolt Joint	12
2.4.5	Hole Wearout Specimens	15
2.4.6	Load Introduction - Subcomponent Joints	15
3.0	SUBCOMPONENT TESTS	21
3.1	TEST PROCEDURES	21
3.2	TEST RESULTS	21
3.2.1	Tension Tests	28
3.2.1.1	4-Bolt Tension Tests	28
3.2.1.2	8-Bolt Tension Tests	33
3.2.1.3	12-Bolt Tension Tests	36
3.2.1.4	24-Bolt Tension Tests	39
3.2.2	Compression Tests	43
3.2.2.1	4-Bolt Compression Tests	43
3.2.2.2	8-Bolt Compression Tests	47
3.2.2.3	12-Bolt Compression Tests	53
3.2.2.4	24-Bolt Compression Tests	53
3.2.3	Hole Wearout Tests	59
4.0	ANALYSIS METHODS DEVELOPMENT	60
5.0	ANALYSIS OF MULTIROW BOLTED JOINTS	72
5.1	PARAMETRIC STUDIES	77
6.0	PRELIMINARY SUBCOMPONENT JOINT STRENGTH ANALYSIS.	79

TABLE OF CONTENTS (Continued)

<u>Section</u>		<u>Page</u>
7.0	ANALYSIS/TEST CORRELATION	84
7.1	4-BOLT TENSION AND COMPRESSION	85
7.2	8-BOLT TENSION AND COMPRESSION	87
7.3	12-BOLT TENSION	90
7.4	12-BOLT COMPRESSION	92
7.5	24-BOLT TENSION	93
7.6	24-BOLT COMPRESSION	96
8.0	SPECIMEN INSPECTION AFTER TESTING	97
9.0	CONCLUSIONS	104
10.0	REFERENCES	106
11.0	APPENDICES	
	A - SUBCOMPONENT JOINT TEST DATA	A-1
	B - SUBCOMPONENT JOINT ANALYSIS RESULTS	B-1

LIST OF ILLUSTRATIONS

<u>Figure</u>		<u>Page</u>
1	Relation Between Strengths of Bolted Joints in Ductile, Fibrous Composite and Brittle Materials	2
2	4-Bolt Subcomponent Joint Specimen Configuration	9
3	Interference Fit Fastener System	10
4	8-Bolt Subcomponent Joint Specimen Configuration	11
5	12-Bolt Subcomponent Joint Specimen Configuration	13
6	24-Bolt Subcomponent Joint Specimen Configuration	14
7	Hole Wearout Specimen Configuration	16
8	Load Introduction - Subcomponent Tension Joints	17
9	End Joint Proof Test Specimen	18
10	End Joint Proof Test	19
11	Load Introduction - Subcomponent Compression Joints	20
12	4-Bolt Tension Specimen - JT4CF-503-1	29
13 (a)	4-Bolt Tension Specimen - JT4IF-1-1	30
13 (b)	4-Bolt Tension Specimen - JT4IF-1-2	31
14	4-Bolt Tension Specimen - JT4CF-503-2	32
15	8-Bolt Tension Specimen - JT8CF-505-1	34
16	8-Bolt Tension Specimen - JT8CF-505-2	35
17	8-Bolt Tension Specimen - JT8CF-515	37
18	8-Bolt Tension Specimen - JT8IF-501	38
19	12-Bolt Tension Specimen - JT12CF-1	40
20	12-Bolt Tension Specimen - JT12IF-501	41
21	24-Bolt Tension Specimen - JT24CF-507	42
22	24-Bolt Tension Specimen - JT24IF-509	44

LIST OF ILLUSTRATIONS (Continued)

<u>Figure</u>		<u>Page</u>
23 (a)	4-Bolt Compression Specimen - JC4CF-511	45
23 (b)	4-Bolt Compression Specimen - JC4CF-511 (Cont'd).	46
24 (a)	4-Bolt Compression Specimen - JC4IF-507	48
24 (b)	4-Bolt Compression Specimen - JC4IF-507 (Cont'd).	49
25	8-Bolt Compression Specimen - JC8CF-513	50
26 (a)	8-Bolt Compression Specimen - JC8IF-509	51
26 (b)	8-Bolt Compression Specimen - JC8IF-509 (Cont'd).	52
27	12-Bolt Compression Specimen - JC12CF-503	54
28	12-Bolt Compression Specimen - JC12IF-505	55
29 (a)	24-Bolt Compression Specimen - JC24CF-511	56
29 (b)	24-Bolt Compression Specimen - JC24CF-511 (Cont'd)	57
30	24-Bolt Compression Specimen - JC24IF-513	58
31	Load Deflection Curve - Double-Shear Tension Test (Bearing Failure)	60
32	Load Deflection Curve, Double-Shear Tension Test (Tensile Failure)	61
33	Fastener Load Deflection Characteristics	62
34	Bolted Joint Elastic Spring Rates - Test Versus Prediction	64
35	Additional Displacements Due to Bolt Rotation	65
36	Single-Shear Bolted Joint Elastic Spring Rates - Test Versus Prediction	66
37	Stress Concentration Factors at Failure for Composite Bolted Joints	69
38	Loads and Deformations on Elements of Bolted Joint	73
39	Deformations in Mechanically Fastened Joint	73

LIST OF ILLUSTRATIONS (Continued)

<u>Figure</u>		<u>Page</u>
40	Outer Envelope of Bearing-Bypass Load Interactions . . .	74
41	Effects of Bolt Bending on Laminate Bearing Strength . . .	76
42	Effect of Ancillary Test Results on Multirow Joint Strength Predictions.	77
43	Effect of Joint Configuration on Bolt Load Distribution . .	79
44	Stress Concentration Interactions in Multirow Bolted Composite Joints	81
45	Use of A4EJ Analysis to Improve Bolted Joint Design . . .	82
46	4-Bolt Joint Bearing-Bypass Failure Envelopes	85
47	8-Bolt Joint, Bearing-Bypass Failure Envelopes	87
48	Tapered Joint - Strain Gage Locations	88
49	8-Bolt Joint Load Distribution - Test Vs Analysis	90
50	12-Bolt Joint, Bearing Bypass Failure Envelopes	91
51	24-Bolt Joint Load Distribution - Test Vs Analysis	94
52	24-Bolt Joint, Bearing-Bypass Failure Envelopes	95
53	JT12CF Blade "A" C-Scan	98
54	JT12IF Blade "A" C-Scan	99
55	JT12IF Blade "B" C-Scan	100
56	JT24CF Blade "A" C-Scan	101
57	JT24CF Blade "B" C-Scan	102

LIST OF TABLES

<u>Table</u>		<u>Page</u>
I	Subcomponent Test Program - Specimen Description	6
II	Subcomponent Test Specimen Designation	7
III	4-Bolt Tension and Compression Test Results	23
IV	8-Bolt Tension and Compression Test Results	24
V	12-Bolt Tension and Compression Test Results	25
VI	24-Bolt Tension and Compression Test Results	26
VII	Hole Wearout Test Results	27

1.0 INTRODUCTION

The safe and efficient use of advanced composite materials in primary aircraft structure has become a major topic of research. The principal objective of this investigation is to develop and demonstrate the technology for critical structural joints of a composite wing structure that meets all the design requirements of a 1990 commercial transport aircraft.

To fulfill this objective, procedures were developed for joint design and analysis. A series of ancillary tests were performed to characterize composite bolted joint behavior and provide empirical data for the analysis formulas. In addition to single-bolt tests, a series of subcomponent joint specimens were tested and the results were compared with analytical predictions for multirow joints of the same configurations. The agreement between test and analysis results was found to be very good, and the A4EJ computer analysis program was established as an effective tool for the design and analysis of multirow bolted joints in composite structures.

The work was conducted by Douglas Aircraft Company at Long Beach, California, under contract to NASA Langley Research Center. Significant work on which this research was based includes an earlier NASA Langley contract on small bolted coupon tests in which the failure mechanisms and strengths for composite laminates adjacent to bolt holes were characterized empirically (Reference 1). That work, in turn, was followed by a recent contract with the U.S. Air Force Flight Dynamics Laboratory at Wright Patterson AFB, Ohio, in which one task was to develop the A4EJ nonlinear computer program for load-sharing in multirow bolted joints (Reference 2).

The analysis of load transfer through mechanically fastened joints in fibrous composite laminates must inevitably rely upon some empirically derived input based on test results. This is so because fiber-reinforced resins do not fall as homogeneous one-phase materials, although they are usually modeled as such, but as heterogeneous materials with two distinct phases and an interface. As shown in Figure 1, the efficiency of real composite bolted joints lies roughly halfway between analytical predictions based on purely elastic and perfectly plastic behavior. Analysis based on either extreme does not come close to predicting the strength of these single-row bolted joints, and either extreme would not be

acceptable for design purposes without some form of major modifications. All analyses of composite bolted joints rely on an empirical correlation factor in some form or other. In the case of the A4EJ analysis program, the correlation is achieved by modifying the theoretical elastic stress concentration factor at each bolt hole. The stress concentration factor is reduced, on the basis of test results, to reflect a failure mechanism which starts with fiber pull-out from the resin over a finite length in the most highly strained areas and proceeds through delaminations around the bolt holes before any fibers are broken.

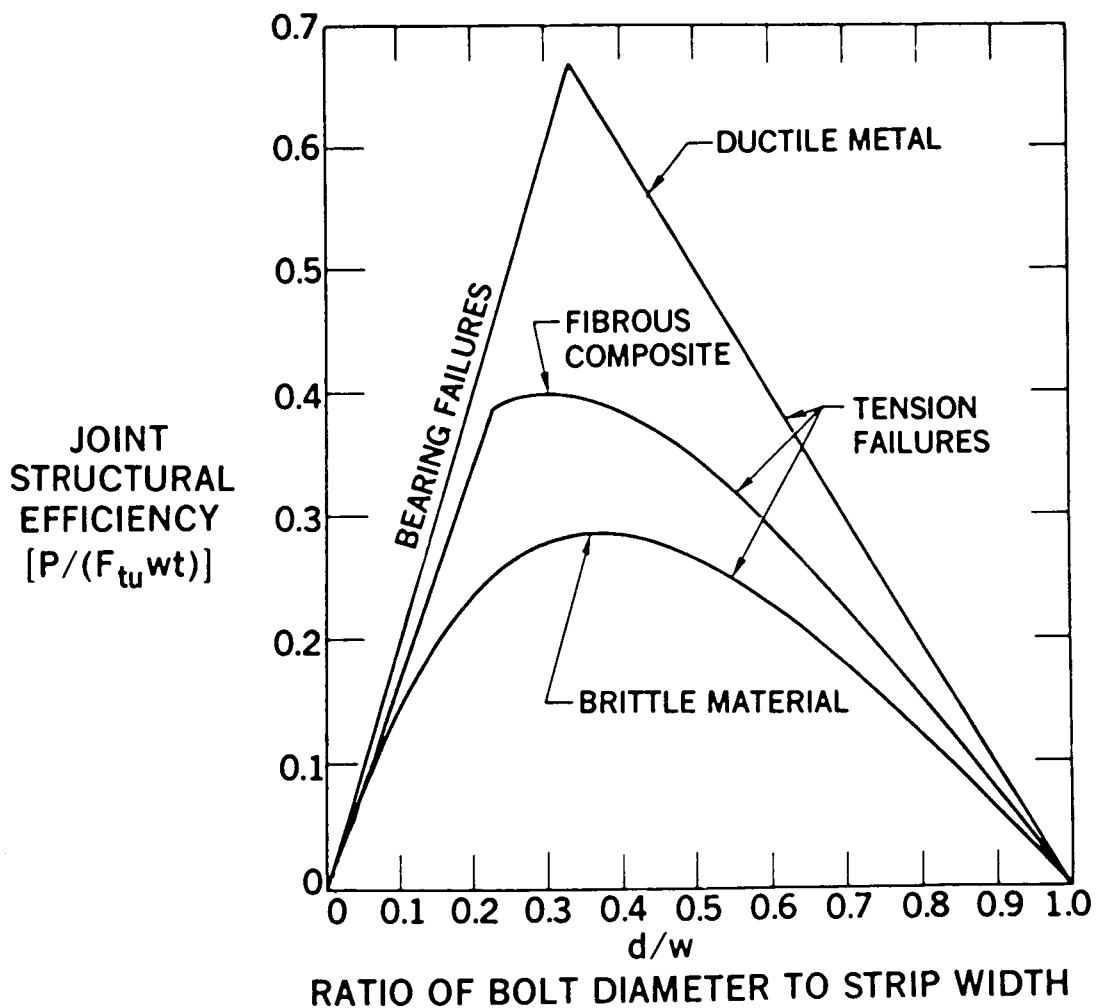


FIGURE 1. RELATION BETWEEN STRENGTHS OF BOLTED JOINTS IN DUCTILE, FIBROUS COMPOSITE AND BRITTLE MATERIALS

The need to characterize this failure mechanism of bolted joints in composites is one of the reasons why bolted joints of various sizes were tested in the ancillary test program which preceded the subcomponent testing discussed in this report. Another reason for the testing was the need to acquire load deflection, or stiffness, measurements to permit determination of the load-sharing between the various fasteners. These test results have shown that an old NACA formula for the stiffness of bolted joints in metal structures (Reference 3) needed only a minor modification to account for the different moduli associated with orthotropic composite laminates.

The stiffness and failure data generated on single fastener joints were used successfully to predict the failure load of various structurally configured multirow bolted joints. This report describes all of the analysis work and test results associated with the subcomponent test program. Discussions of the development of analytical methods and the evaluation of multirow bolted joint performance are included. Finally, the report presents a summary of the multirow joint test results, the A4EJ analysis predictions for joint strength and load distribution, and the correlation between the two for each configuration.

2.0 TEST SPECIMENS

2.1 MATERIALS

Subcomponent joint test specimens were fabricated from laminates made of carbon-epoxy unidirectional tape consisting of Toray high-strength T-300 fibers and Ciba-Geigy 914 resin. This material system was selected for several reasons. The 914 resin was found to have a more extensive data base than most of the so-called "tough resin" systems. It has also been shown to exhibit good handling characteristics for layup. The T-300 generic fiber is in widespread use throughout the industry. For this program, it was supplied as 10 mil tape which consisted of two plies of 5 mil tape combined by the vendor during the preimpregnation process.

The decision to use "thick" plies was made in consideration of the cost savings associated with minimizing the number of plies and layup operations required for thick, composite wing skin structure. This also reduced the fabrication costs of our test program. It should be noted that the use of thicker plies places additional restrictions on the minimum gage of balanced laminates. Certainly for thin-skinned secondary structure, thinner plies would be preferred. Titanium bolts and steel shear nuts were standard throughout the test series except where noted.

2.2 LAMINATE PATTERN SELECTION

Two fiber patterns were selected for the overall program, including ancillary testing. One was pseudo-isotropic pattern A consisting of 25-percent 0-degree, 50-percent \pm 45-degree, and 25-percent 90-degree plies. Pattern B consisted of 37.5-percent 0-degree, 50-percent \pm 45-degree, and 12.5-percent 90-degree plies. The latter was chosen on the basis of its higher stiffness in the wing bending direction and is a likely candidate for highly loaded wing skin structure. Prior test programs have shown that both fiber patterns perform close to the maximum joint efficiency that is attainable (Reference 1). In addition, based on ancillary test data, both patterns exhibit virtually equal bearing strengths and loaded hole tension strengths, while the unloaded hole strengths vary proportionally with the unnotched laminate allowables.

Balanced layup sequences provided 0-degree fibers at the laminate surfaces to facilitate load transfer to the bonded end fitting doublers. Only ± 45 -degree angle changes were permitted between adjacent plies except at the laminate midplane of symmetry. These constraints were aimed at avoiding induced microcracks which may occur between stacks of unidirectional plies. Such microcracks are known to cause edge delamination problems which cause a reduction in static compression strengths and a significant loss of fatigue life under tensile loading.

2.3 FABRICATION

The subcomponent test specimens were constructed from large flat panels that were laid up and cured for each fiber pattern and laminate thickness. A special cure cycle was developed to minimize exotherm effects. Sufficient dwell times at several hold temperatures allowed any heat generated by the continuous reaction to dissipate throughout the panel. The pressure and caul plates were 1/2 inch thick 7075-T6 aluminum reinforced with angle bars. The tendency of thick laminates to be thicker in the central region of the panel due to plate bending (at 350°F and 100 psi) warranted these thicker pressure plates.

The completed panels were C-scanned to insure that no voids or warpage had taken place. The panels were then cut to the proper geometry for each joint configuration. Carbide tipped drills and reamers were used to drill the fastener holes. A diamond tipped boring bit was used for the large end holes in the thick material. The bolt holes in the test section were drilled with the three joint members clamped together to insure proper hole alignment.

Bolts for the sleeved interference fit specimens had a lead taper ground on the bolt shank to facilitate bolt installation. In addition, the bolts and sleeves were treated with an Ann-Ro surface preparation and lubrication process to reduce the force required to drive the bolts through the expansion sleeves. The installation procedure was apparently successful for all bolt sizes.

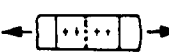


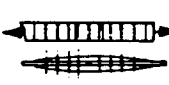
Tapered joint members were fabricated by machining or milling the surface of uniformly thick panels to the proper dimensions. Spot faces were used to accommodate the fasteners on the surfaces of tapered members and were achieved with standard machine tools.

2.4 CONFIGURATIONS

The subcomponent test program consisted of four basic multirow joint configurations to be tested for static strength in double shear for both tensile and compressive loading. The selection of joint geometries was based on the results of a series of preliminary analysis cases using the A4EJ program.

The entire series of static strength test specimens is described in Table I.

TABLE I
SUBCOMPONENT TEST PROGRAM - SPECIMEN DESCRIPTION

COMPONENT	LOAD TYPE	NO. OF SPECIMENS		SPECIMEN CODE	BOLTS PER SPECIMEN	d (IN.)	t LAM (IN.)	w (p) (IN.)	w/d (p/d)
	TENSION	2	2	JT4CF	4	0.500	0.832	2.15	4.30
	COMPRESSION	1	1	IF JC4CF IF					
	TENSION	3	1	JT8CF	8	0.375/ 0.437	0.832	2.15	5.75/ 4.92
	COMPRESSION	1	1	IF JC8CF IF					
	TENSION	1	1	JT12CF	12	0.750	0.996	9.00 (3.00)	(4.0)
	COMPRESSION	1	1	IF JC12CF IF					
	TENSION	1	1	JT24CF	24	0.500/ 0.625	0.996	6.00 (2.00)	(4.0, 3.2)
	COMPRESSION	1	1	IF JC24CF IF					

In addition to these specimens, there were three specimens designed to measure hole wearout in fatigue loading. Table II contains a list of detailed drawings.

All of the multirow joint specimens were fabricated from laminates of the Pattern B layup sequence ($37.5\% 0^\circ$, $50\% \pm 45^\circ$, $12.5\% 90^\circ$). This pattern was chosen because it was considered more representative of high aspect ratio composite wing skin structure. The three hole wearout specimens were made from the pseudo-isotropic layup Pattern A.

TABLE II
SUBCOMPONENT TEST SPECIMEN DESIGNATION

DRAWING NO.	SPECIMEN CONFIGURATION	SPECIMEN CODE
ZJ011263		HOLE WEAROUT
ZJ011264	- 1	JT12CF
↓	- 501	JT12IF
	- 503	JC12CF
	- 505	JC12IF
	- 507	JT24CF
	- 509	JT24IF
	- 511	JC24CF
	- 513	JC24IF
ZJ011264		
ZJ011265	- 1	JT4IF
↓	- 503	JT4CF
	- 507	JC4IF
	- 511	JC4CF
	- 501	JT8IF
	- 505	JT8CF
	- 509	JC8IF
	- 513	JC8CF
ZJ011265	- 515	JT8CF #3*

*Reworked

2.4.1 4-Bolt Joint (ZJ011265)

The 4-bolt specimen is a two-row joint with uniformly thick splice plates as shown in Figure 2. The central skin and splice plates are 0.832-inch-thick and 0.50-inch-thick, respectively. With a width of 2.15 inches and 0.50-inch diameter bolts, the w/d ratio is 4.30. The interference fit fastener system for this configuration consisted of a 7/16 inch bolt driven into a steel sleeve which was 1/32-inch-thick. Strain gages were mounted at the center of both edges on the two splice plates to monitor gross-section strain levels throughout the test.

Each of the subcomponent test specimen configurations included at least one specimen fabricated with interference fit fasteners. Figure 3 describes the general arrangement and specific dimensions of the interference fit fastener system used throughout the test program. The steel sleeves extended beyond the outer laminate surfaces to provide a uniform bolt bearing surface. Washers which were thicker than this extension were used to avoid "bottoming out" of the bolt head against the sleeve so that the clamp-up forces were applied directly to the composite joint members.

2.4.2 8-Bolt Tapered Joint (ZJ011265)

The 8-bolt joint is a single column specimen with four rows of bolts on each side. The splice plates are tapered linearly from just beyond the inner bolt row to the ends of the splice, as shown in Figure 4. The central skin thickness for this specimen was 0.832 inch. The splice plate thickness ranged from 0.50 inch at the center of the joint down to 0.06 inch at the tip. There were a total of six specimens tested in this configuration, four of them in tensile loading. All but one had 3/8-inch-diameter bolts for the first three rows, and 7/16-inch-diameter bolt at the interior rows. One specimen was reworked so that the first three rows of bolts were 7/16-inch-diameter, while the interior rows contained 1/2 inch bolts. All specimens used titanium bolts with the exception of the reworked specimen which had steel bolts of the larger sizes. The tapered surfaces of the splice plates were spot-faced to permit proper seating of the bolt heads and nuts. With a panel width of 2.15 inches, the nominal w/d ratios were 5.75 for three rows and 4.92 for the inner row. The corresponding values for the reworked specimen were 4.92 and 4.30.

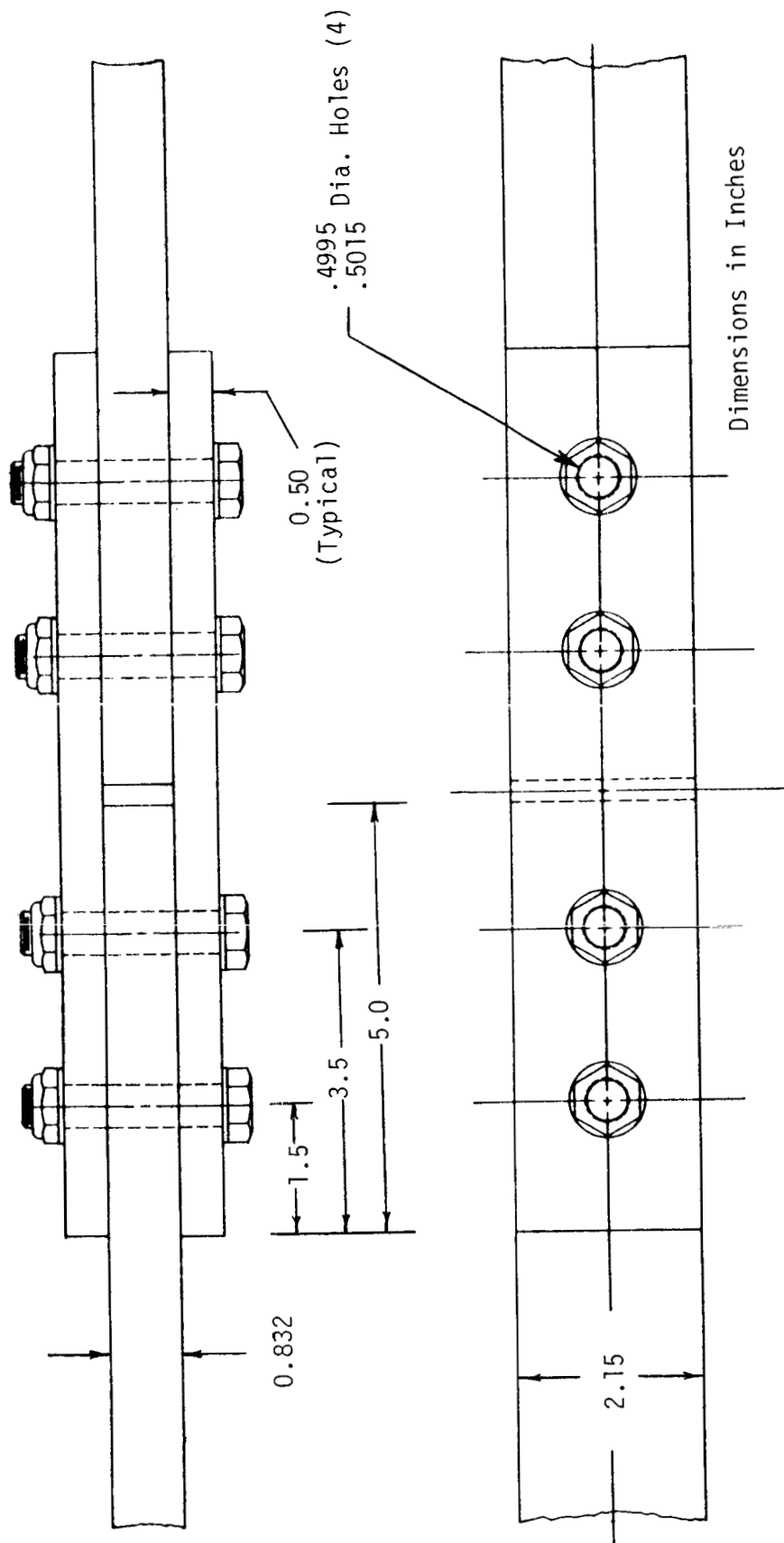
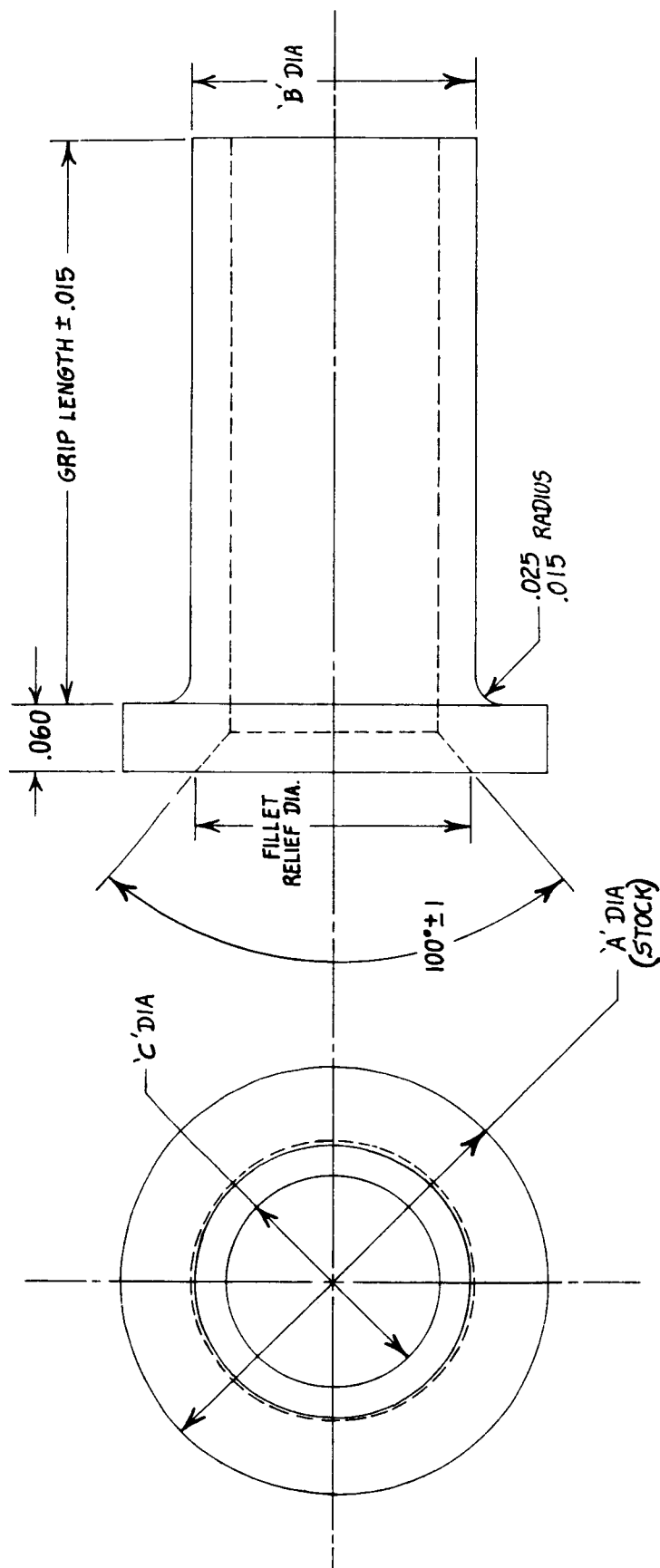


FIGURE 2. 4-BOLT SUBCOMPONENT JOINT SPECIMEN CONFIGURATION



DIA	DASH NO.	STRUCTURE HOLE SIZE (REF.)	'A' DIA STOCK	'B' DIA O.D.	'C' DIA I.D.	FILLET RELIEF DIA.	CORE BOLT DIA (REF) (UNPLATED)
3/8	-12	.3745 .3765	$\frac{9}{16}$.3735 .3745	.3045 .3055	.360 .370	.3115 (5/16) .3120
7/16	-14	.4370 .4390	$\frac{11}{16}$.4360 .4370	.3670 .3680	.425 .435	.3740 (3/8) .3745
1/2	-16	.4995 .5015	$\frac{3}{4}$.4985 .4995	.4295 .4305	.490 .500	.4365 (1/2) .4370
5/8	-20	.6245 .6265	$\frac{15}{16}$.6235 .6245	.4920 .4930	.560 .570	.4990 (1/2) .4995
3/4	-24	.7495 .7515	$1 \frac{1}{8}$.7485 .7495	.6165 .6175	.690 .700	.6235 (5/8) .6240

FIGURE 3. INTERFERENCE FIT FASTENER SYSTEM

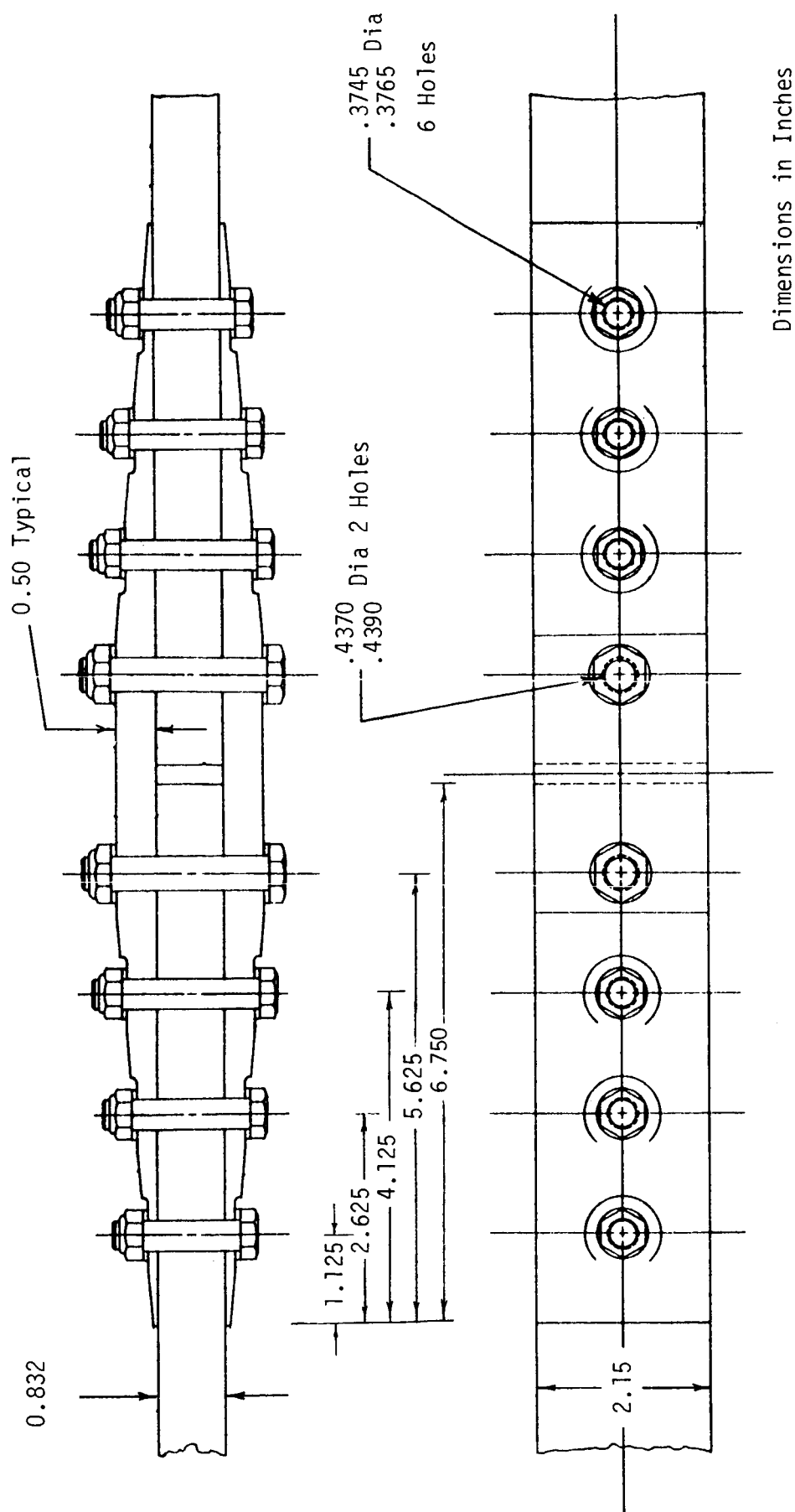


FIGURE 4. 8-BOLT SUBCOMPONENT JOINT SPECIMEN CONFIGURATION

Of the six specimens in this configuration, one tension and one compression specimen were fitted with interference fit fasteners. The 3/8 inch bolts were replaced by 1/32-inch-thick sleeves which were filled with 5/16 inch bolts. The same sleeve thickness was used in 7/16 inch and 1/2 inch holes along with 3/8 inch and 7/16 inch bolts, respectively.

Four of the six 8-bolt specimens were equipped with 18 strain gages mounted along the length of the joint on both sides of the central skin member and one splice member. These gages were located midway between the bolt rows. Additional gages were mounted away from the bolts in all three member to verify the lack of bending deformations.

2.4.3 12-Bolt Joint (ZJ011264)

The 12-bolt joint configuration was similar to the 4-bolt specimen, using uniformly thick splice plates with the fasteners arranged in two rows and three columns as in Figure 5. The base laminate was 1.0-inch-thick, with splice plate thicknesses of 0.67 inch. The fasteners were 3/4-inch-diameter bolts spaced 3.0 inches between columns across the overall width of 9.0 inches. The p/d ratio (pitch-to-diameter) was 4.0. The interference fit specimen used 5/8-inch-diameter bolts driven through 1/16-inch-thick steel sleeves to fill the 3/4 inch bolt holes. Strain gauges were mounted on the splice members as in the 4-bolt configuration.

2.4.4 24-Bolt Tapered Joint (ZJ011264)

A 24-bolt specimen was tested in a similar configuration to the 8-bolt specimen. The fasteners were arranged in four rows and three columns, with tapered splice plates as shown in Figure 6. The central skin member was 1.0-inch-thick. The splice plate thickness was 0.67 inch at the center, tapering down to 0.12 inch at the tips. The interior rows of bolts were 5/8-inch-diameter, while the rest were 1/2-inch-diameter. The specimen was 6.0-inches-wide leaving a p/d ratio of 3.2 at the interior rows, and 4.0 for the outer three rows. The interference fit specimens of this configuration used 7/16 inch bolts with a sleeve 1/32-inch-thick, and 1/2 inch bolts with a sleeve thickness of 1/16 inch. The splice plate surfaces were machine tapered and spot-facing was used to provide flat surfaces for the fastener heads and nuts.

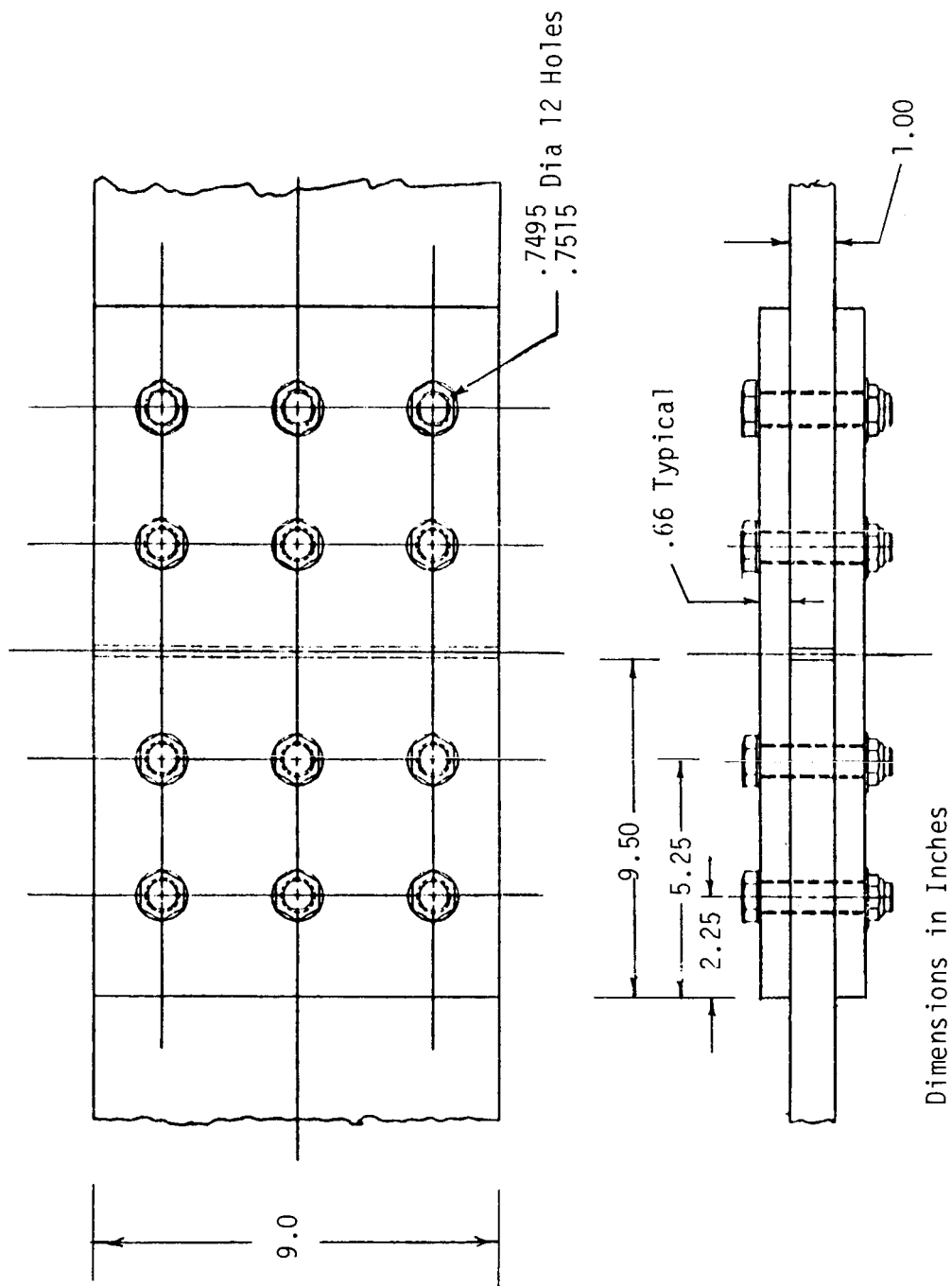


FIGURE 5. 12-BOLT SUBCOMPONENT JOINT SPECIMEN CONFIGURATION

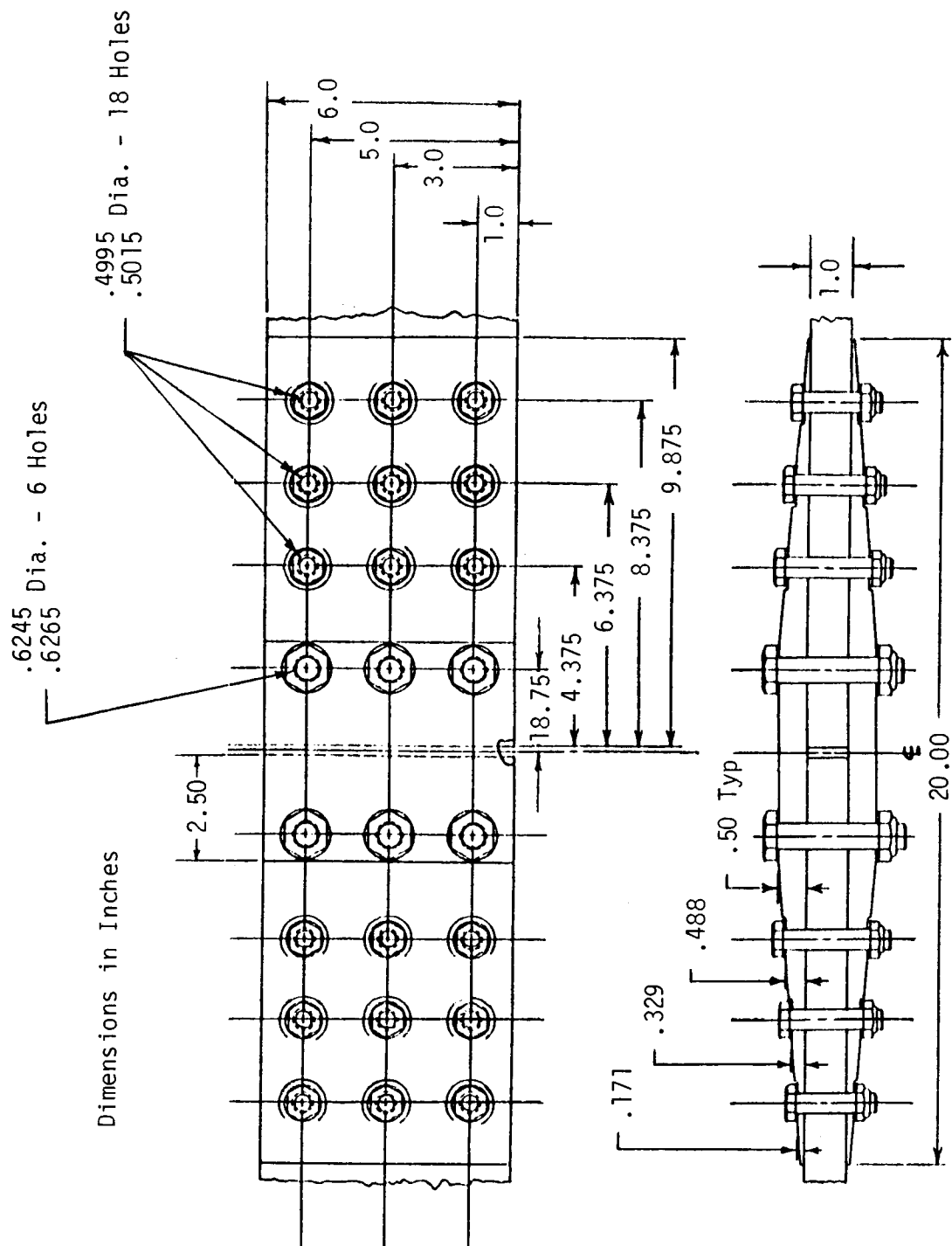


FIGURE 6. 24-BOLT SUBCOMPONENT JOINT SPECIMEN CONFIGURATION

Each of the 24-bolt specimens had 18 strain gages mounted along the length of one side of the joint to monitor internal loads. The gages were located between the rows of bolts and in the cross-section away from the bolts on the central skin member and one splice member.

2.4.5 Hole Wearout Specimen (ZJ011263)

The hole wearout specimens were 0.50 x 2.00 inch in cross section with a 1/2 inch bolt through each end. The two bolts were loaded in double shear by steel plates at each end of the specimen. The pseudo-isotropic Pattern A was used for all three specimens. The specimen configuration is shown in Figure 7.

2.4.6 Load Introduction - Subcomponent Joints

The load introduction technique for the subcomponent tension joint is illustrated in Figure 8. For the 4-bolt and 8-bolt joints, the end joint was sufficiently wider than the test section to avoid the need for additional reinforcement at the ends. However, the higher loads and geometric limitations associated with the larger 12-bolt and 24-bolt joints indicated that such reinforcement was required. This added strength was provided by tapered aluminum doublers which were bonded to each of these specimens to reinforce the pin loaded hole.

An end joint proof test specimen was fabricated to insure that the design was sufficient to carry the high load intensities of these joints. The specimen (Figure 9) was successfully loaded to 400,000 pounds in tension, indicating that the end joint design was satisfactory. The specimen is shown in Figure 10 as it was mounted in the test machine.

Compression specimens were loaded through standard potted ends as shown in Figure 11. The ends were machined flat and parallel to stabilize and align the specimens.

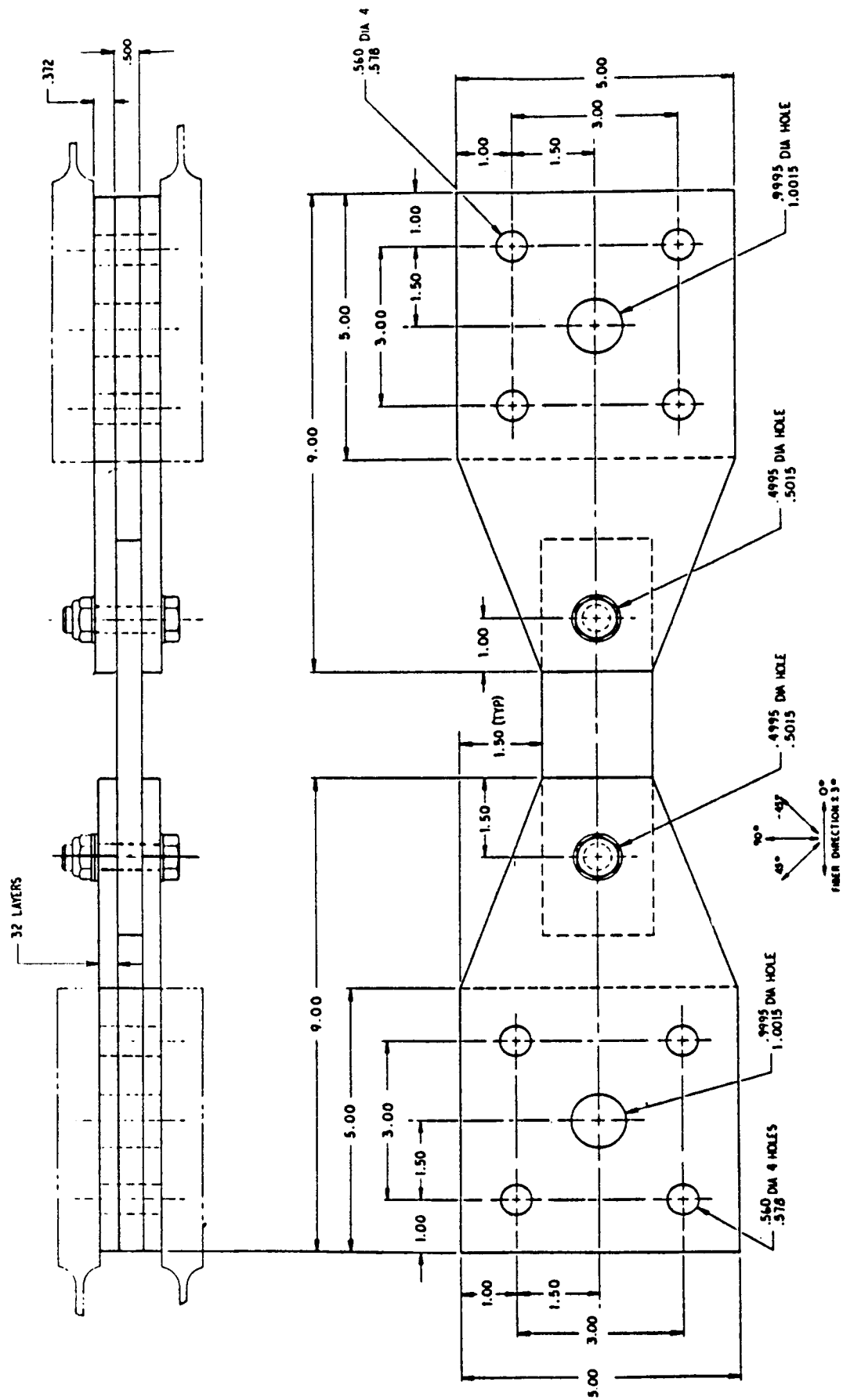


FIGURE 7. HOLE WEAROUT SPECIMEN CONFIGURATION

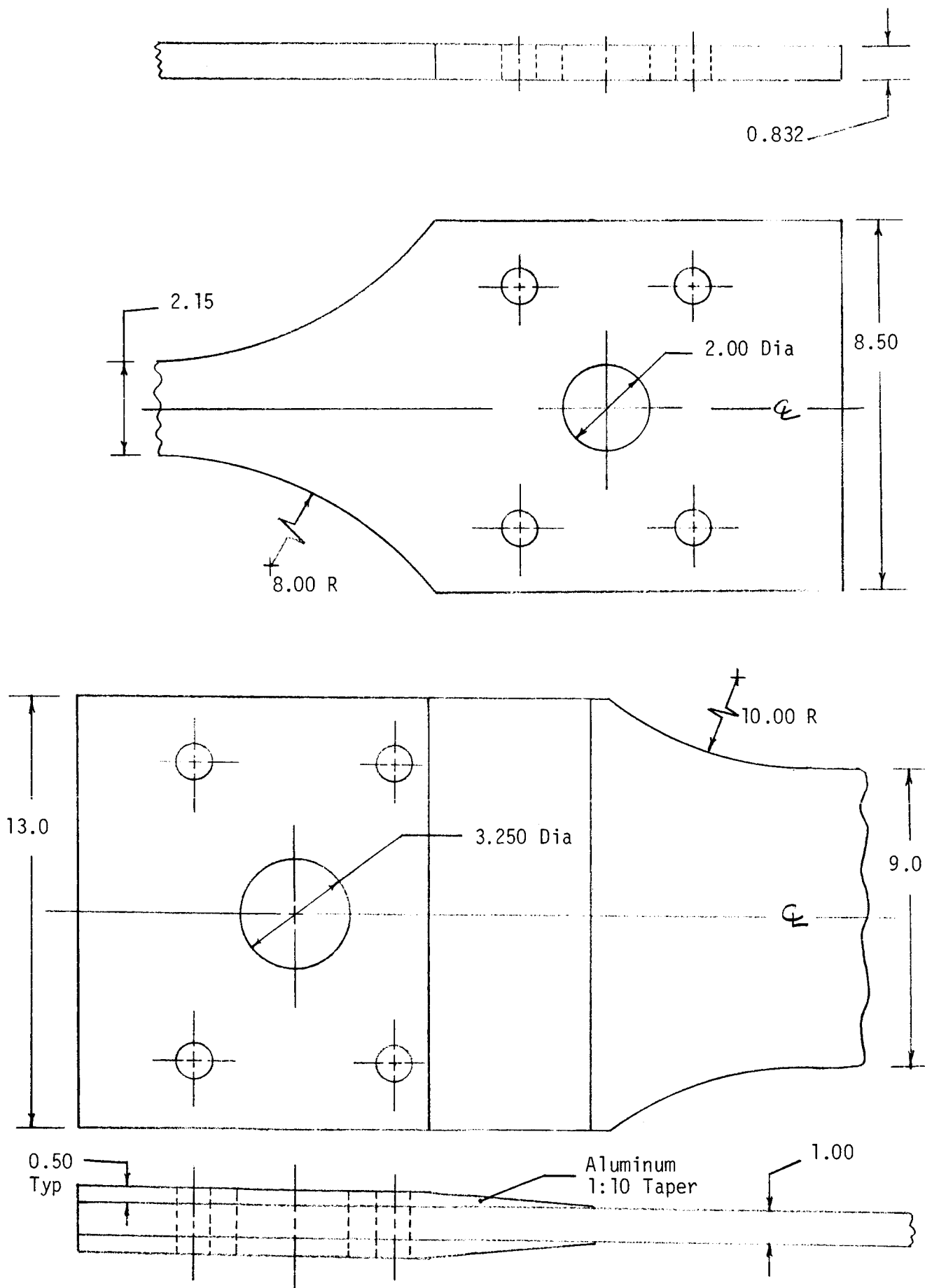


FIGURE 8. LOAD INTRODUCTION - SUBCOMPONENT TENSION JOINTS

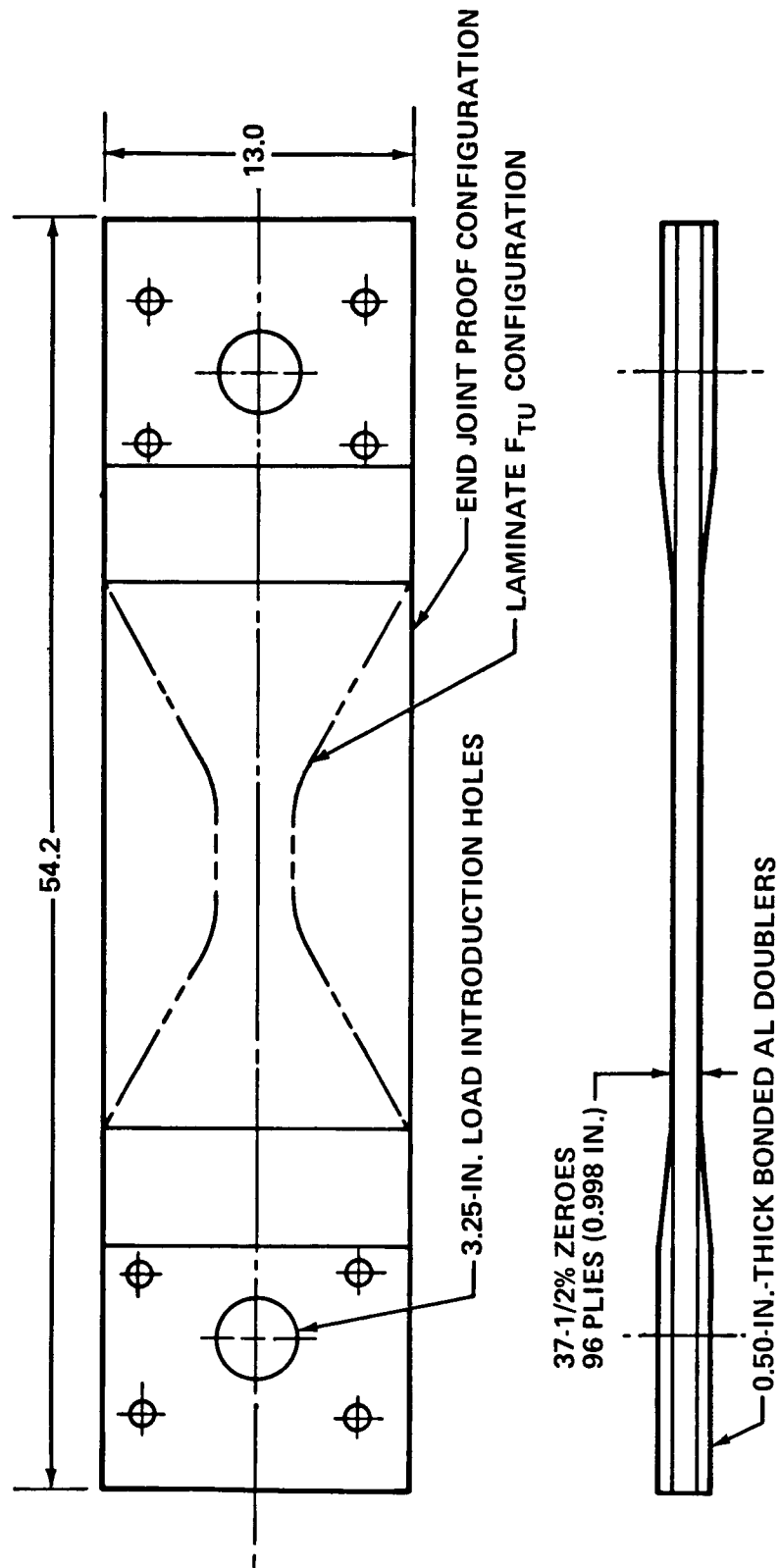


FIGURE 9. END JOINT PROOF TEST SPECIMEN



FIGURE 10. END JOINT PROOF TEST

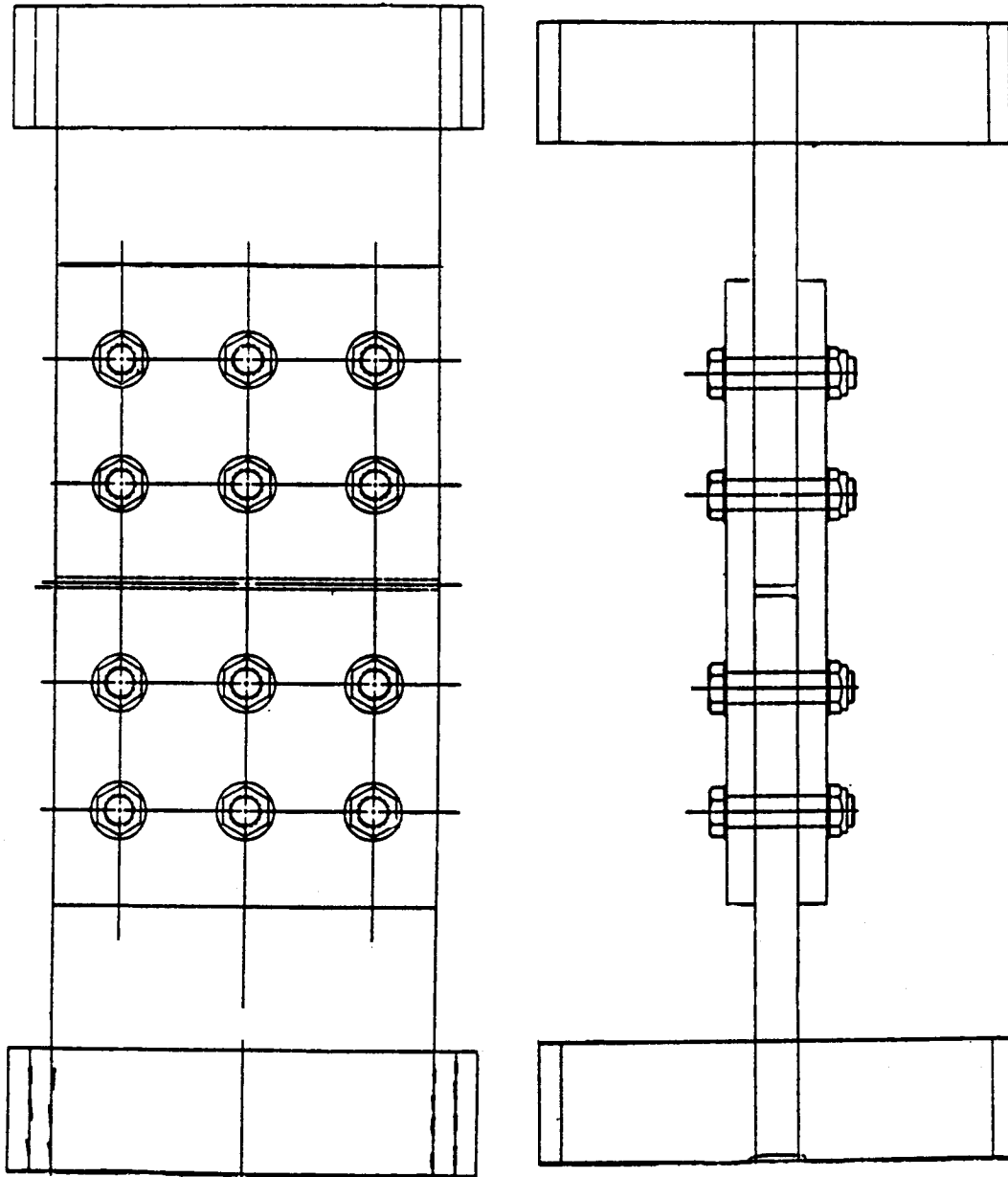


FIGURE 11. LOAD INTRODUCTION - SUBCOMPONENT COMPRESSION JOINTS

3.0 SUBCOMPONENT JOINT TESTS

3.1 TEST PROCEDURES

The subcomponent joint specimens were tested at room temperature using two different test machines, depending on the specimen configuration. The 4-bolt and 8-bolt specimens with one column of bolts and 0.832-inch-thick skins were tested in a 100,000 pound capacity servo-hydraulic MTS test machine. The larger 12-bolt and 24-bolt joints with three columns of bolts and 1.0-inch-thick skins required more load capacity and were tested in a 1,100,000 pound Baldwin test machine (Figure 10). Tension specimens were loaded through the combination of pin loading and clamping forces on the end fittings. Compression specimens were loaded directly through the potted ends with spherical loading heads used to assure specimen alignment in the test machine. The compression specimens were stabilized across the centerline of each side to prevent an Euler buckling failure of the joint occurring prior to a true compression failure. All specimens were loaded to failure using the stroke control (machine head travel) mode of loading.

Single channel, axial foil, resistance strain gages were bonded to each specimen at various locations throughout the joint, depending on the configuration. Strains were recorded at intervals of 20 percent of the predicted limit joint strength, and in 10 percent intervals thereafter until failure. In addition to strain gage readings, plots of joint applied load versus machine head travel were recorded when possible.

Spectrum load data for the hole fatigue wearout specimens was fed into the MTS machine load control system by magnetic tape. No additional instrumentation was required.

3.2 TEST RESULTS

The most significant results of the subcomponent test program was the consistent ability to reach gross-section strains on the order of 0.005 in large composite bolted joints, for both tensile and compressive loading. Throughout the series of tests a variety of failure modes were encountered, some of which were

unanticipated. Of these, the most troublesome was the delamination of the outer plies of tapered splice members in tension tests which induced a premature tension failure of the splice plates at a reduced thickness. Some specimens experienced excessive bolt bending which occasionally led to bolt failure, prior to the anticipated failure of the laminate.

Subcomponent compression tests also displayed various modes of failure. The phenomena associated with these failures (to be explained in subsequent discussions) further verify the importance of interlaminar stresses in the performance of bolted composite joints under compressive load. Failure of the compression joint splice members under bearing-bypass load levels below that of initial predictions suggests the existence of a new failure mode, the source of which shall also be discussed.

The entire set of test results is presented in Tables III through VII, including ultimate loads, strain levels, and a brief description of the failure modes. Strain gage data and load deflection curves from each test (if available) are contained in Appendix A.

TABLE III
4-BOLT TENSION AND COMPRESSION TEST RESULTS

SPECIMEN CODE	BOLT HOLE DIAMETER(S) (inches)	SPLICE THICKNESS MAX. (inches)	SKIN THICKNESS (inches)	FAILURE MODE (lbs)	STRAIN AT FAILURE CENTRAL SKIN (μ in./in.)	STRAIN AT FAILURE SPLICE PLATES (μ in./in.)	GROSS-SECTION STRESS AT FAILURE (psi)	RUNNING LOAD IN SKIN AT FAILURE (lb/in)	FAILURE MODE	FIGURE NUMBER
JT4IF #1	1/2	.499	.832	70,200	4390	3650	39,240	32,650	Bolt Bending, Bolt Tension Failure, Failure of Threads in Shear Nut	13 (a)
JT4IF #2	1/2	.499	.832	69,500	4410	3670	38,850	32,330	Same as JT8IF #1	13 (b)
JT4CF #1	1/2	.499	.832	71,600	4690	3900	40,030	33,300	Failure of Castellated Shear Nut Followed by Bolt Pull Through	12
JT4CF #2	1/2	.499	.832	75,400	4970	4140	42,150	35,070	Net-section Tension Central Skin Member Outer Row of Bolts	14
JC4IF	1/2	.499	.832	-58,400	-4640	-3860	-32,650	-27,160	Edge Delamination in Gross Section of One Splice Plate	24
JC4CF	1/2	.499	.832	-63,400	-4510	-3750	-35,440	-29,490	Column Buckling Due to Omission of Lateral Supports	23

TABLE IV
8-BOLT TENSION AND COMPRESSION TEST RESULTS

SPECIMEN CODE	BOLT HOLE DIAMETER(S) (inches)	SPLICE THICKNESS MAX. (inches)	SKIN THICKNESS (inches)	FAILURE MODE (lbs)	STRAIN AT FAILURE CENTRAL SKIN (μ in./in.)	STRAIN AT FAILURE SPLICE PLATES (μ in./in.)	GROSS SECTION STRESS AT FAILURE (psi)	RUNNING LOAD IN SKIN AT FAILURE (lb/in)	FAILURE MODE	FIGURE NUMBER
JT81F	3 - 3/8 1 - 7/16	.499	.832	60,500	3640	3080	33,820	28,140	Splice Delamination Bolt Failure at 3rd Row	18
JT8CF #1	3 - 3/8 1 - 7/16	.499	.832	70,100	4220	3860	39,190	32,600	Splice Delamination and Net Tension Failure at Reduced Thickness	15
JT8CF #2	3 - 3/8 1 - 7/16	.499	.832	65,600	4070	3640	36,670	30,510	Same as JT8CF #1	16
JT8CF #3	3 - 7/16 1 - 1/2	.499	.832	71,300	4290	3850	39,860	33,160	Same as JT8CF #1	17
JC81F	3 - 3/8 1 - 7/16	.499	.832	-67,900	-4080	3520	-37,960	-31,580	Edge Delamination in Gross Section of One Splice Plate	26
JC8CF	3 - 3/8 1 - 7/16	.499	.832	-75,000	-4790	-3980	-41,930	-34,880	Compressive Delamination Failure at Inner Row of Bolts in Splice	25

TABLE V
12-BOLT TENSION AND COMPRESSION TEST RESULTS

SPECIMEN CODE	BOLT HOLE DIAMETER(S) (inches)	SPLICE THICKNESS MAX (inches)	SKIN THICKNESS (inches)	FAILURE LOAD (lbs)	STRAIN AT FAILURE CENTRAL SKIN (μ in./in.)	STRAIN AT FAILURE SPLICE PLATES (μ in./in.)	GROSS-SECTION STRESS AT FAILURE (psi)	RUNNING LOAD IN SKIN AT FAILURE (LB/IN)	FAILURE MODE	FIGURE NUMBER
JT12CF	3/4	.667	.996	354,000	4170	3130	39,330	39,330	Net-section tension in central skin at outer row of bolts	19
JT12IF	3/4	.667	.996	350,000	3990	2990	38,890	38,890	Bolt bending yield	20
JC12CF	3/4	.667	.996	-408,000	-4800	-3600	-45,330	-45,330	Compressive delamination failure at inner row of bolts in splice	27
JC12IF	3/4	.667	.996	-370,000	-4250	-3190	-41,110	-41,110	Same as JC12CF	28

TABLE VI
24-BOLT TENSION AND COMPRESSION TEST RESULTS

Specimen Code	Bolt Hole Diameter(s) (inches)	Splice Thickness max (inches)	Skin Thickness (inches)	Failure Load (lbs)	Strain at Failure Central Skin (μ in./in.)	Strain at Failure Splice Plates (μ in./in.)	Gross-Section Stress at Failure (psi)	Running Load in Skin at Failure (lb/in)	Failure Mode	Figure Number
JT24CF	3 - 1/2 1 - 5/8	.667	.996	259,000	4710	3710	43,170	43,170	Splice delamination and net-tension failure at reduced thickness	21
JT24IF	3 - 1/2 1 - 5/8	.667	.996	265,000	4960	3800	44,170	44,170	Same as JT24IF	22
JC24CF	3 - 1/2 1 - 5/8	.667	.996	-297,000	-6189	-5500	-49,500	-49,500	Compressive delamination failure at inner row of bolts in splice	29
JC24IF	3 - 1/2 1 - 5/8	.667	.996	-302,000	-6230	-5000	-50,330	-50,330	Same as JC24CF	30

TABLE VII
HOLE WEAROUT TEST RESULTS
Drawing ZJ011263

1 Spectrum repetition = 57,849 cycles/profile
30 reps. = 1,735,470 cycles = 2 lifetimes

Specimen Number	1	2	3
Gross Area (in ²) at Hole 1 at Hole 2	1.001 0.9945	1.0124 0.9886	1.006 0.9934
Initial Brg Area (in ²) Hole 1 Hole 2	0.2507 0.2485	0.2531 0.2474	0.2520 0.2491
Peak Loads (lbs) Max Min	13,300 -2,260	19,950 -3,389	26,955 -4,579
Initial Clearance 1 2	.0020 .0021	.0028 .0031	.0022 .0022
Peak Brg Stress (ksi) 1 2	53.051 53.521	78.823 80.639	106.96 108.25
Total Cycles (Millions)	1.7355	1.7355	0.3653
Hole Clearance After Test (in) 1 2	0.0021 0.0030	0.0033 0.0041	0.0662 0.0362
"Wear" 1 2	0.0001 0.0009	0.0005 0.010	0.064 0.034
Clamping Torque (in-lb)	40	40	40 (3 reps) 100 (to fail)

3.2.1 Tension Tests

3.2.1.1 4-Bolt Tension Tests

The JT4 test series was characterized by extensive bolt bending, and of the four tests in this configuration, three were ultimately critical in the fasteners. These specimens were designed to fail the net-section in the central skin members, and the failure modes resulting from insufficient bolt stiffnesses were not anticipated, or predicted. Adequate consideration of the bolt diameter-to-laminate thickness ratio (or more appropriately, bolt bending stiffness-to-laminate thickness ratio) is warranted for future joint design to assure that the fasteners are not the weak link.

Specimen number JT4CF-503-1 was a clearance fit specimen and the first to be tested in this configuration. The failure was initiated by severe bending of the 1/2 inch bolts which resulted in failure of the castellated shear nuts (at a gross-section stress of 40,030 psi and gross-section strain of .0047) which could not withstand the induced tension load on the fasteners. With the consequent loss of clamp-up on those bolts, they were then dragged through the splice plates, with the massive damage shown in Figure 12. The two interference fit specimens of this configuration (JT4IF-1-1, 2) exhibited essentially the same failure mode. The combination of high bending and induced tension loads on the fasteners (7/16 inch for interference fit) led to either a failure of the threaded connection between nut and bolt or a combined bending-tension failure of the fastener. The two interference fit specimens are shown in Figure 13. The interference fit fastener systems were typically bent more severely than clearance fit fasteners for the same size bolt hole. Gross-section stresses at failure for the two specimens were 39,240 psi (-1) and 38,850 psi (-2). In an attempt to suppress the bolt bending failure mode, specimen number JT4CF-503-2 was equipped with larger tension nuts to resist the loads induced by the now anticipated bolt bending. This modification was sufficient to maintain the integrity of the fasteners long enough to fail the joint at the outer row of bolts in net-tension, as was originally predicted. Figure 14 shows that this joint also suffered extensive bolt bending before a net-section failure occurred at a gross-section stress of 42,150 psi and strain of 0.005.

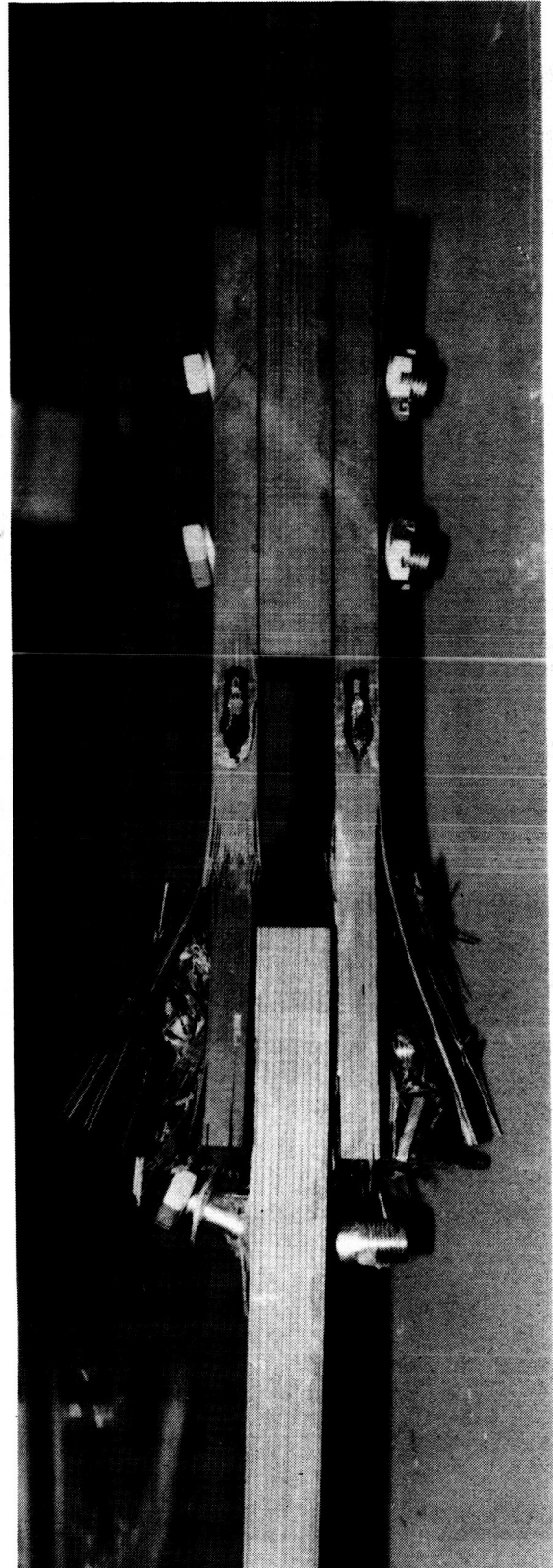
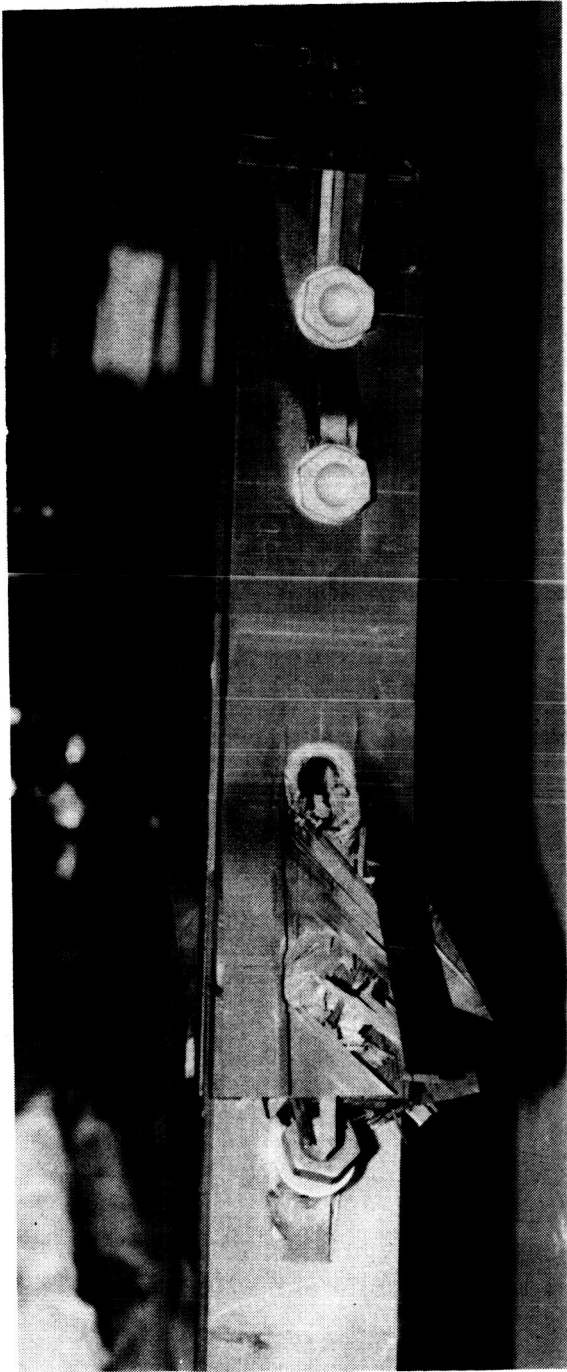


FIGURE 12. 4-BOLT TENSION SPECIMEN - JT4CF-503-1

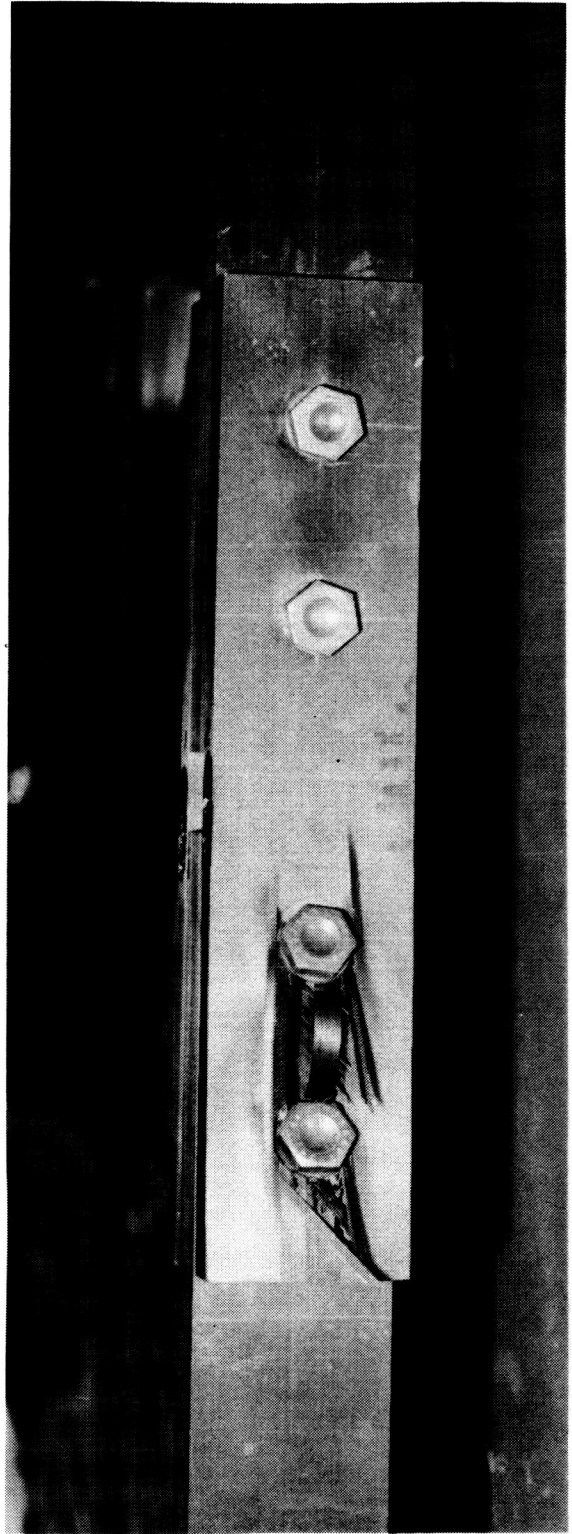
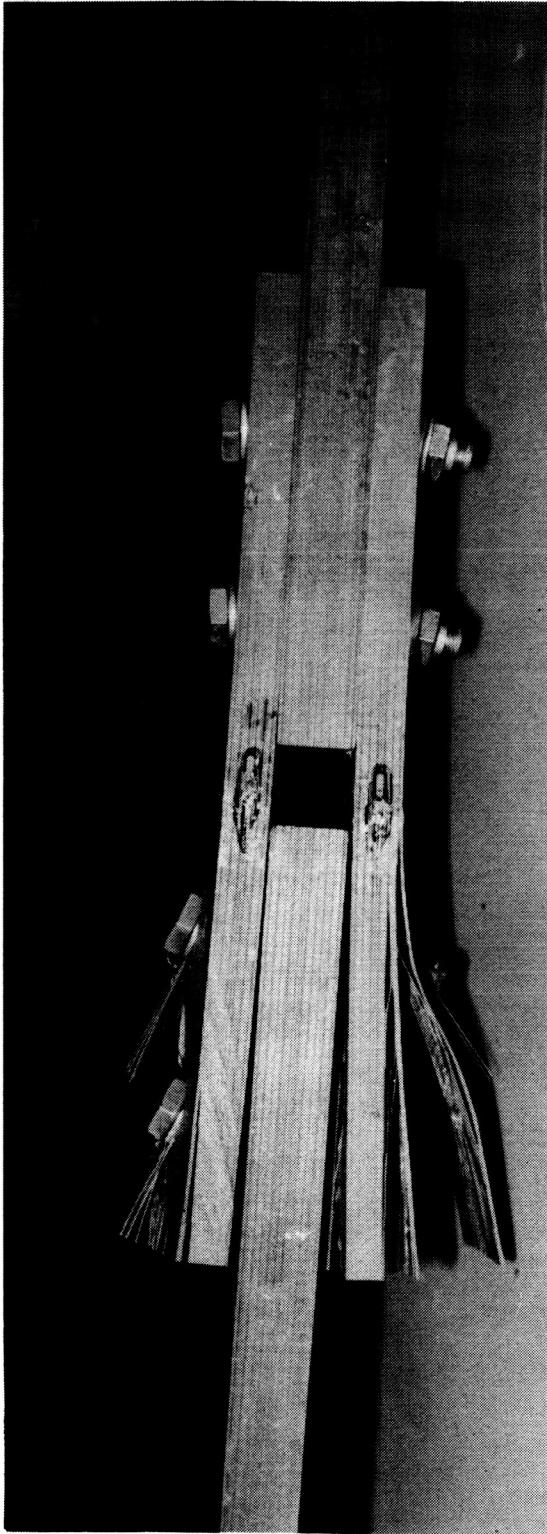


FIGURE 13 (a). 4-BOLT TENSION SPECIMEN - JT4IF-1-1

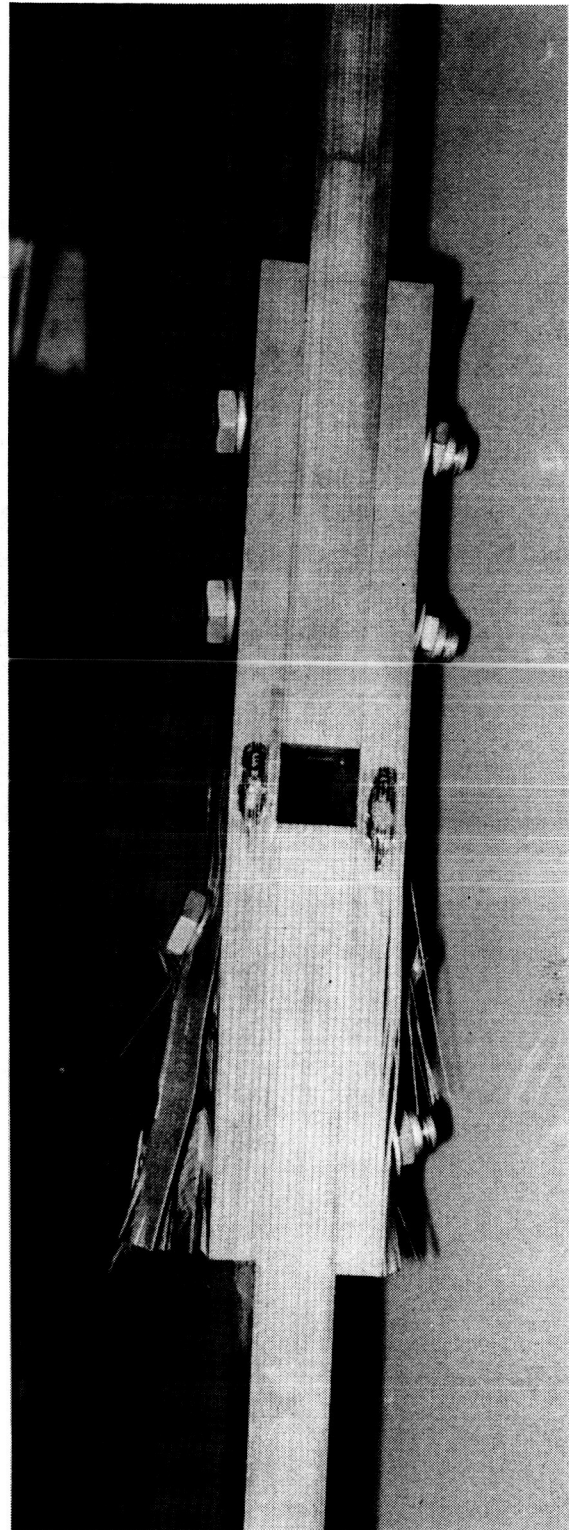
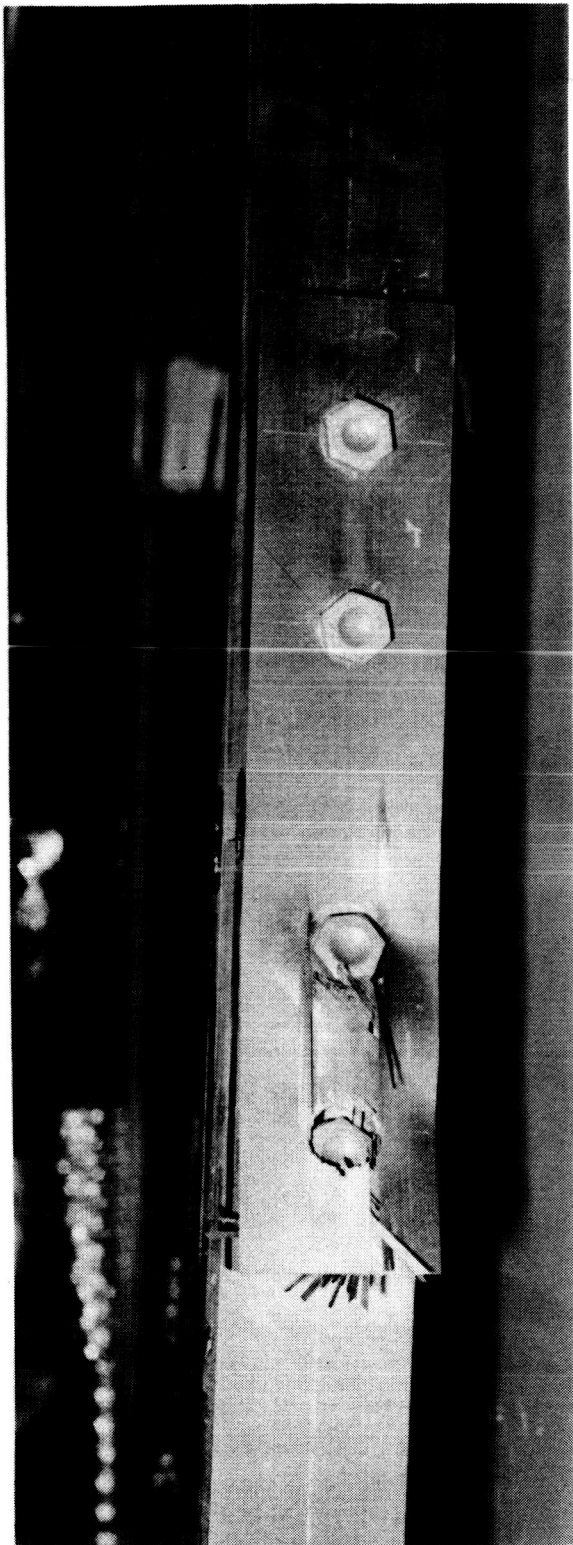


FIGURE 13 (b). 4-BOLT TENSION SPECIMEN - JT4IF-1-2

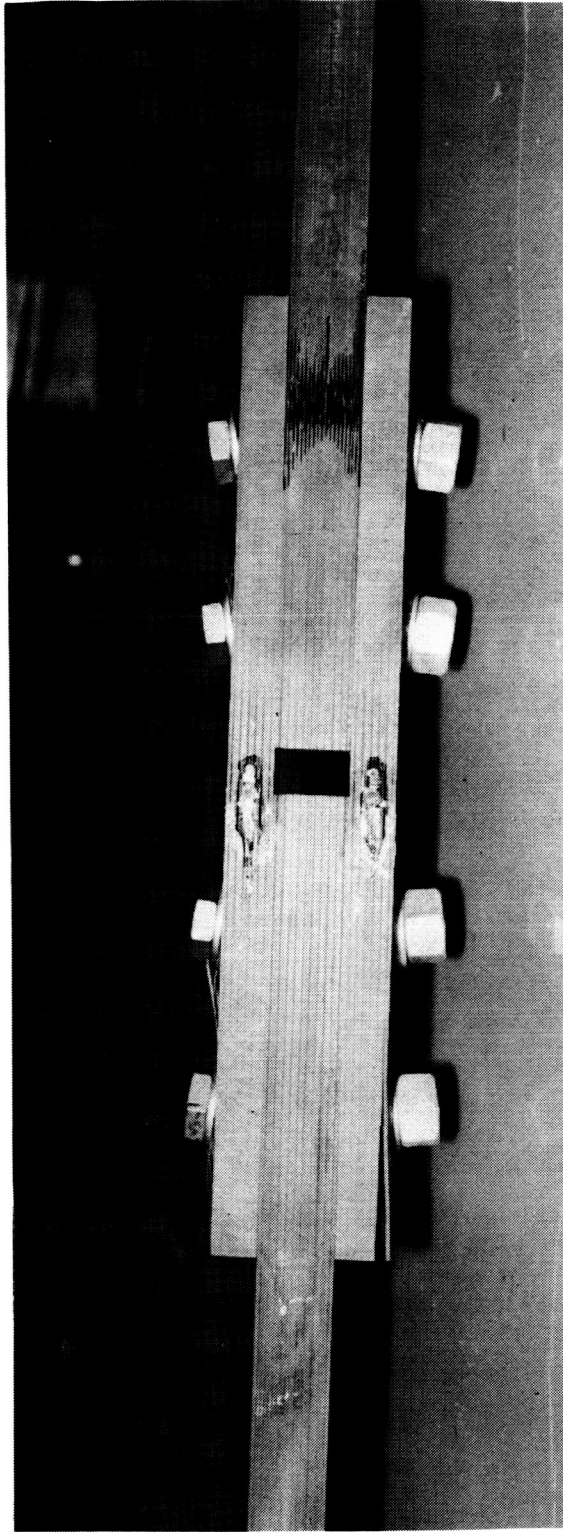


FIGURE 14. 4-BOLT TENSION SPECIMEN - JT4CF-503-2

In general, this series of tests exemplified the need to avoid using inadequately stiff fasteners in order to minimize their weight, solely on the basis of apparent shear strength. The bending of bolts should also be avoided because of its effect on laminate bearing strengths. As a bolt which is too small bends, it relieves the through-the-thickness clamp-up on the composite laminate which, in turn, drastically reduces the bearing strength of the laminate on the surface. This results in delaminations at local bearing stresses as low as those for simple shear pins - only about half of the strength for torqued bolts of larger diameter. The initial delaminations resulting from this phenomenon are visible in Figure 14, the effects of which will be discussed in subsequent sections of this report.

3.2.1.2 8-Bolt Tension Tests

The tapered, double-lapped, 8-bolt joint tests all resulted in an unanticipated mode of failure. These joints were designed to fail in a high-bypass, low-bearing load combination with a net-tension failure at the outer row of fasteners in the central skin member. Despite the additional reinforcement of the splice plates to stiffen them up and so modify the bolt load distribution favorably, most of the failures occurred in the splice plates rather than in the skins which, being in the middle of the sandwich, had greater allowable strengths. A frequent failure mode associated with the machine-tapered doublers was the delamination of the splice plates, as shown in Figures 15 and 16. The prime cause of that mode of failure was believed to be the spot facing for the bolt heads, nuts, and washers. Tapered washers would be preferred in the future. However, the possibility remains that the delaminations were initiated at small cracks on the surface due to machining, and it should be noted that such tapered laminates have been laid up and cured net by other investigators.

For three of the four specimens, the failure occurred when a delamination originating at the second row of bolts propagated beyond the fourth row. This reduced (by approximately 50 percent) the effective area of the splice members for carrying bypass loads at that most highly loaded row of bolts. A net-section failure at the reduced thickness followed instantaneously. In addition to premature splice plates failures, these specimens were also

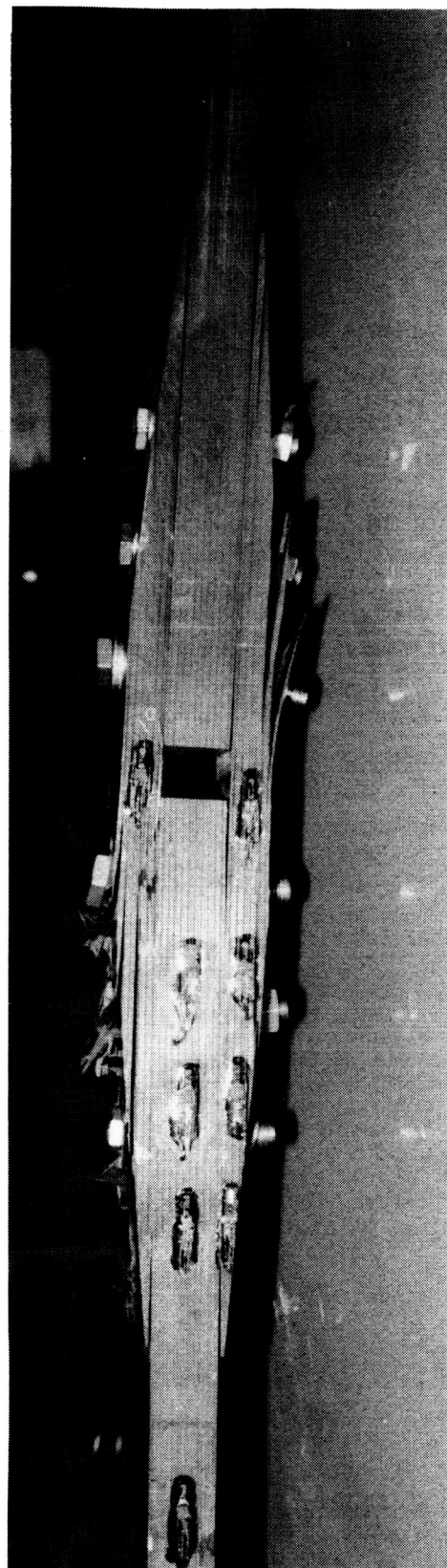
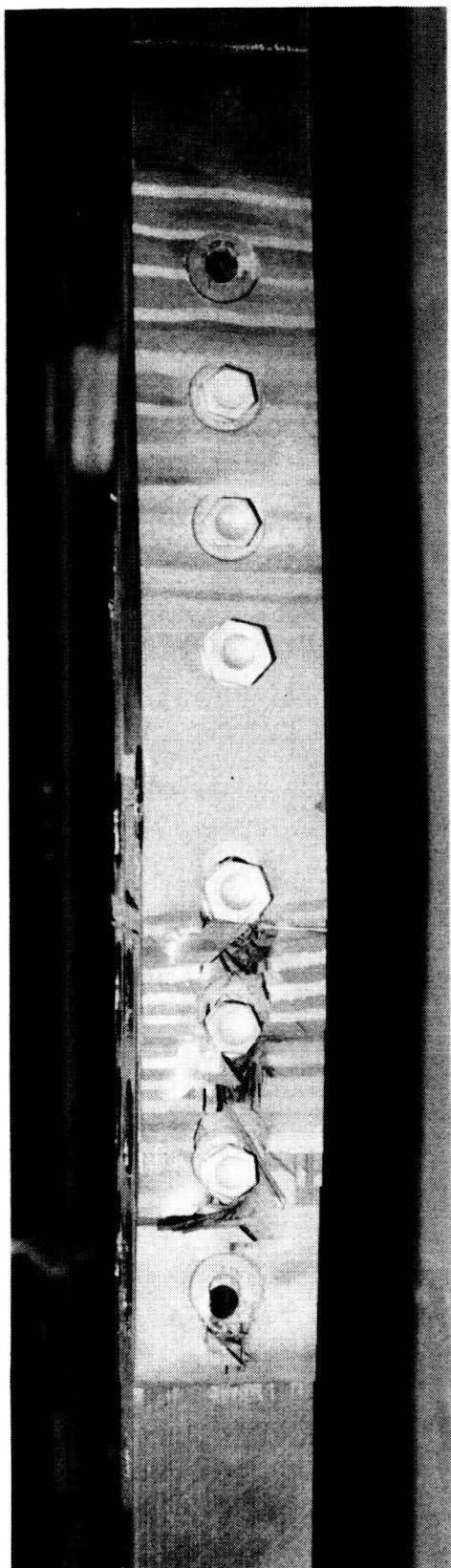


FIGURE 15. 8-BOLT TENSION SPECIMEN - JT8CF-505-1

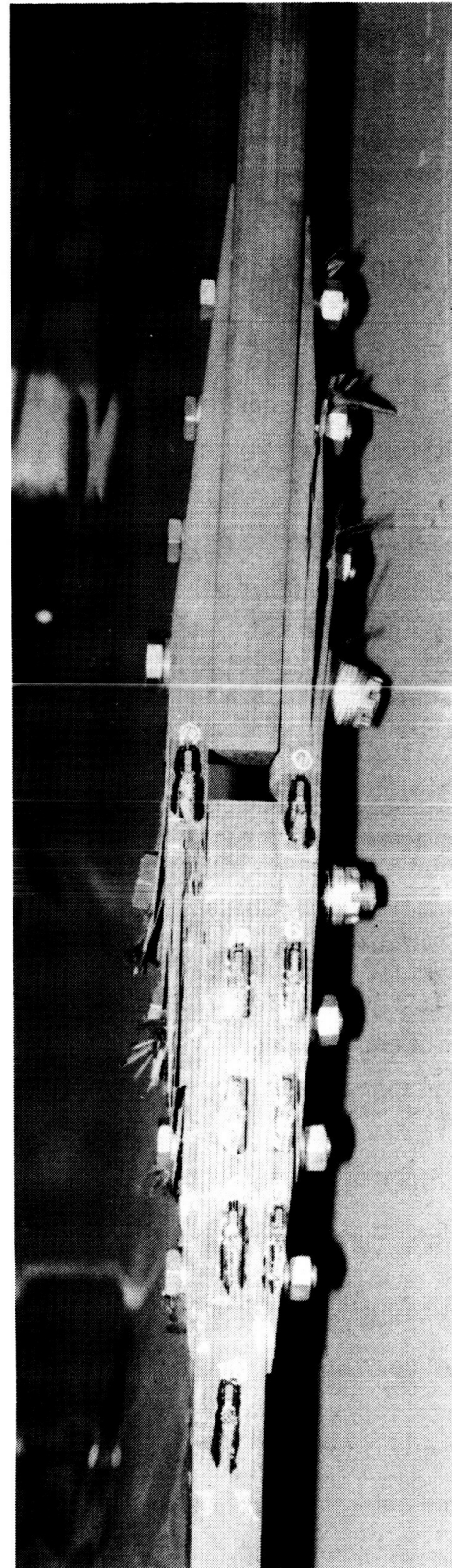
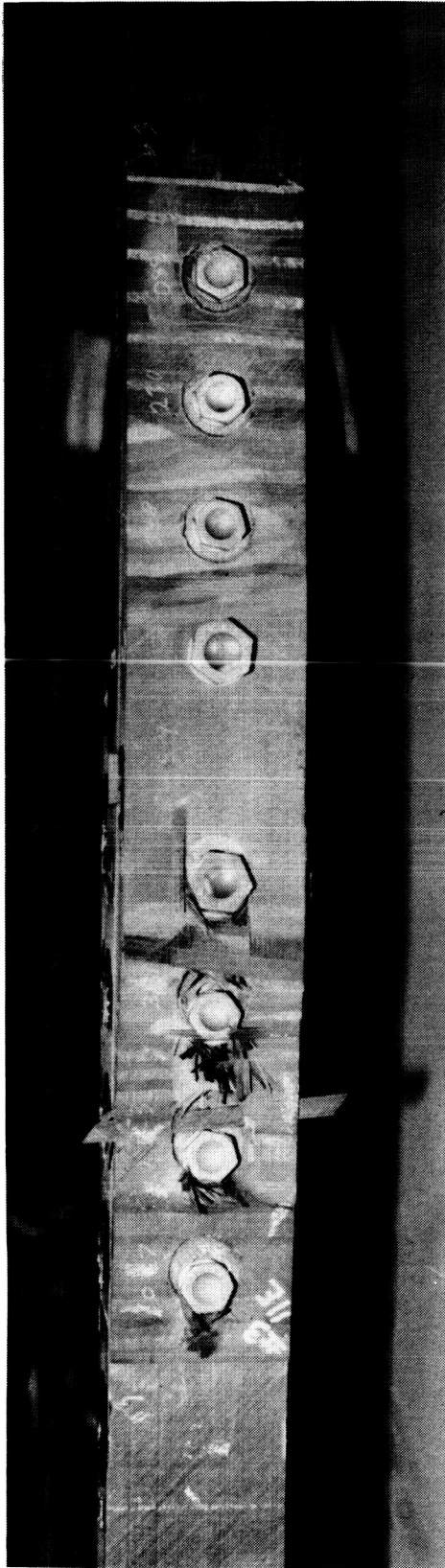


FIGURE 16. 8-BOLT TENSION SPECIMEN - JT8CF-505-2

subjected to extensive bolt bending. Specimen number JT8CF-505 shown in Figure 17 was reworked to 1/16 inch larger bolt sizes, and stiffer, steel bolts were used in place of titanium. This greatly reduced the amount of bolt bending which also limited the apparent damage due to delaminations of the splice plate external surfaces and theoretically increased the overall strength of the joint. However, the splice delaminations followed by a net-section failure at a reduced thickness was still the mode of failure. Strains at failure ranged from 0.0036 to 0.0048, depending on the onset and propagation rate of the surface delaminations in the splice members, regardless of fastener diameter.

The JT8IF specimen shown in Figure 18 was the interference fit specimen for this configuration. As was the case for the 4-bolt joint, these fasteners were substantially less stiff in bending, resulting in extensive bolt bending and splice delaminations. The test was stopped when one fastener (third from the end) failed due to the high bending and induced tension loads.

These tests demonstrated the ineffectiveness of machine tapered doublers with spot facing for the fasteners. None of these specimens reached their anticipated ultimate strengths, but they did generally perform as the analysis predicted. Improved design and manufacturing concepts should allow subsequent joints of this type to reach their predicted strengths, showing the high level of efficiency expected for this configuration. The delamination failure mode encountered by all of the JT8 specimens precludes a direct comparison between tested and predicted strengths. However, several of these specimens were equipped with strain gages (as previously described) to monitor joint internal loads throughout the test. These readings were used to generate histories of the bolt load distributions at increasing load levels, and are compared to analysis solutions later in this report. Appendix A contains the strain gage readings and load-deflection curves for this series of tests.

3.2.1.3 12-Bolt Tension Tests

There were two specimens of the 12-bolt configuration tested for tensile loading, and a different failure mode was observed for each of them. A tension-through-

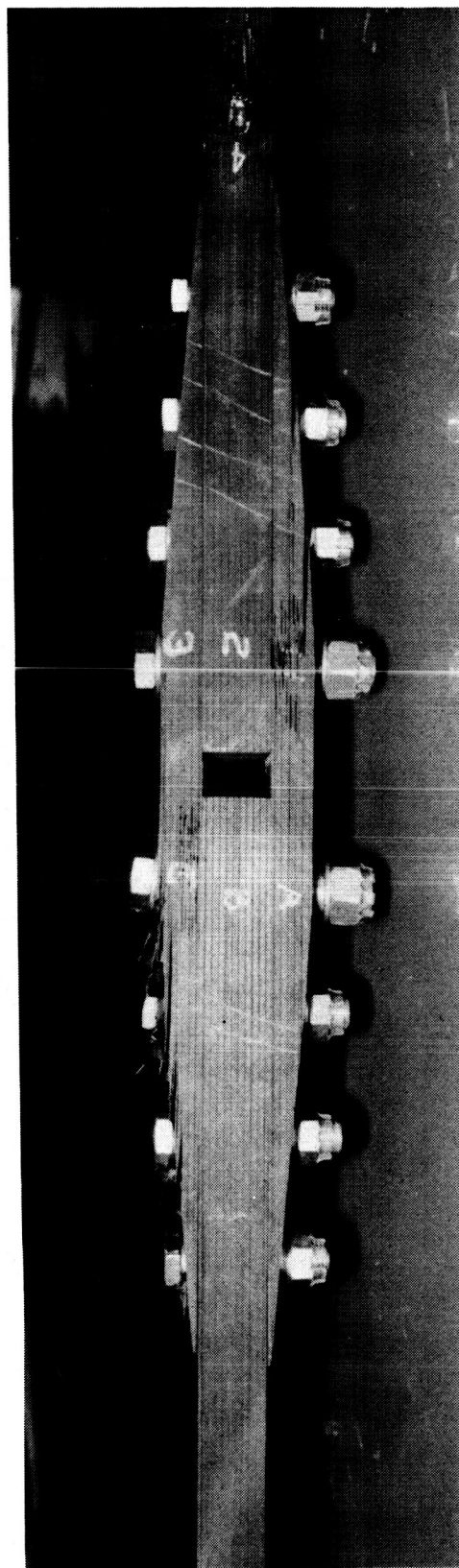
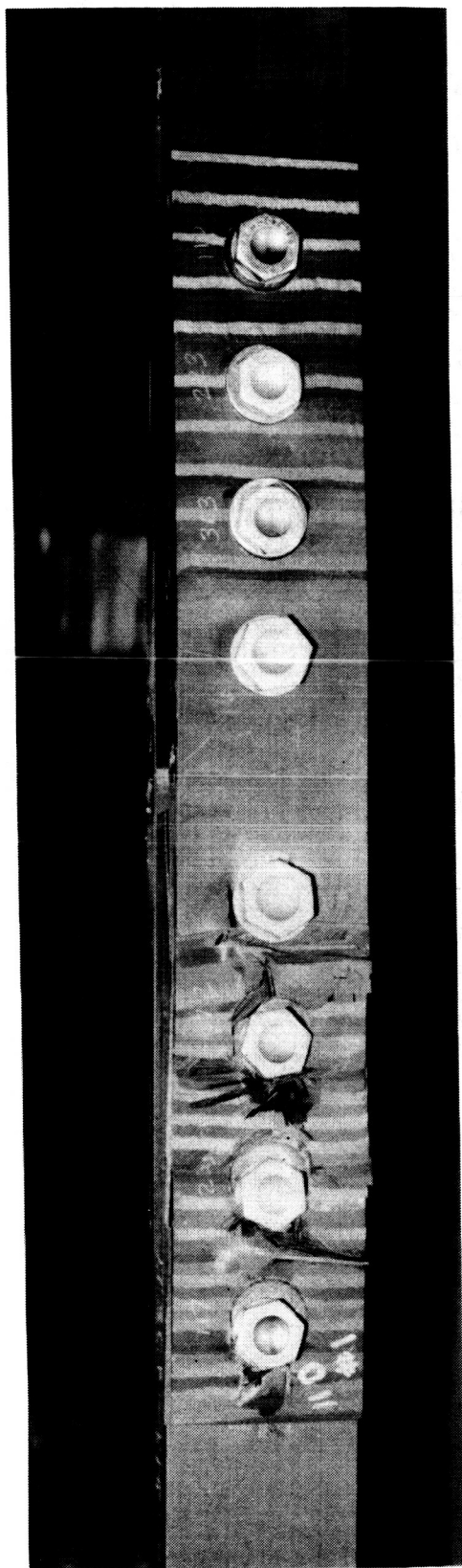


FIGURE 17. 8-BOLT TENSION SPECIMEN - JT8CF-515

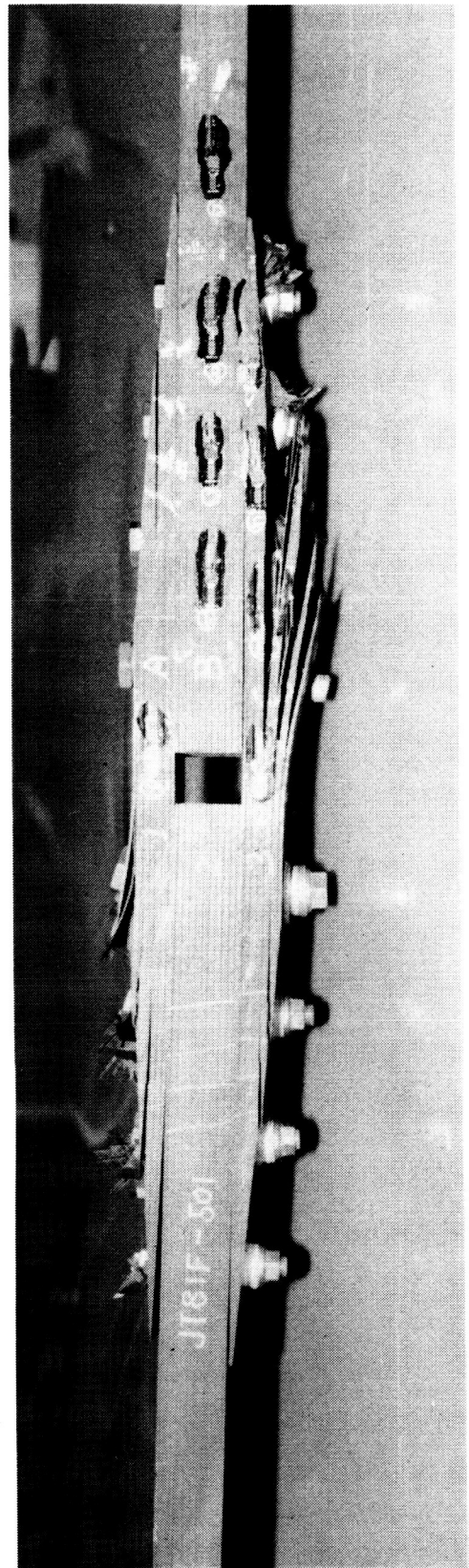
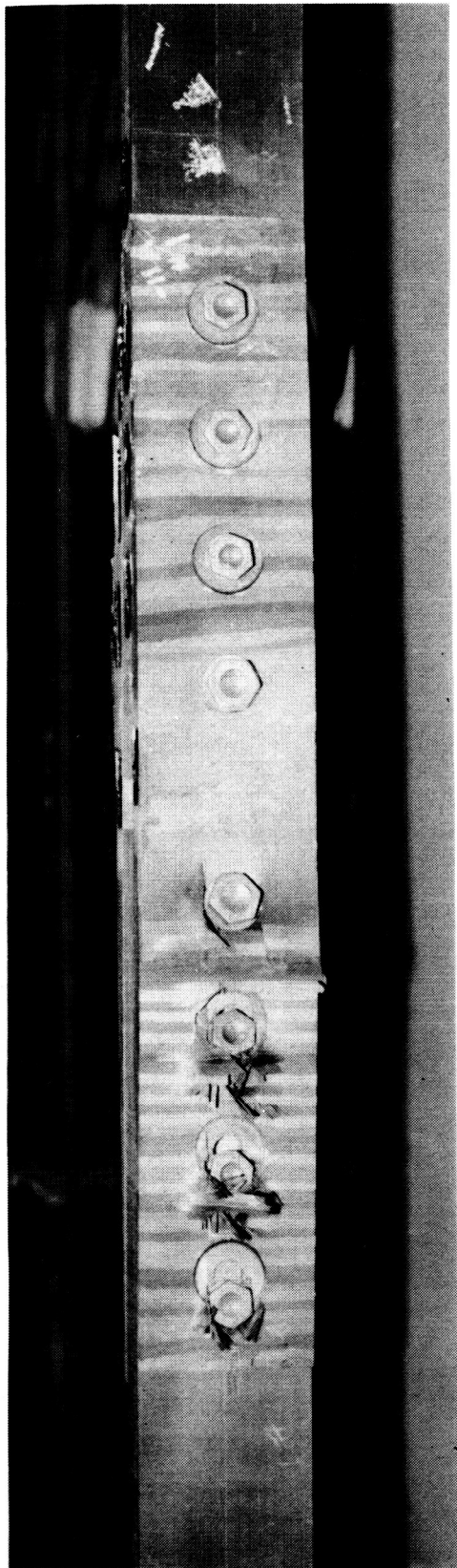


FIGURE 18. 8-BOLT TENSION SPECIMEN - JT8IF-501

the-hole failure has been predicted at the outer row of fasteners in the central skin member. This is consistent with the appearance of the failed (clearance fit) specimen, with a clean textbook fracture at a gross stress of 39,330 and a gross section strain of .0042 as shown in Figure 19. The specimen performance was essentially linear to failure, with no evidence of bolt bending during the test.

The interference fit specimen used 5/8 inch bolts with 1/16 inch-thick-sleeves to fill the 3/4 inch bolt holes. The lower bending stiffness of the interference fit fasteners was again evident in this test, when at a load level of 340-345 kips, the bolts began to yield in bending. This specimen is shown in Figure 20. The joint could sustain but not accept an increase in load above 350 kips and the test was stopped. The load level being so close to that of the clearance fit specimen suggests that a net-tension failure was nearly achieved. Strain gage data from these two tests may be found in Appendix A.

It should be noted that the 12-bolt clearance fit specimen and one of its 4-bolt counterparts were the only two subcomponent tension joints to fail with clean, net-section failures in the central skin as was originally intended. Various other failure modes prevented this for the rest of the tension specimens.

3.2.1.4 24-Bolt Tension Tests

The 24-bolt joint specimens were similar to the 8-bolt joints in both configuration and performance. The clearance fit specimen (JT24CF) shown in Figure 21 failed at an applied gross stress of 43,170 psi (.0047 gross-section strain), when delaminations in the splice members propagated beyond the inner row of bolts and a net-tension failure occurred through the reduced thickness. The onset of these initial delaminations has not been analyzed. In any case, it would be more fruitful to learn how to design joints not subject to this phenomenon, which is believed to have been induced by the spot faces at the bolt holes as was the case for the 8-bolt joints discussed earlier.

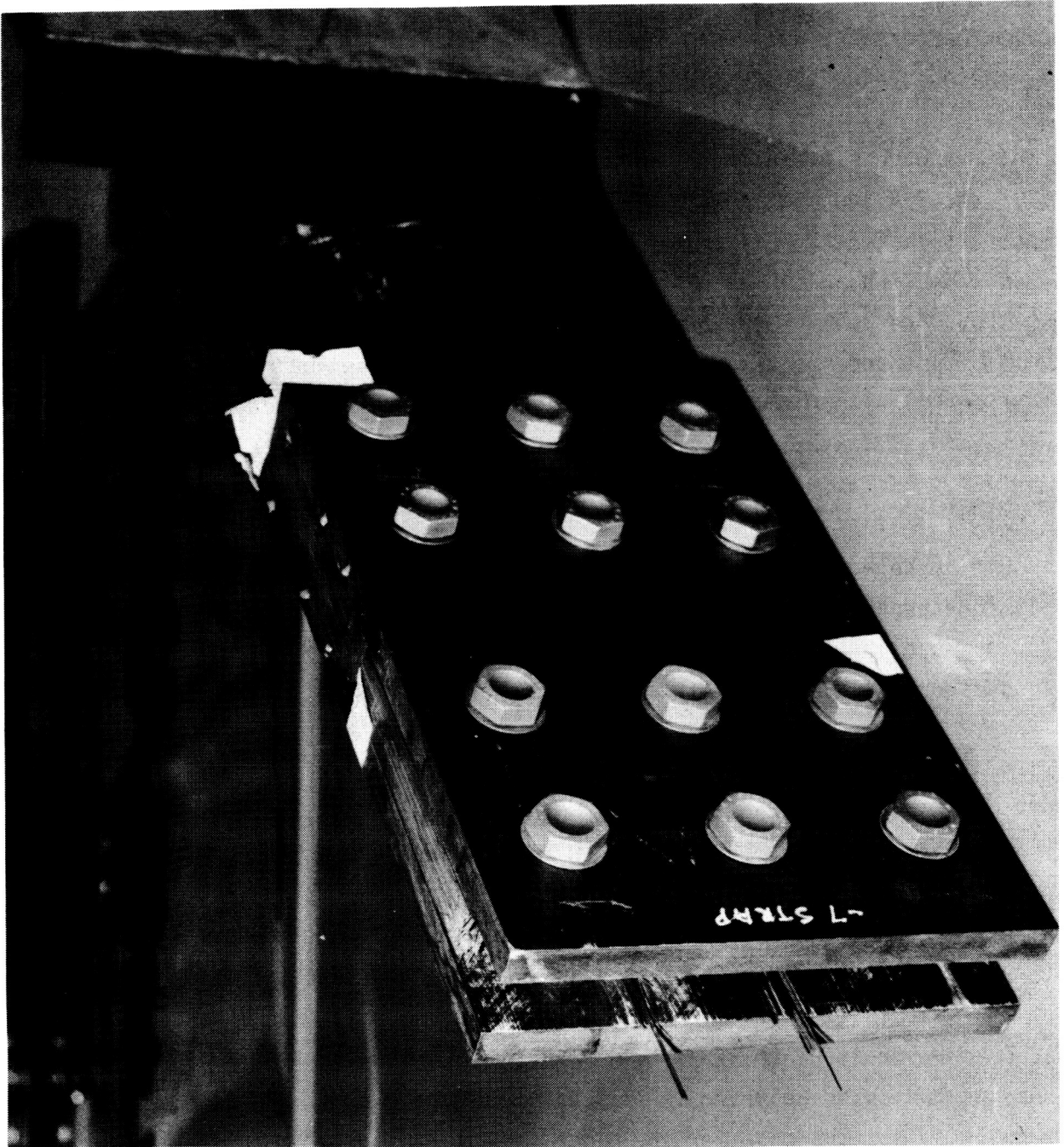


FIGURE 19. 12-BOLT TENSION SPECIMEN - JT12CF-1

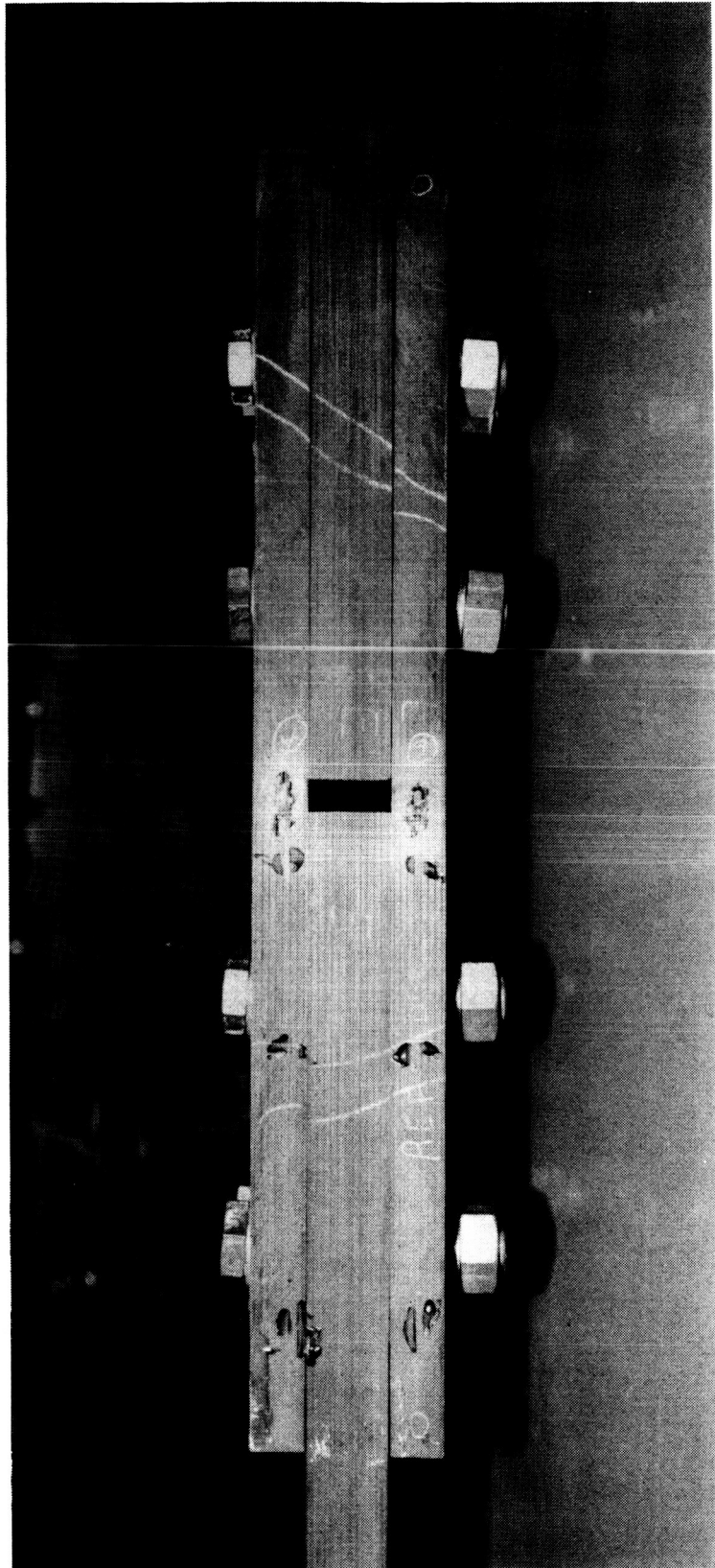


FIGURE 20. 12-BOLT TENSION SPECIMEN - JT12IF-501

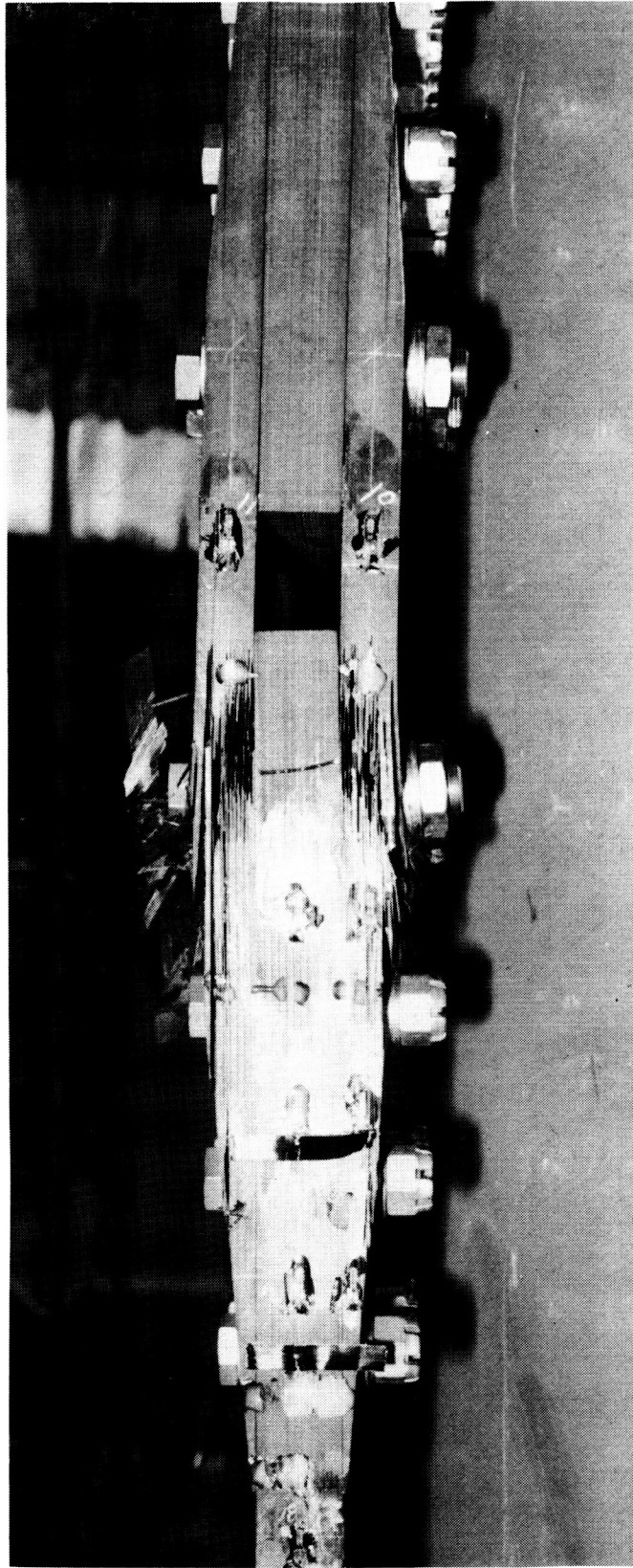


FIGURE 21. 24-BOLT TENSION SPECIMEN - JT24CF-507

The presence of bolt bending persisted in these specimens, though to a much lesser extent than in previous single column tests. For the interference fit specimen, the inferior ability of the sleeve bolts to resist bending loads prompted a change from titanium to steel bolts for this test.

This modification did provide more bolt stiffness throughout the joint, but the same failure mode persisted - splice plate delaminations followed by secondary net-tension failure, as shown in Figure 22. The failure stress of 44,170 psi and .0049 gross-section strain were somewhat higher than the clearance fit joint, but still falls well within the experimental scatter that could be expected when the mode of failure is conditioned by such delaminations.

Despite the emergence of these unforeseen failure modes, these specimens did attain 90 percent of the predicted joint strengths. One might infer from this that there are small but significant benefits to be realized by improving the detailed design or fabrication of such splices. But beyond this reasoning, the lack of any credible method of predicting these surface delaminations of the splice plates warrants the development of a design which precludes such failures altogether. Plans for future work include an investigation into tapered splice plate design and fabrication concepts.

3.2.2 Compression Tests

3.2.2.1 4-Bolt Compression Tests

Two subcomponent joint specimens were tested in this configuration under compressive loading. The first was the JC4CF (clearance fit) specimen, but the gross stress at failure of -35,440 psi is misleading. The specimen was tested without the lateral buckling supports that were supposed to be used for all compression tests. The joint failed when it began to buckle laterally, delaminating the outer plies of one splice plate on the compression side, as shown in Figure 23. The 1/2-inch-diameter bolts had also begun to bend. Care was taken throughout the remaining compression tests to insure that the lateral support devices were properly in place.

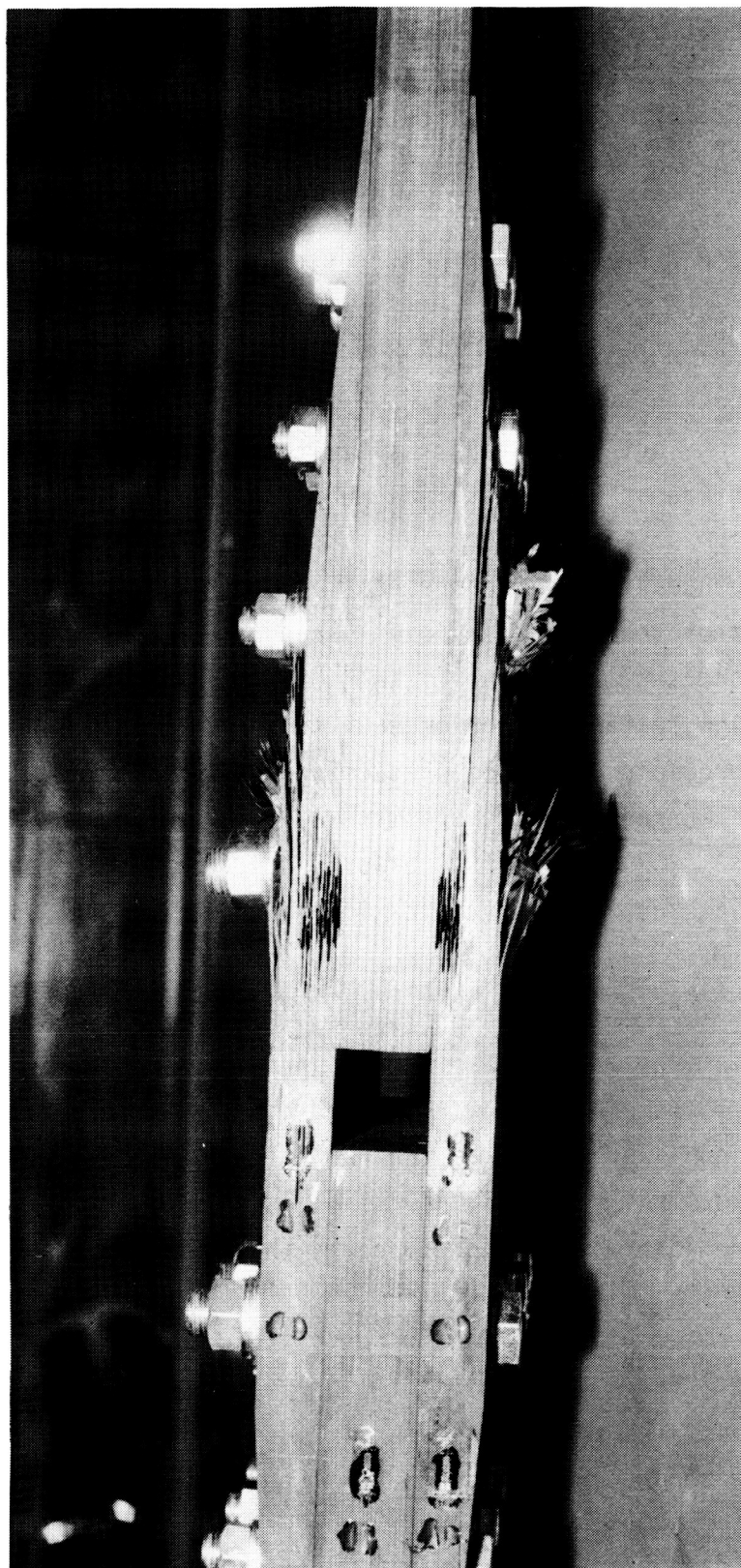


FIGURE 22. 24-BOLT TENSION SPECIMEN - JT24IF-509

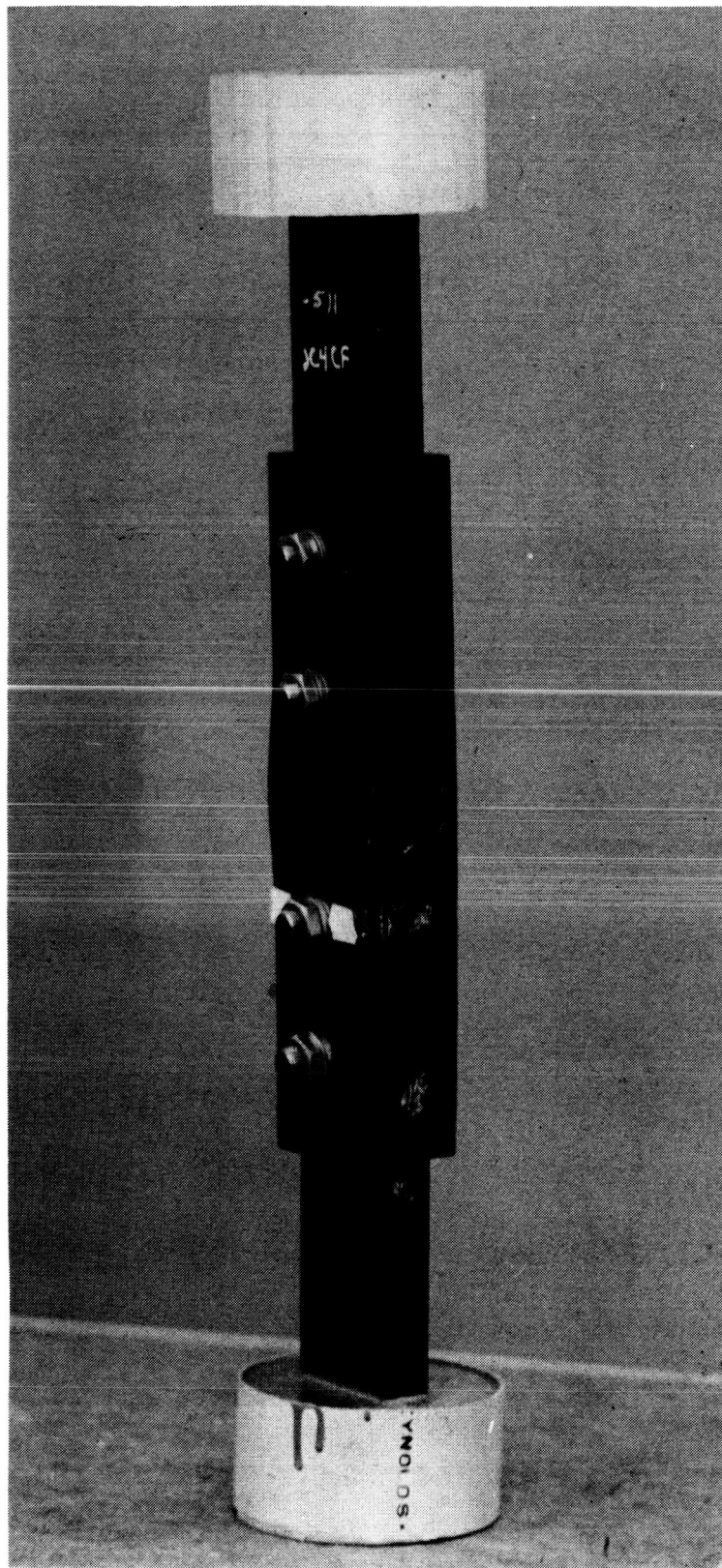


FIGURE 23 (a). 4-BOLT COMPRESSION SPECIMEN - JC4CF-511

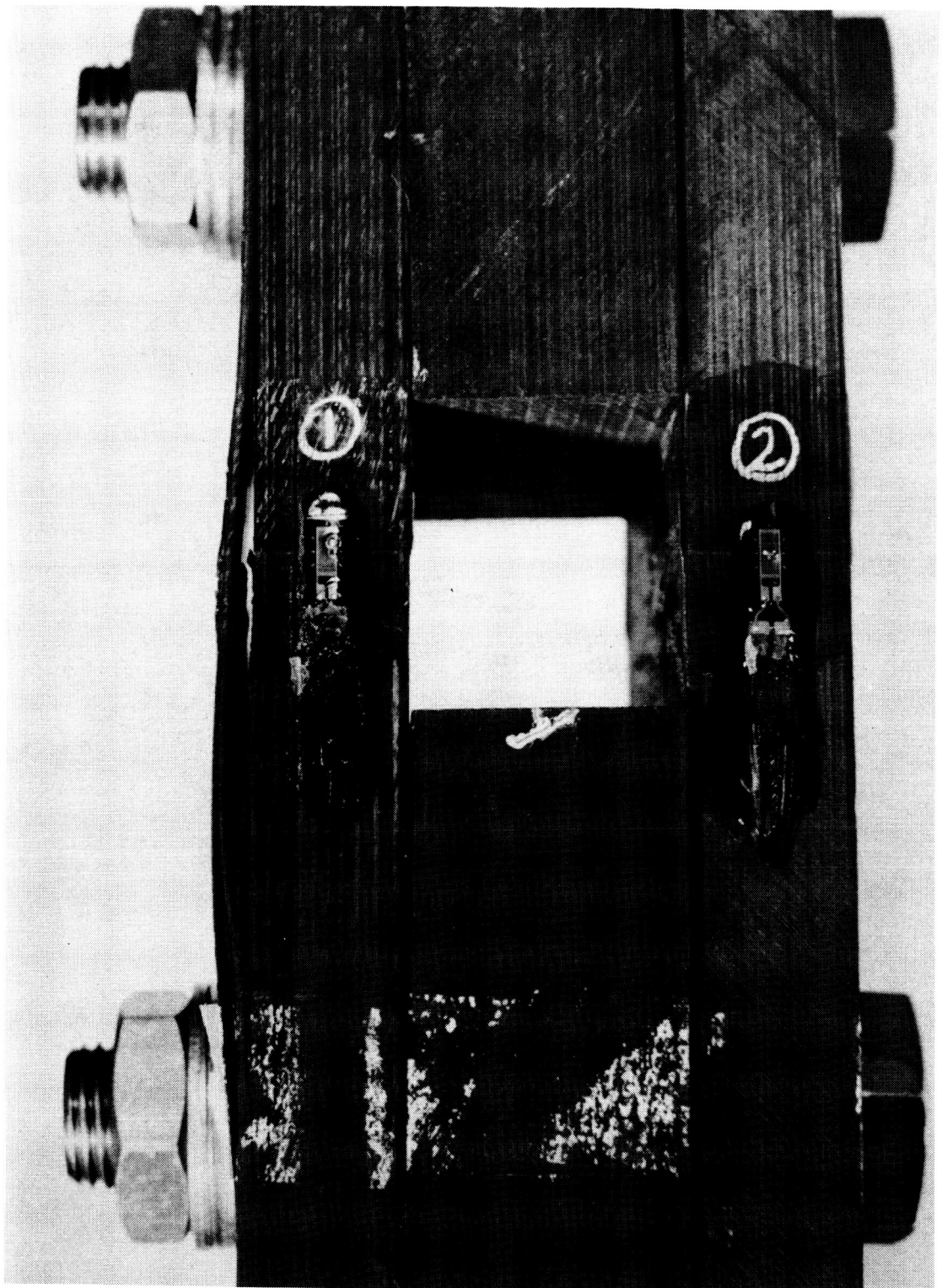


FIGURE 23 (b). 4-BOLT COMPRESSION SPECIMEN - JC4CF-511 (Continued)

The failed JC4IF (interference fit) specimen shown in Figure 24 failed at an even lower gross stress of -32,650 psi. The failure occurred when one splice plate began to delaminate immediately inside one of the interior bolt rows. Although a catastrophic failure had not yet occurred, the specimen was not able to withstand an increase in load and the test was stopped. (Note that had the tests been run with load control rather than stroke control, the failure would most likely have been instantaneous.) Appendix A contains strain readings and load-deflection curves for these tests.

3.2.2.2 8-Bolt Compression Tests

One clearance fit and one interference fit specimen were tested in the 8-bolt tapered joint configuration. The failed JC8CF specimen shown in Figure 25 reached a gross stress of -41,930 psi with a gross-section strain of -.0048. The observed failure was by compressive delamination of the splice plates at the innermost bolts, initiated immediately in front of the bolts, where the bearing and bypass loads combine. A significant amount of nonlinear behavior (bolt bending and bearing deformation) had taken place prior to failure. This failure mode is not surprising since the central skin member should have much higher compression allowables than the splice plates because of the clamp-up support the splices provide. In fact, this type of failure was prevalent throughout the compression tests series.

The JC8IF specimen in Figure 26 (a) did not perform as well as expected. The failure occurred when one splice plate delaminated at about mid-thickness in the central gross-section away from the bolt holes. Whether or not a flaw existed prior to the test is unknown, but the failure mode shown in Figure 26 (b) does not appear related to the presence of a joint. The failure strain for this joint was 0.0041, substantially lower than its clearance fit counterpart. Specific test data is contained in Appendix A.

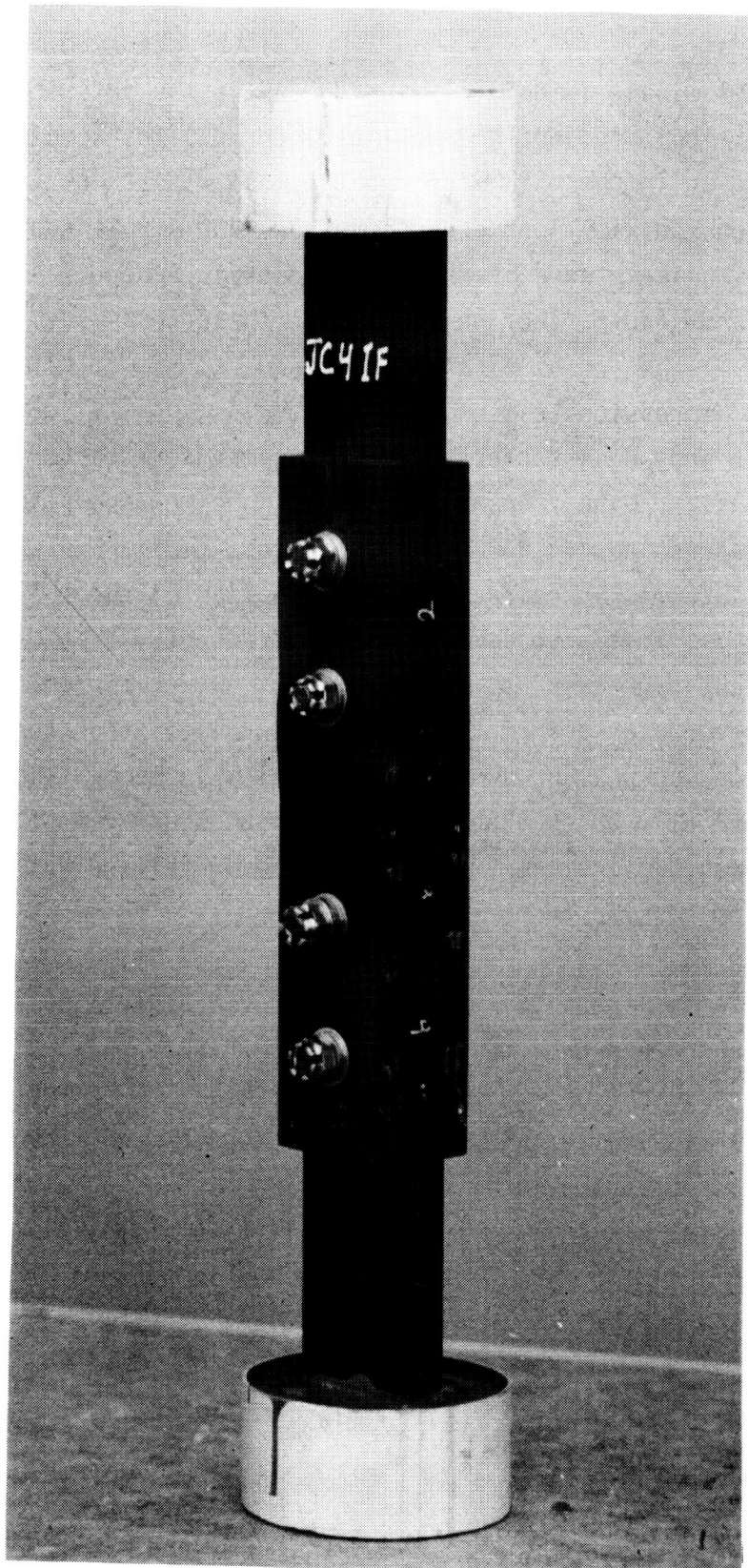


FIGURE 24 (a). 4-BOLT COMPRESSION SPECIMEN - JC4IF-507

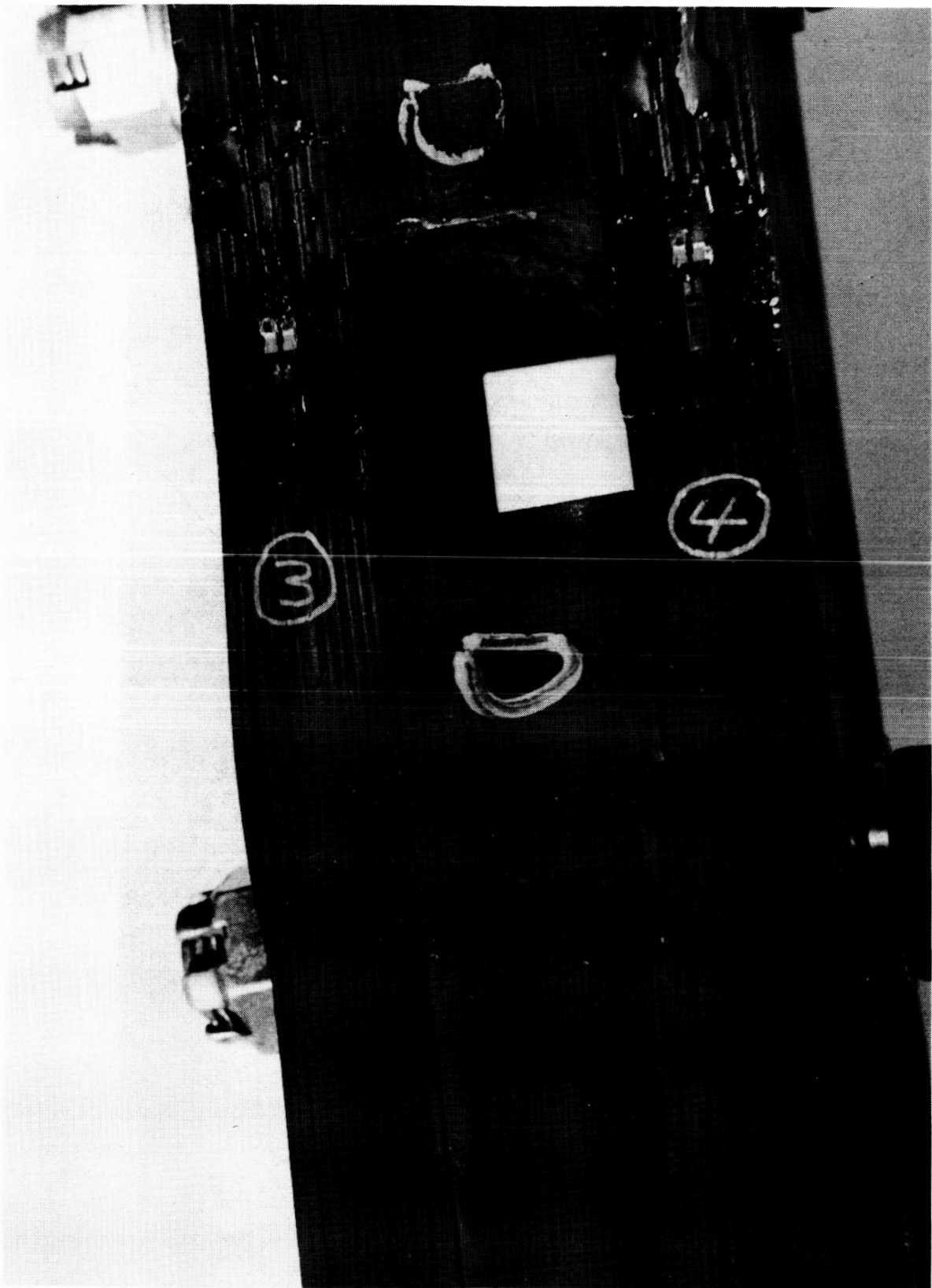


FIGURE 24 (b). 4-BOLT COMPRESSION SPECIMEN - JC4IF-507 (Continued)

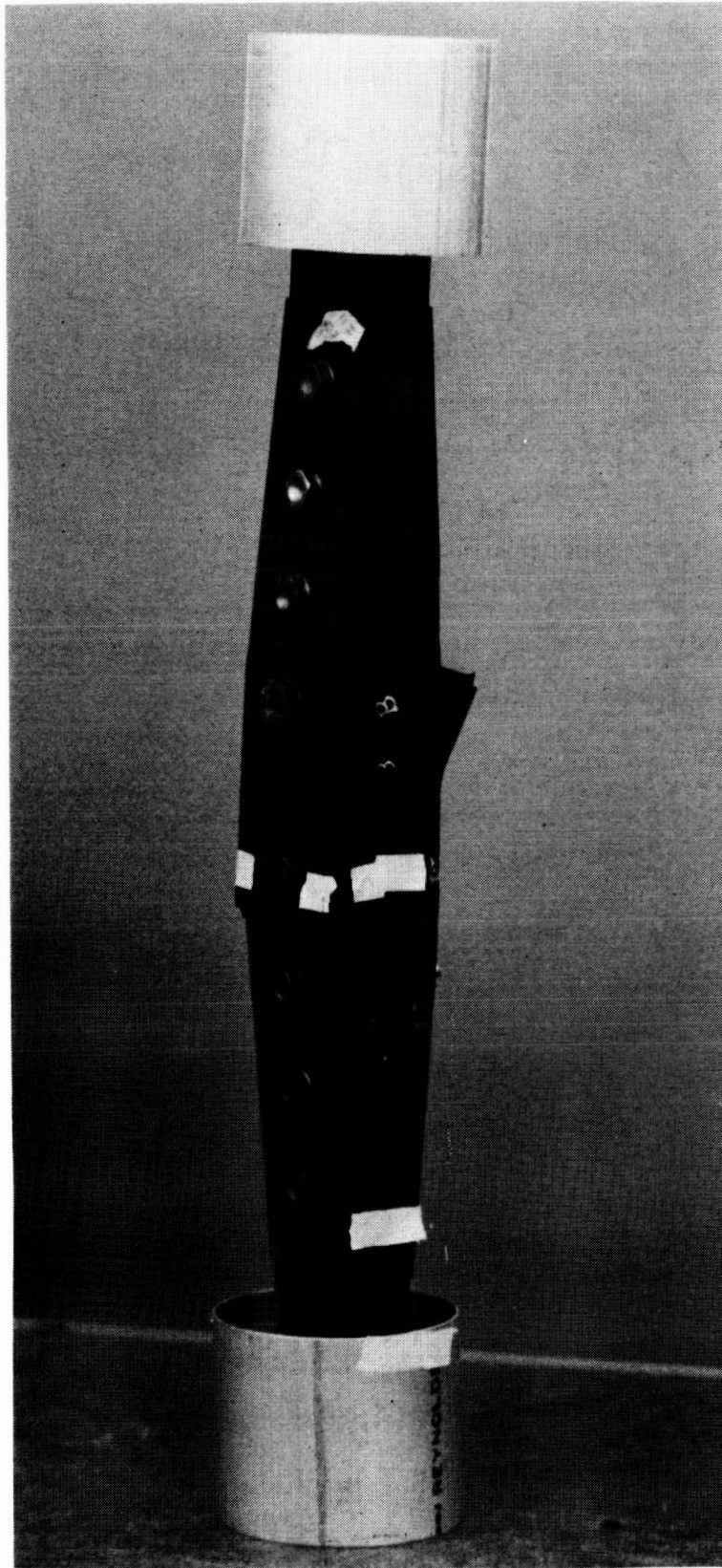


FIGURE 25. 8-BOLT COMPRESSION SPECIMEN - JC8CF-513

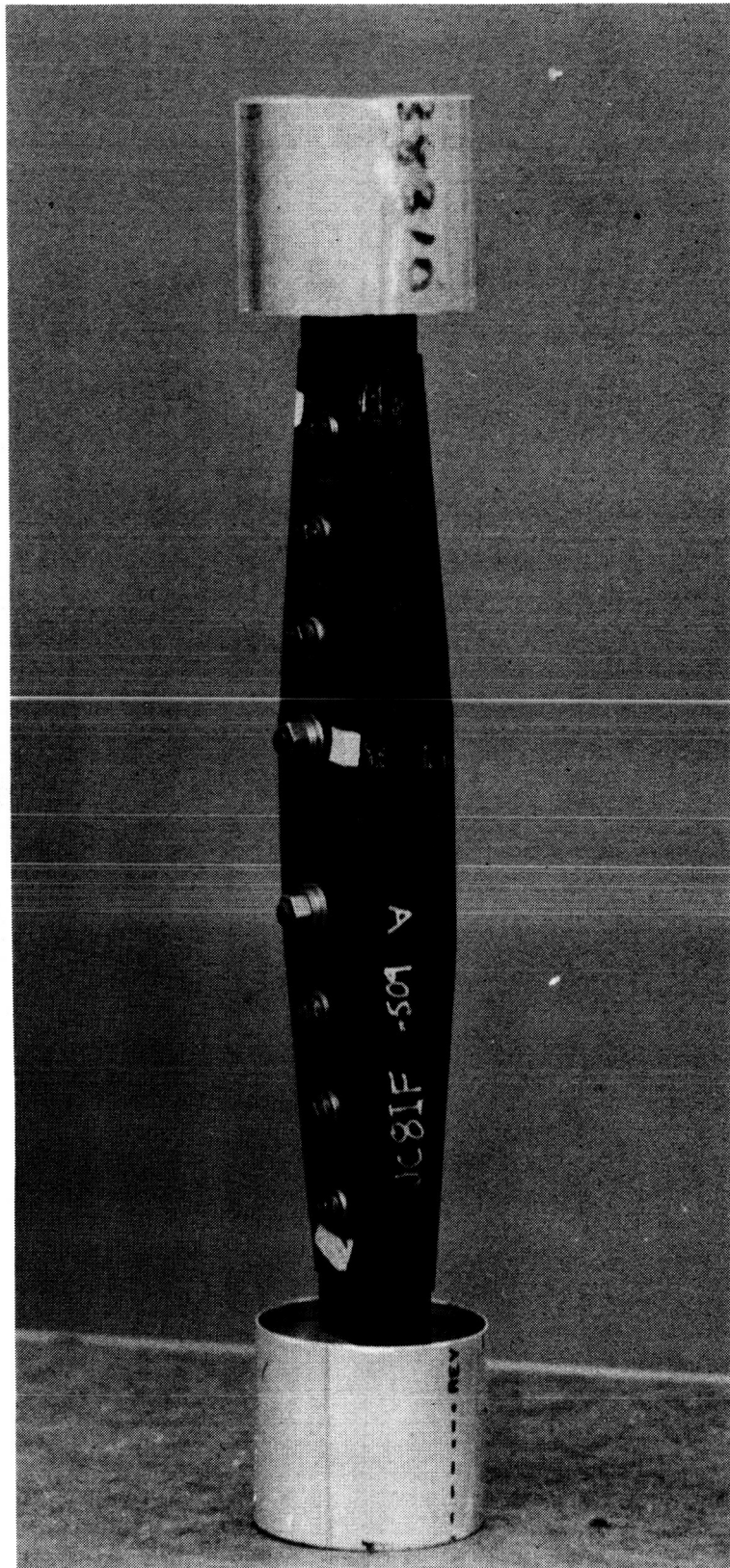


FIGURE 26 (a). 8-BOLT COMPRESSION SPECIMEN - JC8IF-509

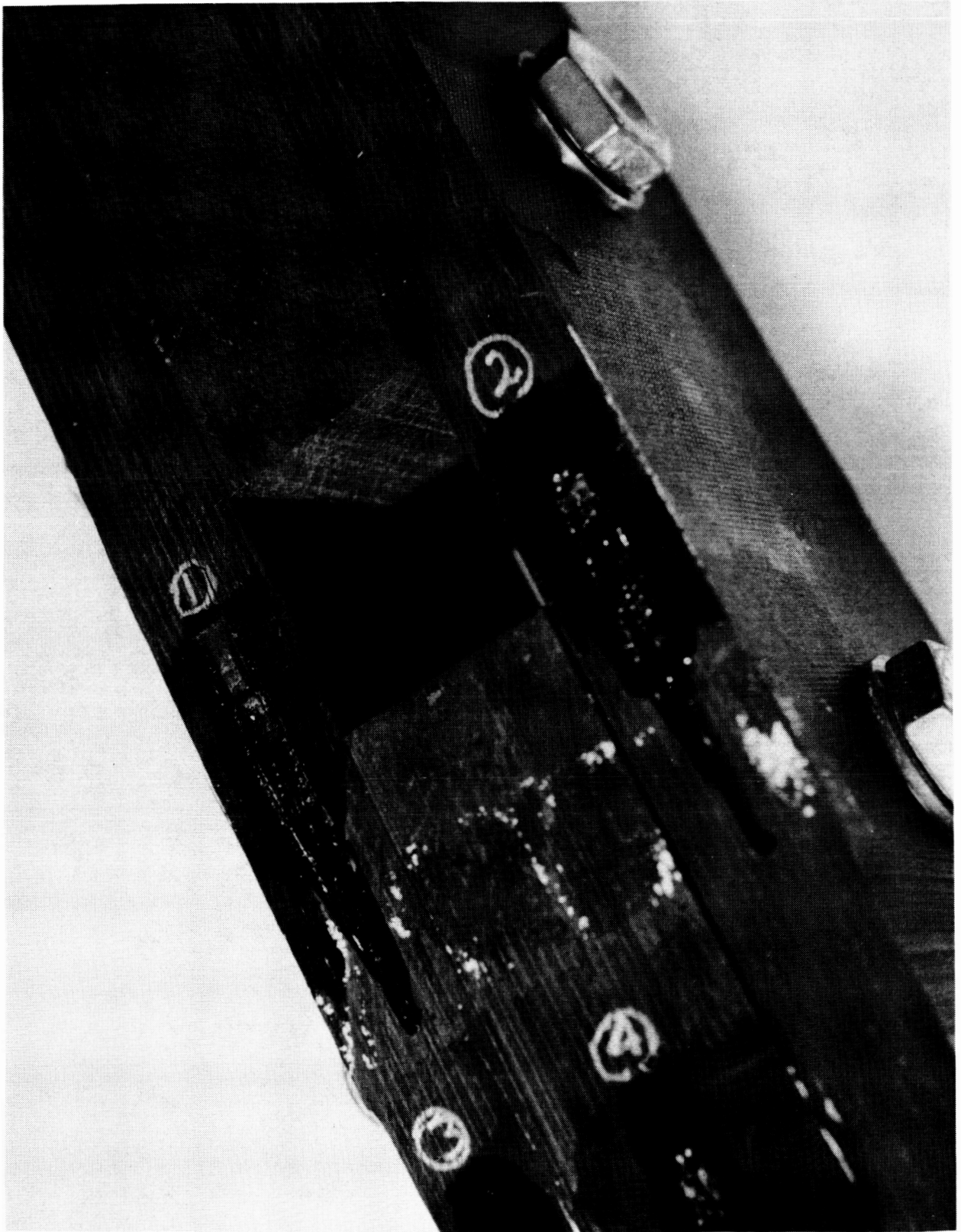


FIGURE 26 (b). 8-BOLT COMPRESSION SPECIMEN - JC8IF-509 (Continued)

It should be noted that the JC8CF ultimate load of 75,000 pounds exceeds that of identical joints tested for tensile loads. This trend was typical throughout the test program, although the premature splice plate failures under tensile load prevents a true comparison between joints with tapered splices.

3.2.2.3 12-Bolt Compression Tests

The 12-bolt clearance fit and interference fit compression specimens reached gross-section strains of -0.0036 and -0.0032, respectively. The mode of failure was the same for both tests as shown in Figures 27 and 28, the damage looking much the same as that of the JC8CF specimen. The failures occurred in the splice members on the bearing load side of the inner row of bolts with massive delamination and buckling of plies, commonly associated with laminate compression failures. The damage was located not actually across the net-section, but in most cases just inside the inner bolt rows. The central skin members remained essentially intact. Some bolt bending did take place in both specimens, more so in the interference fit joint which at this point was expected. The more severe bolt bending of the JC12IF joint is believed to have triggered the earlier failure of that specimen. A more detailed discussion on the cause of these failures is contained in the test/analysis correlation section, and strain gage data from the tests is given in Appendix A.

3.2.2.4 24-Bolt Compression Tests

The two 24-bolt specimens closely followed the behavior of the 12-bolt joints as the same compression failure mode persisted. The JT24CF specimen shown in Figure 29 (a) failed at a gross stress of -49,500 psi and gross-section strain of -0.0062. Figure 29 (b) presents a close-up photograph of the damaged area, clearly showing the compression failure occurring across the splice members immediately inside the last row of bolts. A similar failure occurred in the JT24IF specimen as shown in Figure 30 at a gross stress of -50,330 psi. It is believed that this type of failure will be typical of composite multirow bolted joints loaded in compression and efforts to improve performance should be made in consideration of this phenomenon.

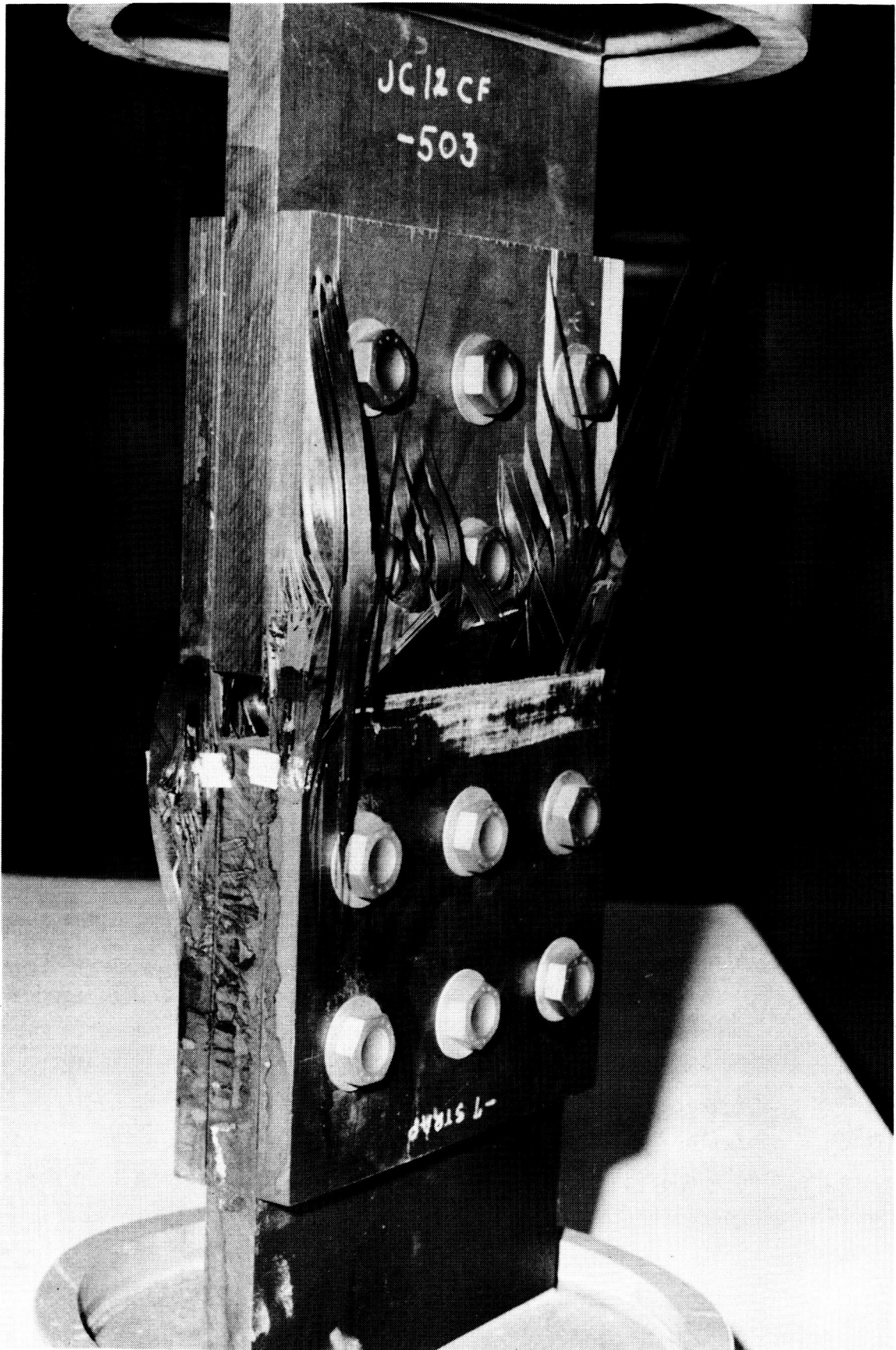


FIGURE 27. 12-BOLT COMPRESSION SPECIMEN - JC12CF-503

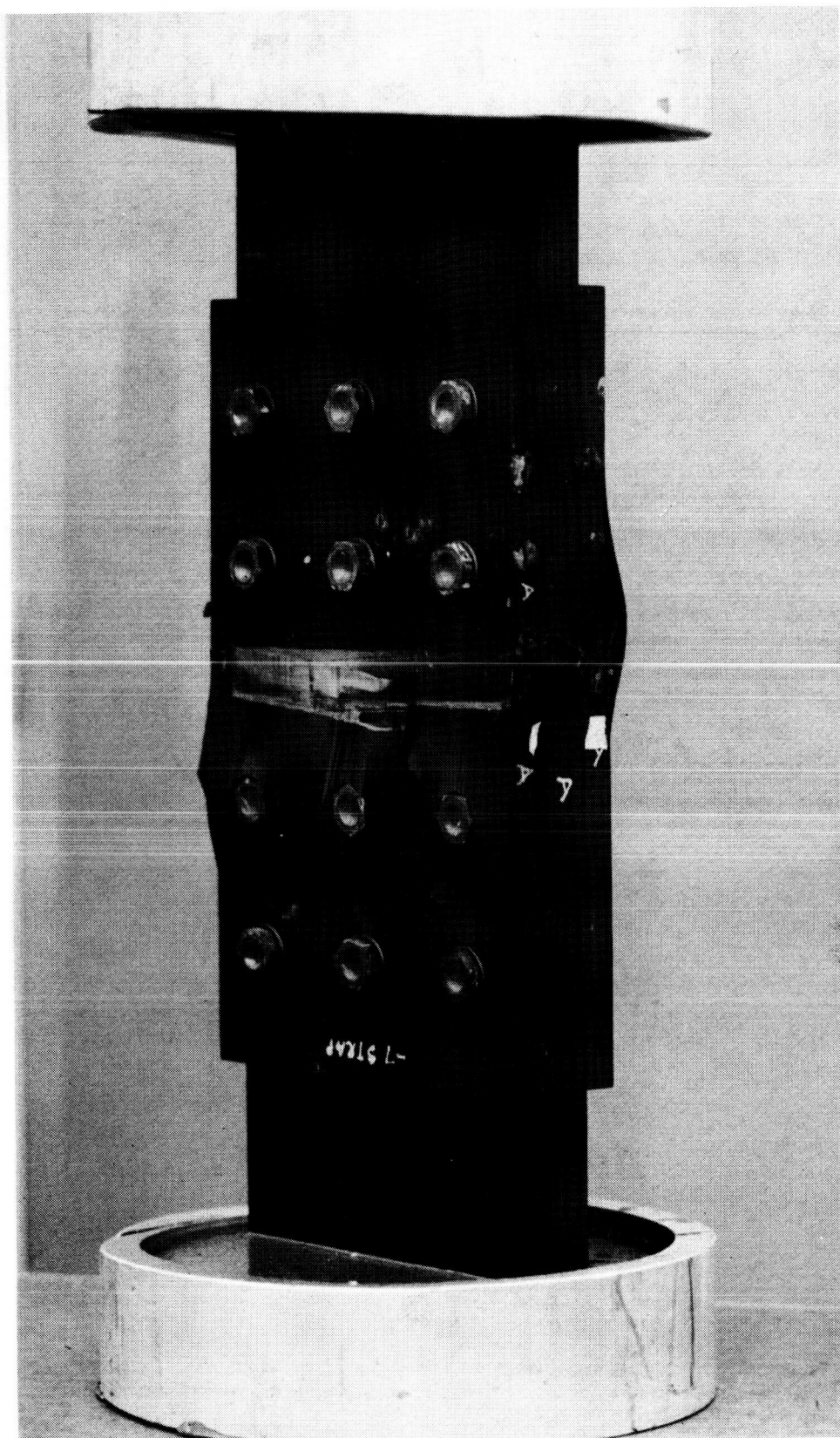


FIGURE 28. 12-BOLT COMPRESSION SPECIMEN - JC12IF-505

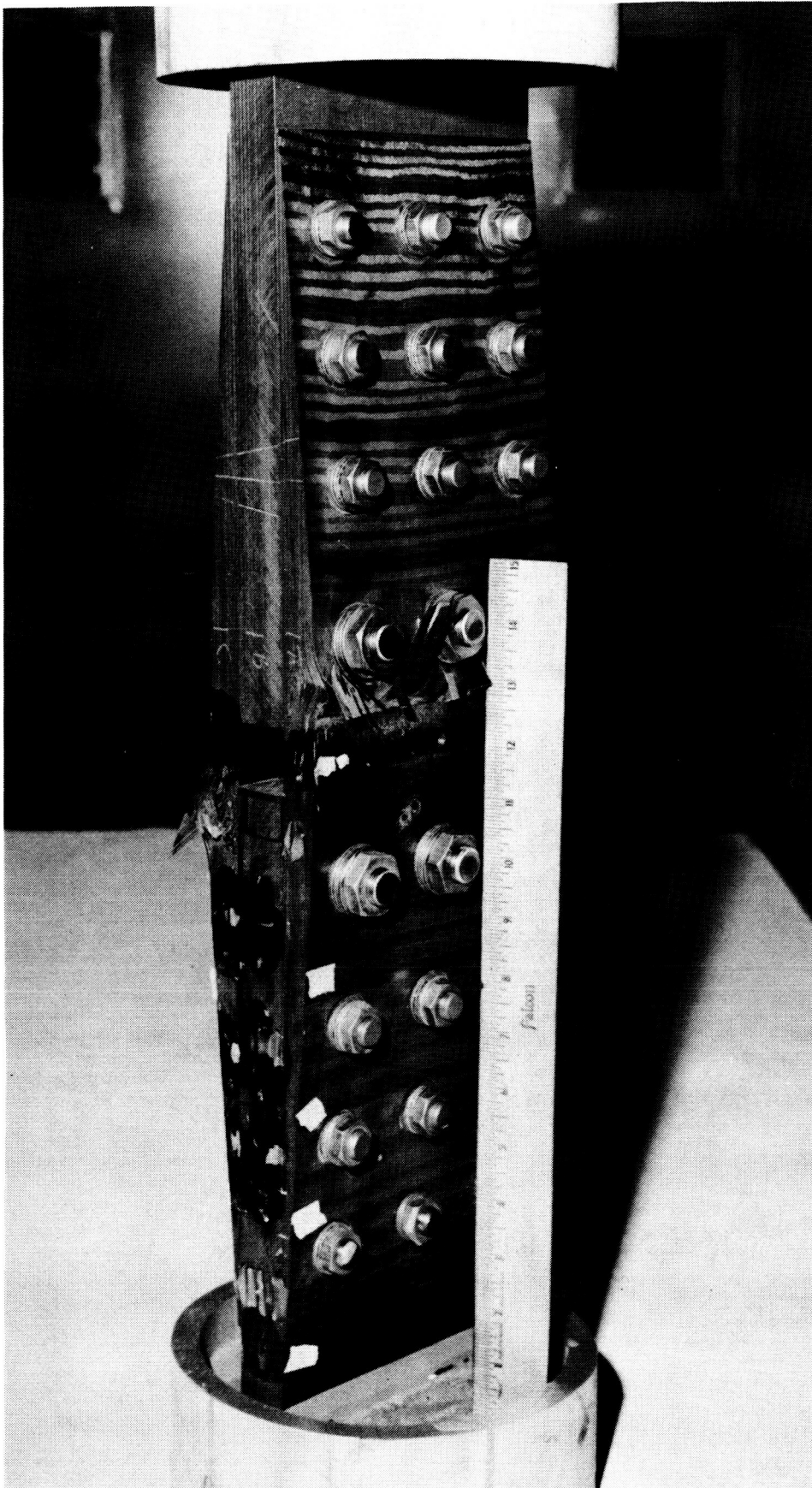


FIGURE 29 (a). 24-BOLT COMPRESSION SPECIMEN - JC24CF-511

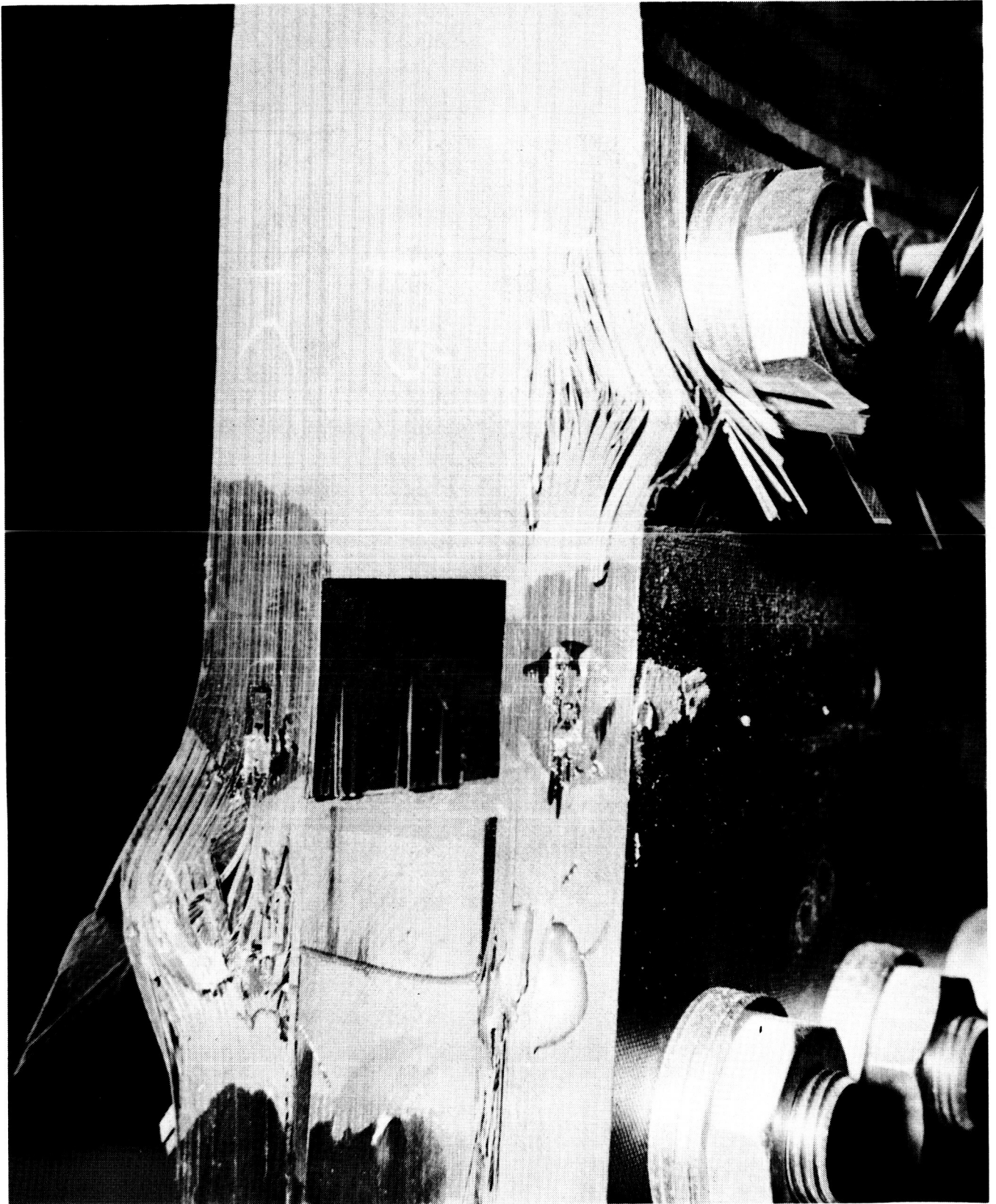


FIGURE 29 (b). 24-BOLT COMPRESSION SPECIMEN - JC24CF-511 (Continued)

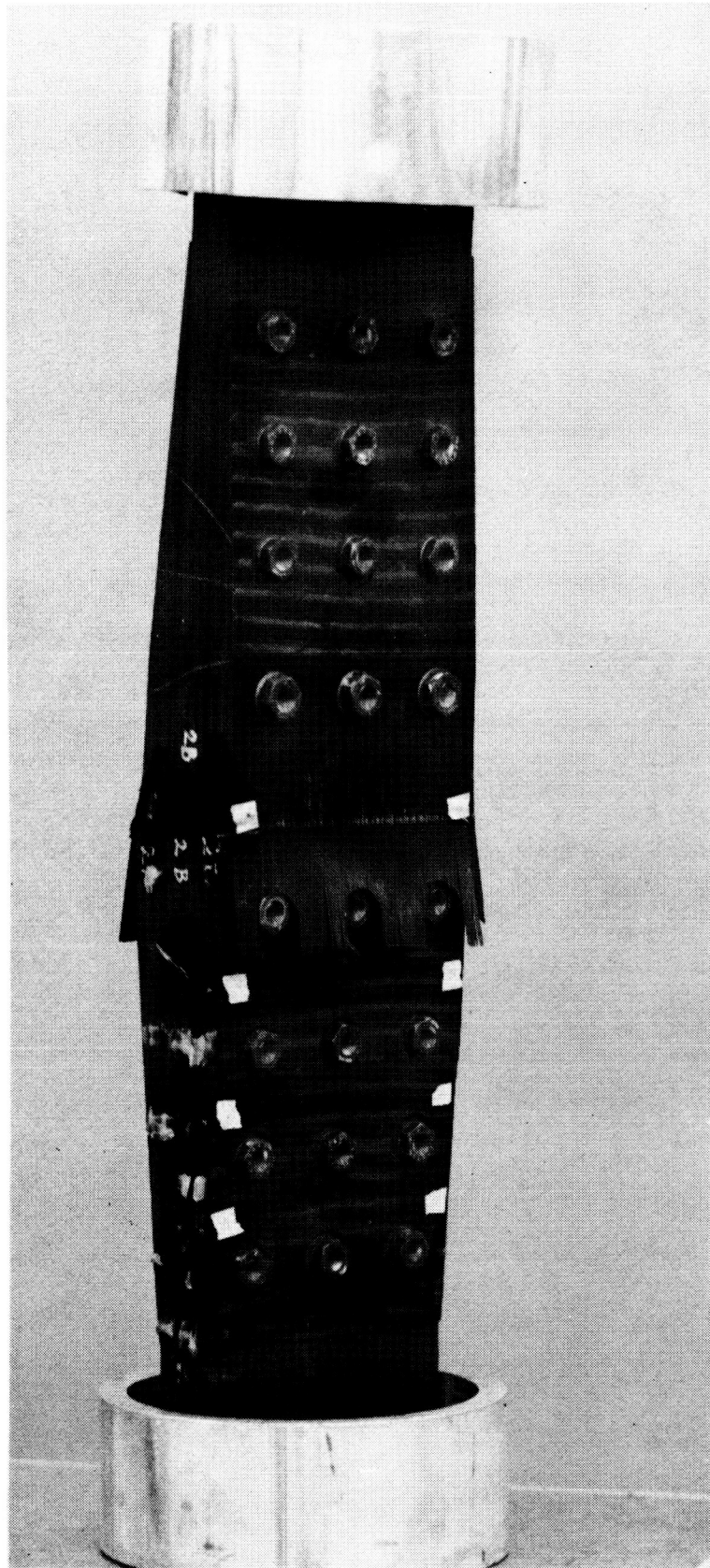


FIGURE 30. 24-BOLT COMPRESSION SPECIMEN - JC24IF-513

These compression joints were loaded to levels above the tested and predicted strengths of the identical tension specimens, and the same holds true for the 12-bolt joints. A direct comparison is deceptive, however, because the critical location for tension loading is theoretically the central skin member while in compression the splice members are critical. Strain gage readings for these two tests are presented in Appendix A.

3.2.3 Hole Wearout Tests

A total of three specimens (ZJ011263) were fabricated and tested to measure the effects of fatigue loading on hole wearout. The results of these tests are presented in Table 6. The first two tests were completed with no significant hole elongation. Specimen Number 1 was tested through two life-times with a peak hole bearing stress of 53,200 psi which represented 80 percent of limit load. Having completed the test with virtually no damage to the first specimen, the peak stress was increased for specimen Number 2 to 79,700 psi - approximately limit load - and still very little elongation took place. For specimen Number 3 the peak stress level was raised to about 107,600 psi and evidence of hole damage was noted after the third profile repetition (173,547 spectrum cycles) at which time the nominal light bolt torque of 40 inch-pounds was increased to 100 inch-pounds and loading was continued. At 365,315 cycles the computer control was unable to track the specimen and the test was concluded with a change in hole dimensions in the load direction of 0.063 and 0.034 inch for the two holes. This specimen was working to approximately 90 percent of the ultimate bearing stress allowable for peak tension loads.

The only anomaly in this test series was the hole sizes. The drawing had called for approximately 0.006 inch clearance fit holes, however, good quality close fit (2-3 mil clearance) holes were supplied. Therefore, the "pounding" effect of loose tolerance holes possible during routine manufacture was not obtained. It would be desirable in the future to test possible bearing 'fatigue strength reductions due to clustered plies and higher percent zero degree plies as well as for excessive hole clearances.

4.0 ANALYSIS METHODS DEVELOPMENT

In the first phase of the test program, 180 single-hole ancillary specimens were tested in a variety of configurations for both tensile and compressive loading

These tests examined loaded and unloaded holes, various laminate thicknesses and bolt diameters, and considered single and double shear joints. The tests were conducted to develop a sufficient data base to be used for analytically predicting the behavior of large multirow bolted joints in composites. The influence of various phenomena on the performance of composite bolted joints was examined, though several important parameters warrant future investigation, such as the effects of flush head fasteners bolted through exterior skins.

The ancillary test program generated load-deflection curves to failure, characterizing both the linear and nonlinear range of behavior. A typical load deflection curve for a composite single bolted joint ($w/d = 8$) is shown in Figure 31. This particular specimen failed in bearing and the large amount

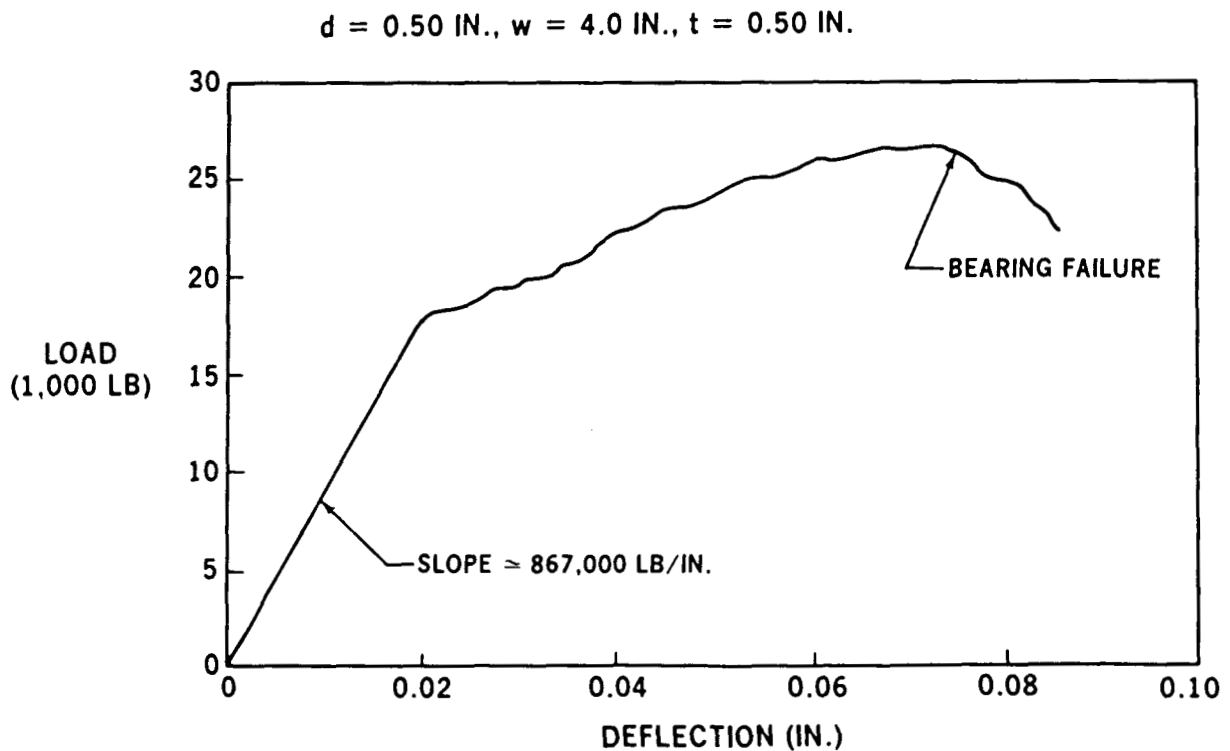


FIGURE 31. LOAD DEFLECTION CURVE, DOUBLE-SHEAR TENSION TEST (BEARING FAILURE)

of nonlinear behavior due to hole elongation was typical of this failure mode. Even the tension-through the hole failures exhibited an observable amount of nonlinear behavior. This was the result of either bearing deformation of the fastener hole (many of these specimens reached or exceeded the characteristic bearing yield stress) or plastic bending of the bolt prior to failure. An example of this load-deflection behavior for a narrow specimen ($w/d = 3$) is shown in Figure 32, where a double shear tension specimen had begun to yield in bearing before finally failing in the net-section.

$$d = 0.50 \text{ IN.}, w = 1.50 \text{ IN.}, t = 0.50 \text{ IN.}$$

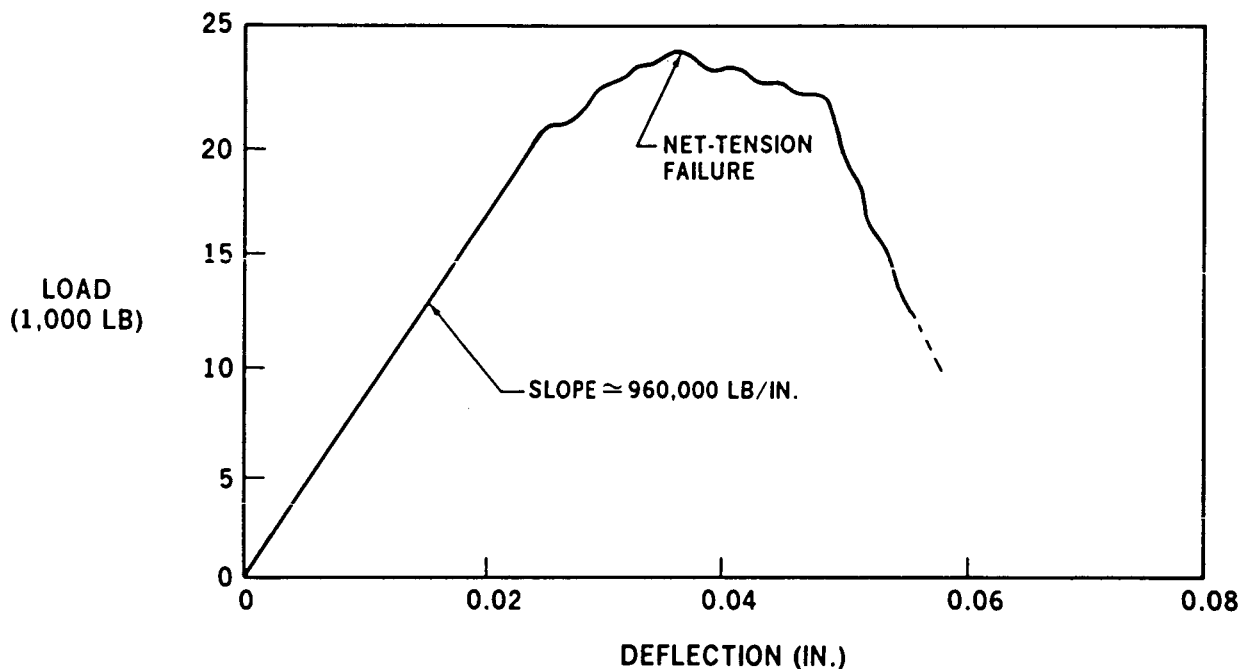


FIGURE 32. LOAD DEFLECTION CURVE, DOUBLE-SHEAR TENSION TEST (TENSILE FAILURE)

The A4EJ program uses a simple bi-linear model as shown in Figure 33 to represent the linear and nonlinear range of bolted joint load-deflection behavior. This nonlinear behavior can be significant to the performance of a multirow joint since its presence permits the most highly loaded bolts to sustain their load without failure, while other more lightly loaded bolts can accept more load due to the added deformation at those bolts that have reached the nonlinear range of behavior. Consequently, a reasonable prediction of the

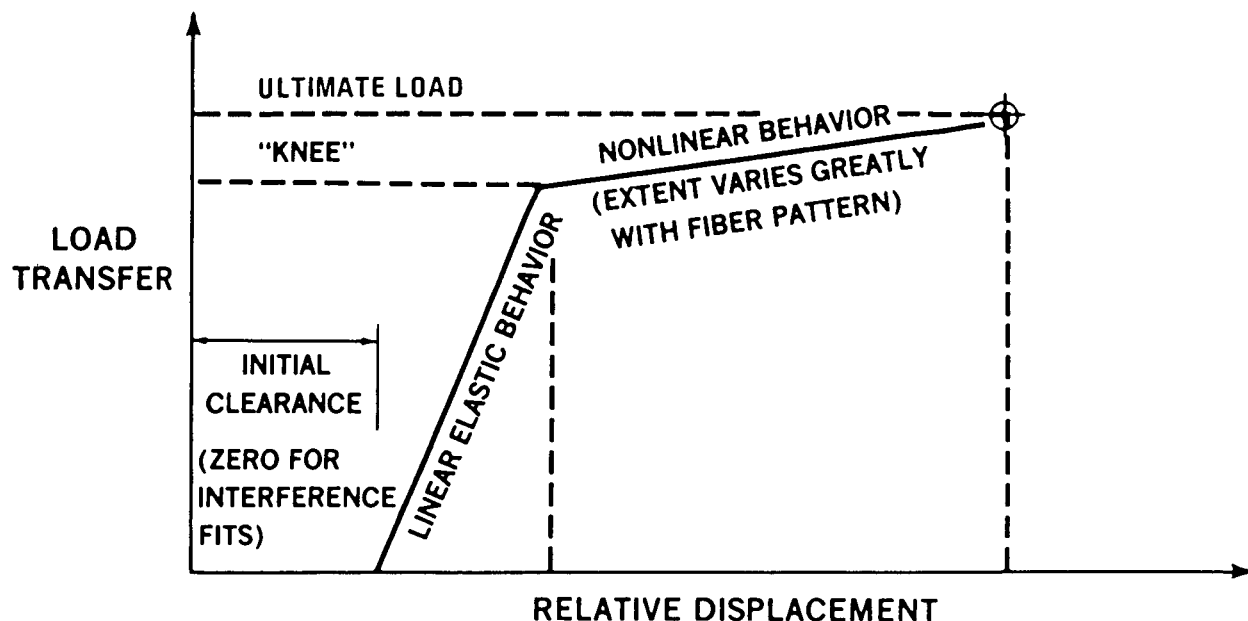


FIGURE 33. FASTENER LOAD DEFLECTION CHARACTERISTICS

onset, allowable extent, and plastic stiffness of the nonlinear range of behavior is fundamental to the accurate analytical prediction of multirow joint strengths.

Included in this investigation were efforts toward developing analytical methods for predicting basic bolted composite joint behavior, which is required to perform multirow joint solutions. It was found that the linear portions of the load-deflection curves could be represented accurately by minor modifications of an old NACA formula (Reference 3). The results from this formula are plotted against test results in Figure 34 for a variety of joint configurations in double shear. The stiffness formula is given as the sum of four components. Thus.

$$\frac{1}{K} = \frac{2\delta}{P} = C_{bs} + C_{bb} + C_{b_{br}} + C_{p_{br}}$$

Here, δ is the deflection of the bolt in inches, P is the double shear bolt load in kips, and the various contributions to the bolt constant (or flexibility) in inches per kip are C_{bs} for shear deformation of the bolt, C_{bb} for bending

deformation of the bolt, $C_{b_{br}}$ for the bearing deformation of the bolt, and $C_{p_{br}}$ for the bearing deformation of the laminates or plate. The empirical expressions deduced by Tate and Rosenfeld (Reference 3) for this expression give, for bolts loaded symmetrically in double shear,

$$\frac{1}{K} = \frac{2t_s + t_p}{3G_b A_b} + \frac{8t_s^3 + 16t_s^2 t_p + 8t_s t_p^2 + t_p^3}{192 E_{bb} I_{bb}} + \frac{2t_s + t_p}{t_s t_p E_{b_{br}}} + \frac{1}{t_s \left(\frac{E_L}{E_T} \right)_s^{.5}} + \frac{2}{t_p \left(\frac{E_L}{E_T} \right)_p^{.5}}$$

in which the first subscript b refers to the bolt and the second to bending, s refers to each of the splice straps (which are assumed to be identical), and p to the basic plate (or skin). The various thicknesses are given by t, as shown in Figure 34 and the various elastic moduli are signified by E for a Young's modulus and G for the shear modulus of the bolt, which has an area $A = d^2/4$ and section modulus $I = \pi d^4/64$ since d is the bolt diameter. The laminate moduli E_L and E_T refer to the longitudinal (or load) direction and lateral (or transverse) direction, respectively, and would be identical for quasi-isotropic laminates. These laminate moduli represent the only change from the original expression which used the moduli E_{sbr} and E_{pbr} instead.

All attempts to interpret the stiffness data for the single-shear tests in terms of existing formulas for metal joints failed. So the double-shear formula above was modified to account for the bolt rotation that occurs in single shear joints.

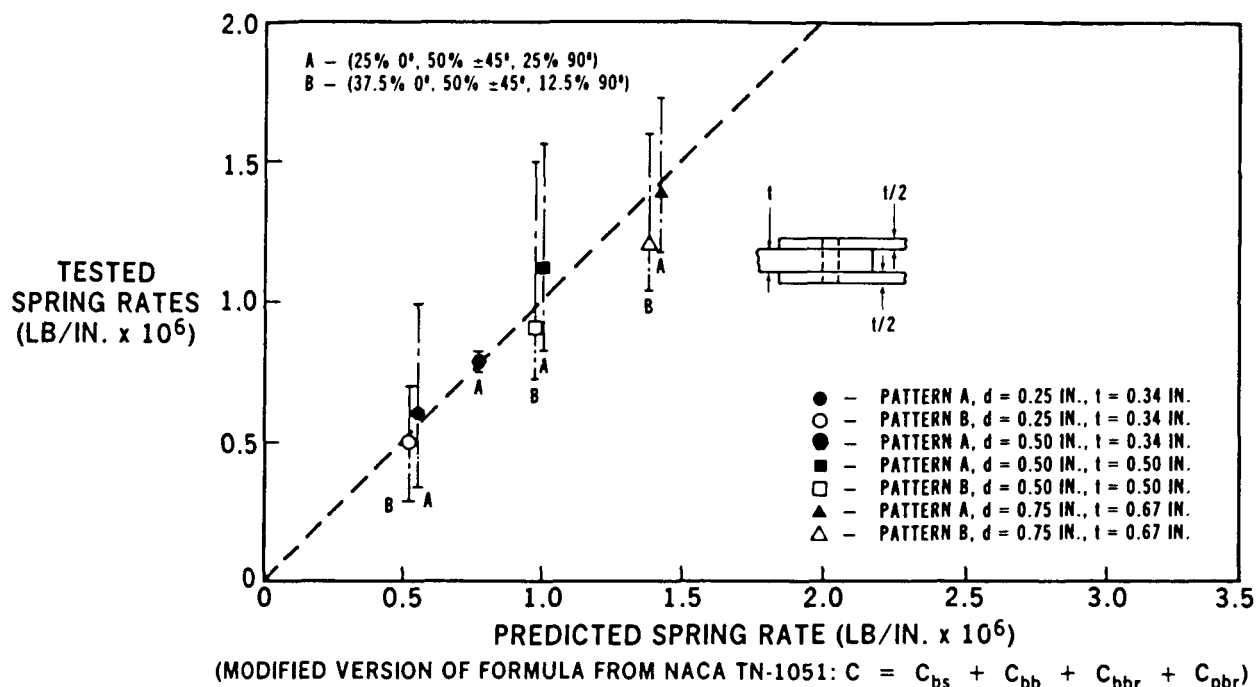
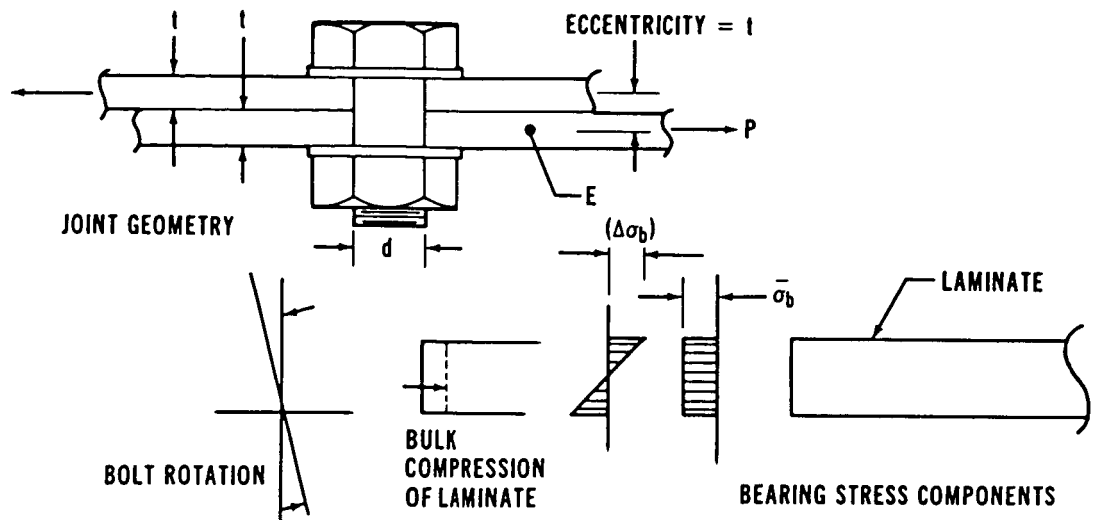


FIGURE 34. BOLTED JOINT ELASTIC SPRING RATES - TEST VERSUS PREDICTION

The first term, representing the shear deformation of the bolt, was taken to be unaltered. The second term, accounting for bolt bending, was deleted and the remaining three terms were all multiplied by the factor $(1 + 3\beta)$, where β represents the fraction of the bending moment on the bolt that is reacted by the nonuniform bearing stresses across the thickness. This is explained in Figure 35. The remaining fraction $(1 - \beta)$ is reacted by the head and nut on the bolt. Therefore, β would vary from a maximum value of 1.0 for a simple shear pin, through a value of about 0.5 for countersunk fasteners, to a small fraction for torqued bolts with protruding heads, becoming very small for the combination of large washers with a large diameter-to-thickness ratio. The interpretation of the data from these tests, with a d/t ratio of about 2 and relatively small washers, indicates that β is on the order of 0.15 here. The need for the correction factor β arises because, as the fasteners rotate under single-shear loading, the bearing stresses become more concentrated near the interface between the members than is the case with double-shear loading. Consequently, the relative motion is increased by those locally higher bearing stresses.



$$\text{BASIC MOMENT} = Pt = \bar{\sigma}_b dt^2$$

$$\text{INCREMENTAL MOMENT} = \beta pt = (\Delta\sigma_b) dt^2/3, \text{ COUNTING BOTH MEMBERS}$$

$$\text{BASIC RELATIVE DEFLECTION} = \frac{2\bar{\sigma}_b d}{E} = \frac{2P}{Et}, \text{ COUNTING BOTH MEMBERS}$$

$$\text{ADDITIONAL RELATIVE DEFLECTION AT INTERFACE} = \frac{2(\Delta\sigma_b) d}{E} = \frac{6\beta P}{Et}, \text{ COUNTING BOTH MEMBERS}$$

$$\text{RATIO OF TOTAL TO BASIC RELATIVE DEFLECTION} = (1 + 3\beta)$$

FIGURE 35. ADDITIONAL DISPLACEMENTS DUE TO BOLT ROTATION

The joint flexibility in single shear is thus expressed by the relation

$$\frac{1}{K} = \frac{\delta}{P} = \frac{2(t_1+t_2)}{3G_b A_b} + \left[\frac{2(t_1+t_2)}{t_1 t_2 E_{bbr}} + \frac{1}{t_1 \left(\frac{1}{E_L E_T} \right)_1^5} + \frac{1}{t_2 \left(\frac{1}{E_L E_T} \right)_2^5} \right] (1+3\beta).$$

in which the subscripts 1 and 2 identify the two members. Figure 36 compares the stiffness predictions of this formula with the measured results. Had the term not been included the stiffness would have been overestimated by about 50 percent.

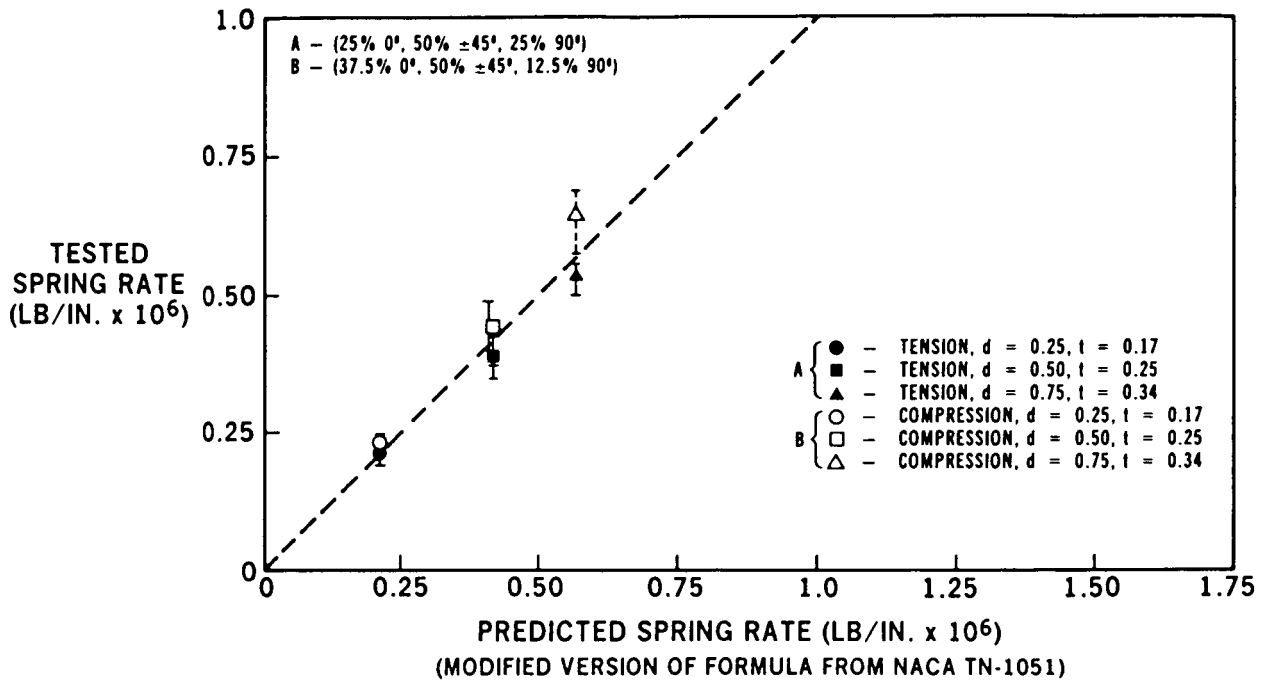


FIGURE 36. SINGLE-SHEAR BOLTED JOINT ELASTIC SPRING RATES - TEST VERSUS PREDICTION

No universal formulas have been derived to express the nonlinear portions of the load-deflection curves. No attempts were made at this because of the great variation between tested nonlinear stiffnesses. This variation is attributed to the nature of the nonlinear behavior, which invariably consists of bearing deformation or bolt bending.

Nevertheless, many analyses have confirmed that two simple rules cover most practical joint geometries. The first is that there is no significant non-linear behavior for unloaded bolt holes, as was shown by our ancillary tests. The other is that the knee in Figure 33 can be located at about 80 percent of the ultimate failing stress in bearing. The secondary stiffness can be taken to be approximately 20 percent of the elastic stiffness. The validity of these approximations can be gaged from the ancillary test data. When there is significant nonlinear behavior, particularly in the larger w/d values, the relative motion between the members is so great as to be unacceptable for

design purposes, so it is useful to then add a displacement cutoff, perhaps as some percentage of the fastener diameter, much as for bolted joints in metal alloys.

The nonlinear portions of the load deflection characteristics influence the load-sharing in a multirow bolted joint only after some plastic deformation has occurred at one or more fastener locations, so the precision needed for that part of the analysis is less than for the linear analysis. However, it is important to represent the end of the linear elastic behavior accurately and to distinguish between the "brittle" or "ductile" behavior which may follow. Those effects are the key to any possible load distribution. The actual predictions of the test results for the multirow bolted joints were based on the stiffness formulas for the elastic behavior, with the definition of the nonlinear behavior taken from the actual load deflection curves from the appropriate single-hole tests because there was often considerable deformation prior to failure.

In addition to generating stiffness data, the ancillary test program provided the data for generalizing the measured section strengths at the bolt holes. Joint geometries were selected carefully to establish both net-section strengths and bearing failures, under both tensile and compressive loads. The tension-through-the-hole failure data were acquired with a width-to-diameter ratio of 3.0 for loaded holes and 2.0 and 8.0 for unloaded holes.

The individual section strengths for multirow analyses may be taken directly from the test data, or the observed stress concentration factors at failure may be related to the elastic isotropic stress concentration factors as in Figure 37 for a given joint geometry. Such an elastic factor is determined for loaded bolt holes (Reference 4) by the equation

$$k_{te} = 2 + \left(\frac{w}{d} - 1\right) - 1.5 \frac{(w/d - 1)}{(w/d + 1)} \theta$$

where

$$\begin{aligned} \theta &= 1.5 - 0.5/(e/w) \text{ for } e/w > 1 \\ \theta &= 1.0 \text{ for } e/w = 1 \end{aligned}$$

The stress concentration factor is evaluated with respect to the net rather than gross section in order to avoid factors which diverge toward infinity at extreme ratios of d/w .

As in prior test programs, the single-hole tests demonstrated considerable stress concentration relief (relative to elastic behavior) prior to failure in the fibrous composites. The linear relation

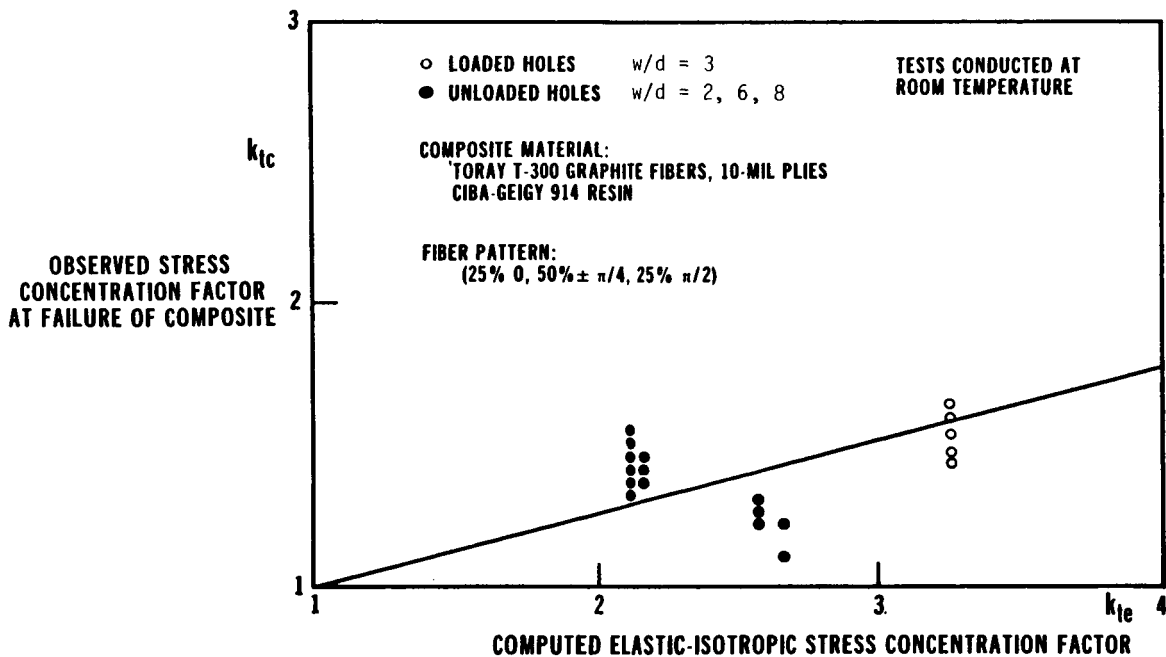
$$(k_{tc} - 1) = C (k_{te} - 1)$$

is used to postulate a linear relationship between the elastic isotropic stress concentration factors and those observed at failure for composite materials. The observed stress concentration factor (k_{tc}) at failure is given by

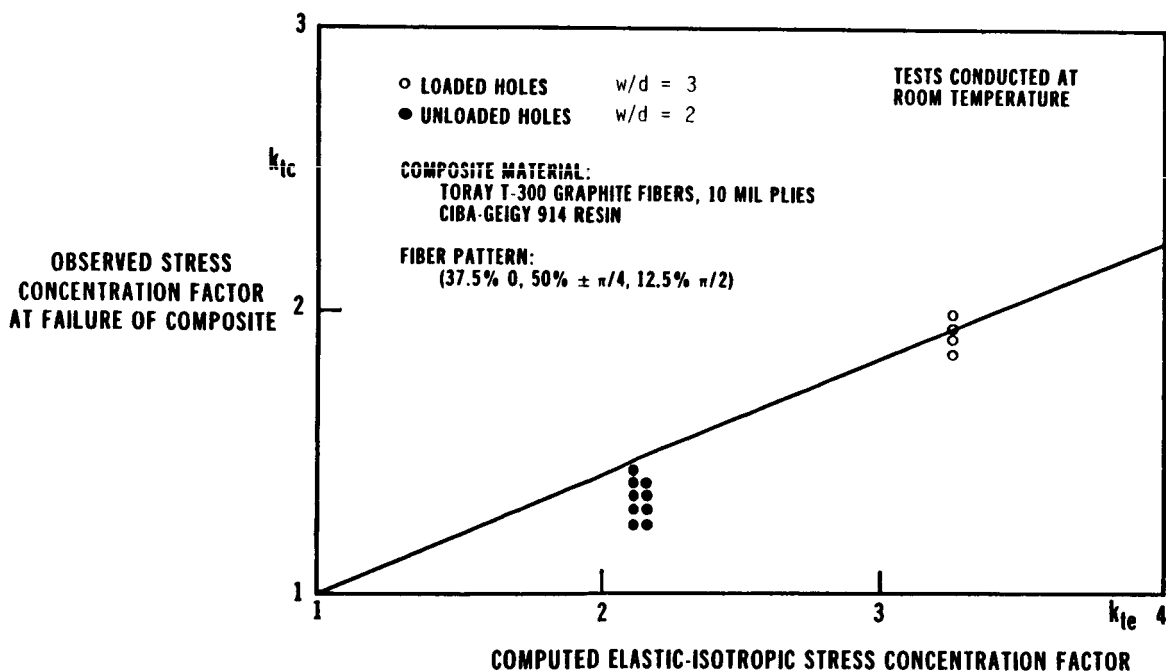
$$k_{tc} = F_{tu} t(w-d)/P_{ult}$$

This relationship may then be used to predict the single-hole section strengths of a given composite joint, based upon the corresponding elastic isotropic stress concentration factor for the same geometry.

The values of C so deduced for loaded hole net-tension failures are 0.26 for the quasi-isotropic Pattern A and 0.42 for the orthotropic Pattern B. These are almost precise matches with Hart-Smith's measurements for graphite-epoxy composites (Reference 1), which adds considerable confidence in the use of this approach to generalize test results. Unfortunately, several of the test coupons failed in the doublers at the load introduction holes instead of the test area. Therefore, it was not possible to characterize the influence of the bolt diameter on the coefficient C , which is anticipated to increase with bolt size. The reason for selecting a w/d ratio of 3 for the loaded holes is that this value had been identified in prior tests as the geometry associated with the maximum strength of single-row bolted joints in graphite-epoxy composites. A value of 8 for the bearing tests was selected to ensure that there would be no interaction with the tension-through-the-hole failure mode. The edge distances, e , were made equal to the strip widths, w , to preclude shear-out failures.



Fiber Pattern A



Fiber Pattern B

FIGURE 37. STRESS CONCENTRATION FACTORS AT FAILURE FOR COMPOSITE BOLTED JOINTS

The w/d ratios of 2 and 8 for the unloaded holes were selected with the intent of maximizing the range of values of elastic stress concentration factors, k_{te} . However, the narrow strips failed prematurely, in quite a different failure mode, with a clean tensile fracture rather than the massive delaminations associated with the wider strips. It is recommended that, henceforth, the minimum w/d ratio for unloaded holes be at least 3. Actually, since the bypass strength is needed primarily for multirow joints, for which the optimum w/d is in the range of 4 to 5 rather than the closer pitch of 3 for single-row joints, a case can be made for an even higher minimum w/d ratio. The unloaded hole results included in Figure 37 clearly show the different behavior for the narrow strips, in the form of abnormally high stress concentration factors k_{tc} . Some wider specimens of Pattern A were necked down slightly to a w/d of 6 in order to prevent failures in the grip area. The results indicate that the notched strength ratio between patterns is about the same as the relative number of 0-degree plies in each laminate.

The elastic isotropic stress concentration factor for a strip with an unloaded hole is given (Reference 4) by the equation

$$k_{te} = 2 + (1 - d/w)^3$$

This elastic factor may be related in some way the observed stress concentration factors for composite laminates with unloaded holes. However, the results of the unloaded hole tension tests suggest that the simple linear relationship between k_{te} and k_{tc} values of Figure 37 may be inadequate for predicting unloaded hole strengths. Variations in hole size, laminate thickness, and possibly ply thickness appear to have a significant effect on the precise failure mode and ultimate strength of laminates with holes. A larger matrix of tests in this area is required to reach a full understanding of the phenomena involved and the significance of each one.

The unloaded hole test results for compression were quite similar to the geometrically equivalent specimens loaded in tension. Such similarities were also evident in the loaded-hole tests

The gross-section

failure stresses were on the order of 30 ksi for both patterns, with $w/d = 3$, while the ultimate bearing stresses were on the order of 100 ksi for both patterns for the wider strips ($w/d = 8$).

The great majority of the single-shear tests failed in bearing, at a stress of about 100 ksi, for both tensile and compressive loading. The w/d ratio of 8 was used throughout the single-shear tests. A special test fixture allowed the bolts to rotate, as they would on a wing spar, for example, but prevented the abnormal rotation of the laminates which would have occurred in a standard single-lap test coupon.

The basic unnotched laminate properties, used as a reference to establish the stress concentration factors k_{tc} , were measured as follows:

Pattern A: $E = 7.4 \times 10^6$ psi, $F_{tu} = 68,350$ psi, $F_{cu} = 69,100$ psi

Pattern B: $E = 9.3 \times 10^6$ psi, $F_{tu} = 94,830$ psi, $F_{cu} = 97,300$ psi

The stiffness and section strength data discussed here provides the required empirical base from which A4EJ analyses may be performed. Although some of the ancillary data is directly applicable to the analysis, some inherent inconsistencies between test coupons and real structure should be considered. The possible effects of these dissimilarities will be discussed in subsequent sections on multirow joint analysis.

5.0 ANALYSIS OF MULTIROW BOLTED JOINTS

Having completed the ancillary testing which generated the single-hole data, an explanation is now presented of how the analysis of large multirow joints is performed. Several methods were evaluated, but the key to the analysis used here is the nonlinear computer program A4EJ (Reference 2). This program can predict the load-sharing between fasteners both at the limit of elastic (linear) behavior and after the load redistribution associated with any non-catastrophic initial damage.

The A4EJ program is an iterative Fortran IV digital solution for the load-sharing between multiple parallel springs (the fasteners) and also accounts for the linear or nonlinear stretching of the members between the fasteners as sets of springs in series. Thus, both equilibrium of forces and the compatibility of displacements are ensured.

Figure 38 describes the elements of the mathematical model. At each station, it is necessary to define the load deflection characteristics of the fastener, including the local deformation of the members, as shown in Figure 39. For the members, the elastic behavior of each member between adjacent stations must be defined. A station is located at each fastener and at each discontinuity in either member. A tapered splice plate is represented elastically as a series of steps, with a precise match of properties at each fastener station.

Strength cutoffs are also needed for the fasteners in shear and for the members under combined bearing and bypass loads at each fastener station. The total load in a member, at each station, is the sum of the bearing load at that particular fastener and the bypass load which is reacted at other fasteners. These terms are explained in Figure 40, which also characterizes the bearing-bypass interactions for both tensile and compressive loads. The program could easily be modified to express the load-sharing under in-plane shear, as with torsion loads on a wing, but the failure criteria under those bearing-bypass interactions have yet to be established. The bearing bypass interactions for

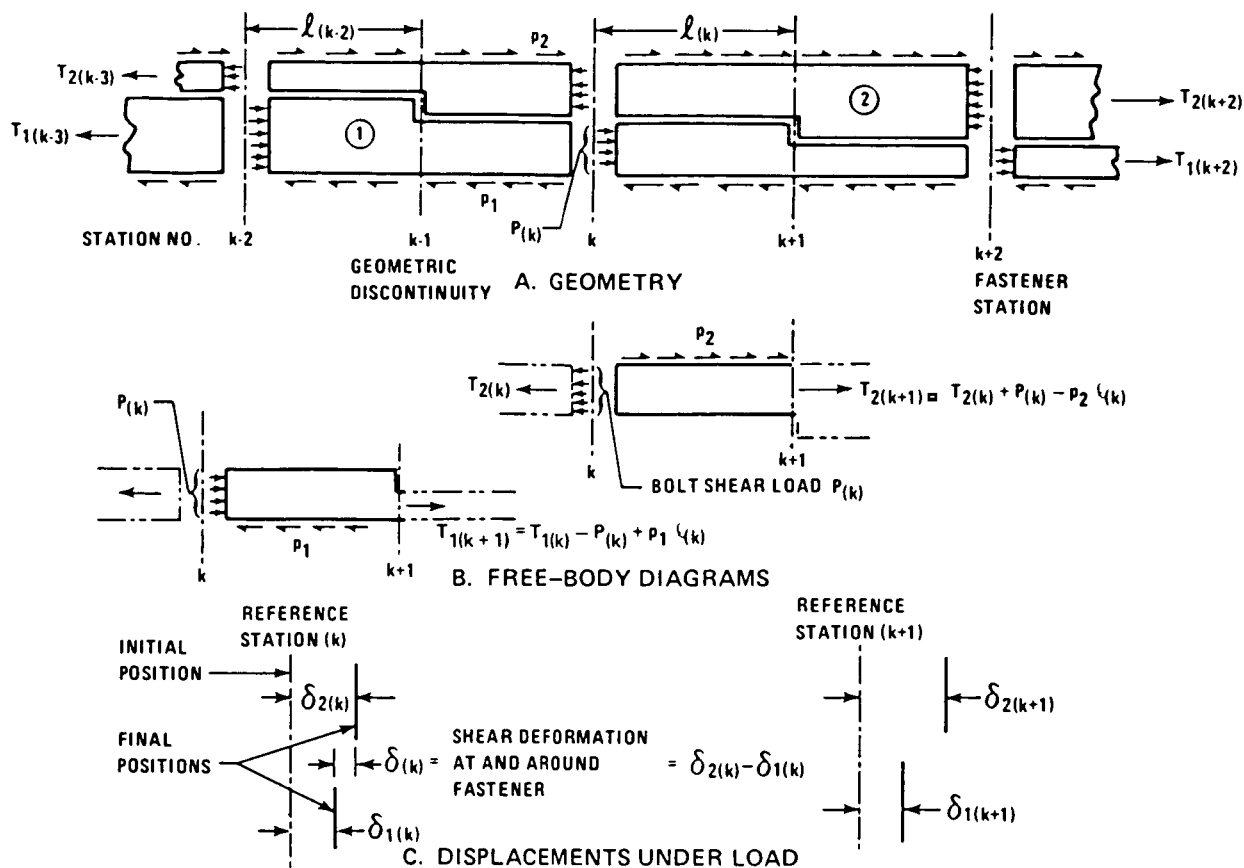


FIGURE 38. LOADS AND DEFORMATIONS ON ELEMENTS OF BOLTED JOINT

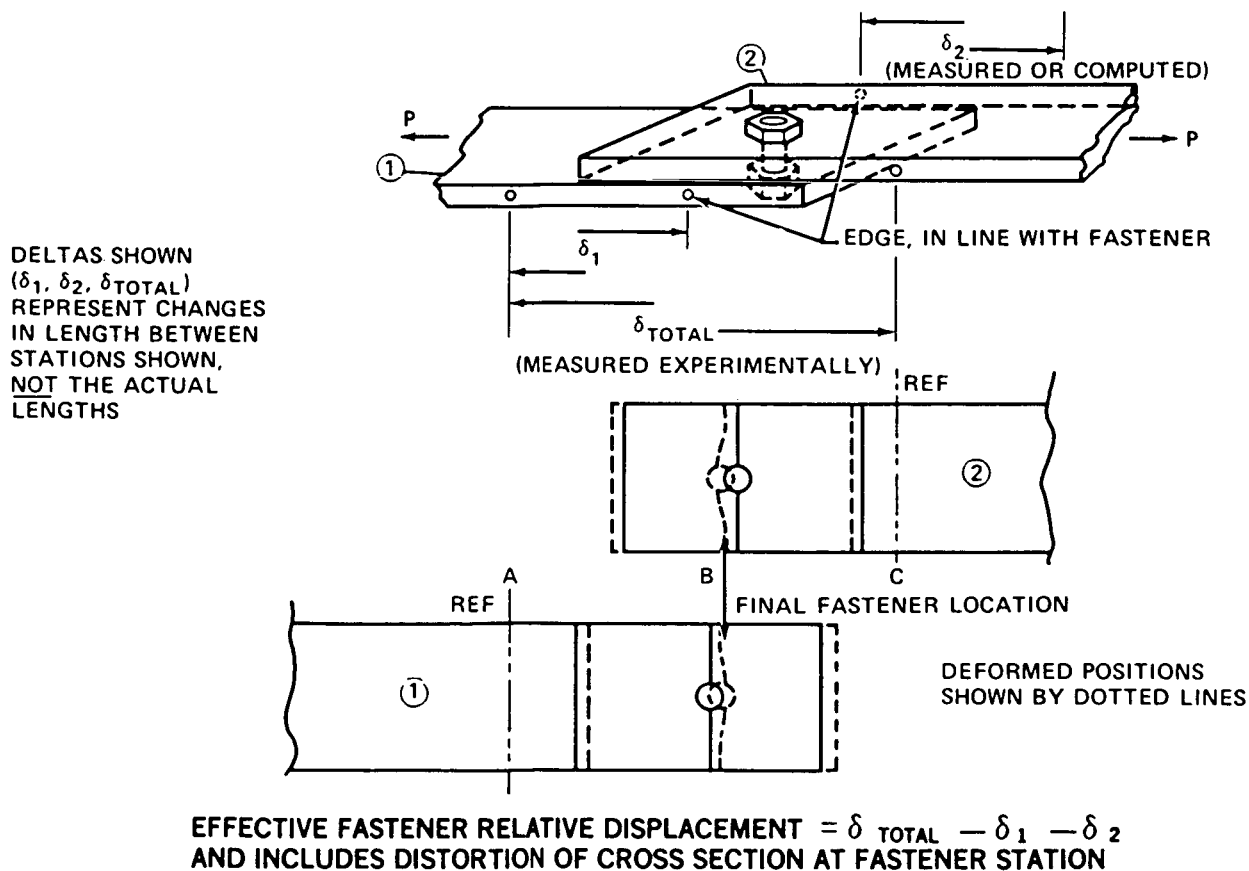


FIGURE 39. DEFORMATIONS IN MECHANICALLY FASTENED JOINT

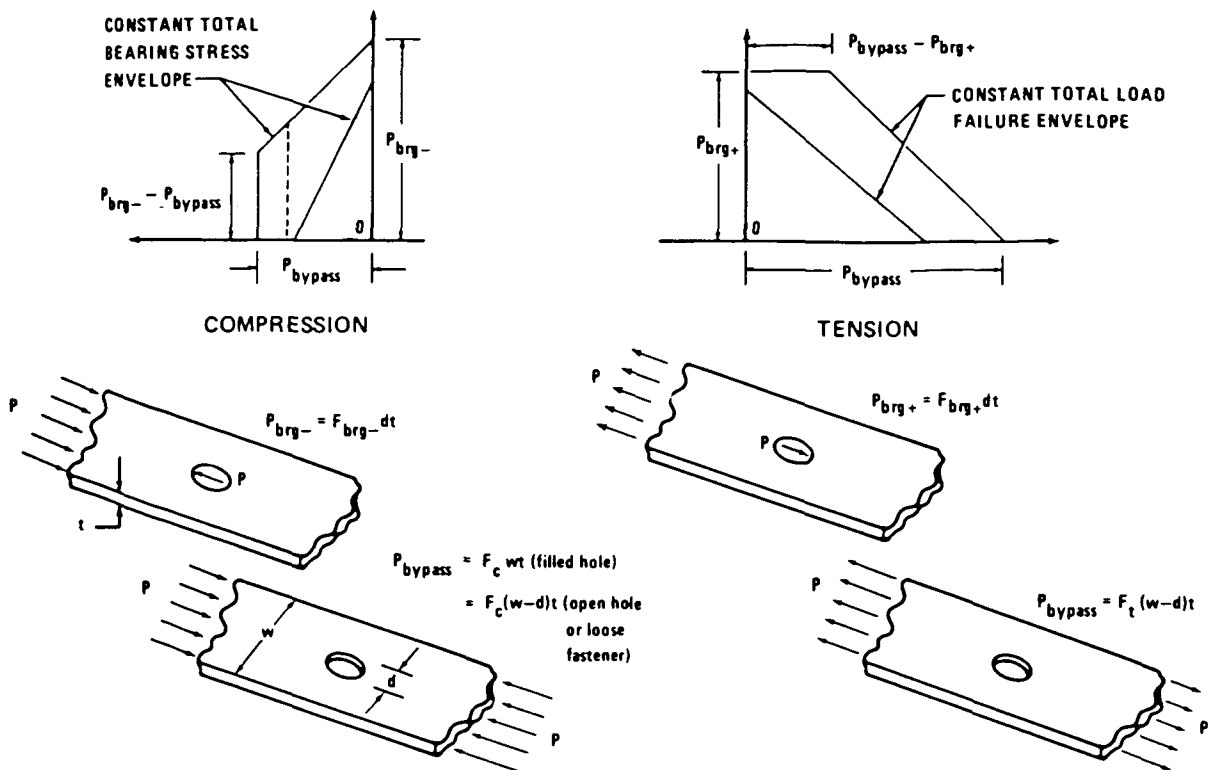


FIGURE 40. OUTER ENVELOPE OF BEARING-BYPASS LOAD INTERACTIONS

tension and compression can be either linear or kinked, depending primarily on the local w/d ratio, as shown in Figure 40. Narrow strips, or closely spaced bolts, fail in tension-through-the-hole for both bearing and bypass loads; however, wide strips exhibit a bearing stress cutoff. Compressive loads have two possible interactions, depending on whether the bolt fits tightly or loosely in the hole. In the case of a tight-fit hole, the combination of bearing and bypass stresses must not exceed the bearing allowable stress. With a loose-fit bolt, none of the bypass load can be transmitted through the bolt, causing a higher stress on the net section. In the case of a bolt hole with a very small clearance, the bolt may pick up a little bypass load as the composite laminate deforms under load.

The intercepts of the bearing bypass interaction curves are established directly from experimental results or by means of the stress concentration formulas and associated reduction factors discussed previously. The following

steps are involved in those calculations. First, the elastic-isotropic stress concentration factor k_{te} is calculated for both loaded and unloaded holes in tension. Those factors are reduced to the equivalent k_{tc} values via the reduction factor C to establish the actual intercepts. A straight line is drawn between the loaded and unloaded hole strength intercepts, and a bearing stress cutoff is added, if necessary, for wider bolt spacings. The same value of k_{tc} would be used for the compressive bypass strength at an unfilled hole and, in the absence of specific data for filled holes, a value half way between that k_{tc} and unity is recommended for filled holes under compression. The compressive bearing limit is self-evident. Usually, joints are more critical in tension than in compression, but the combination of high compressive bypass and bearing stresses may result in joints prone to widespread delaminations.

The analyses presented here rely heavily on the input data generated from the ancillary test program, but the differences between such test data and the actual structure should always be considered. For example, a significant finding of the single-hole tests was that, in double shear, the allowable strength of the central plate was always greater than that of the splice plates despite the matched thicknesses, presumably because of the better clamp-up or slightly unsymmetric loading. Therefore, in analyzing such joints, this extra strength should be accounted for in the input data. Such data would be necessary to truly optimize the design of multirow joints, although in this particular case, the error would be conservative.

In addition to variations in performance, concern must also be given to the sometimes subtle differences in configuration between test coupons and real structure. The unloaded hole ancillary tests were tested as "unfilled" holes, with the undersized bolts providing some clamp-up, while the actual subcomponent joints were tested with close-fit or interference fit fasteners. This discrepancy should be considered when calculating the bypass intercept of the bearing bypass interaction curves for tension and compression if an accurate prediction of joint strength is to be made. Until such variations are more fully understood a conservative approach would be appropriate for real structure applications.

A further strength cutoff, that of failing the fasteners in shear or bending, should never be an effective limit on joint strength. Several of the sub-component specimens suffered extensive bolt bending and it is recommended that a conservative approach to bolt selection be employed to avoid this phenomenon. Attempting to minimize fastener size (and weight) solely on the basis of apparent shear strength may often lead to unexpected bolt bending failures. On the other hand, exceedingly conservative design practices may nullify the potential joint efficiencies that are attained by carefully tailoring proportions. Certainly, a reliable method for efficiently selecting bolt sizes would be quite useful in the optimization of multirow bolted joint designs.

The loss of clamp-up due to bolt bending, as discussed in the test results section, reinforces the desire to avoid the bolt bending problem altogether. Figure 41 explains that the drastic reduction in laminate bearing strength, due to the loss of bolt clamp-up as a result of bolt bending, will occur under both tensile and compressive loading. This results in delaminations at local bearing stresses as low as those for simple shear pins -- only about half of the strength for torqued bolts of larger diameter.

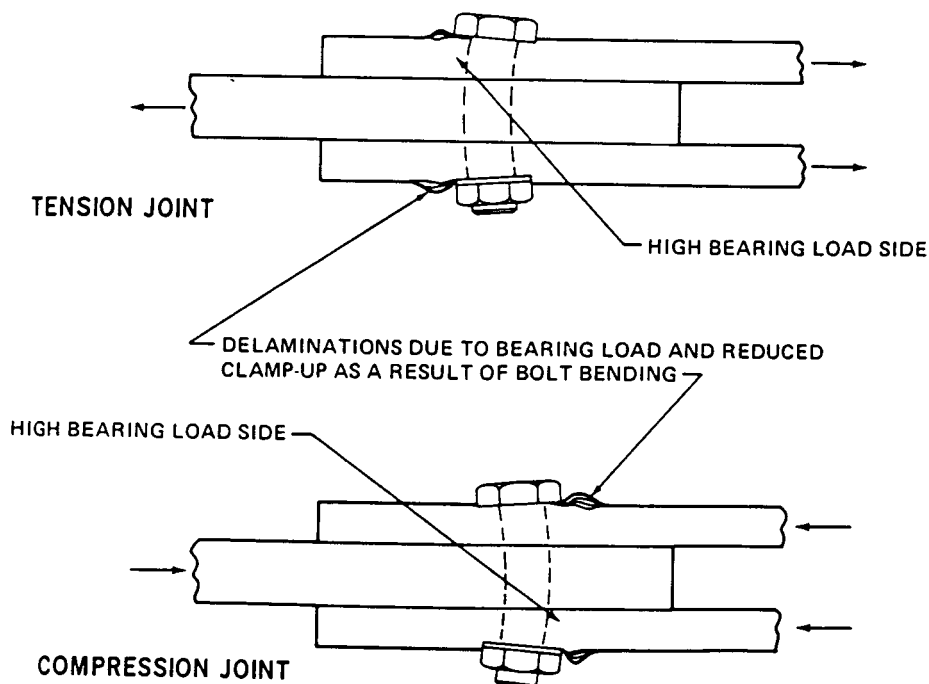


FIGURE 41. EFFECTS OF BOLT BENDING ON LAMINATE BEARING STRENGTH

In evaluating the load deflection characteristics of bolts in fibrous composite laminates, the elastic stiffness can be easily calculated on the basis of the formulas given above. The nonlinear behavior can be determined by the most critical possibility -- the bearing or net-section failures of each member at that station or failure of the bolt in shear (or by yielding under bending).

5.1 PARAMETRIC STUDIES

Several parametric studies were conducted to evaluate the effects of variations or inconsistencies in the input data on the predicted multirow joint strengths from A4EJ solutions. The results of such a study are presented in Figure 42 which shows graphically how variations in the predicted unloaded hole stress concentration reduction factor (C) will influence strength predictions for multirow joint analysis. Variations in predicted unloaded

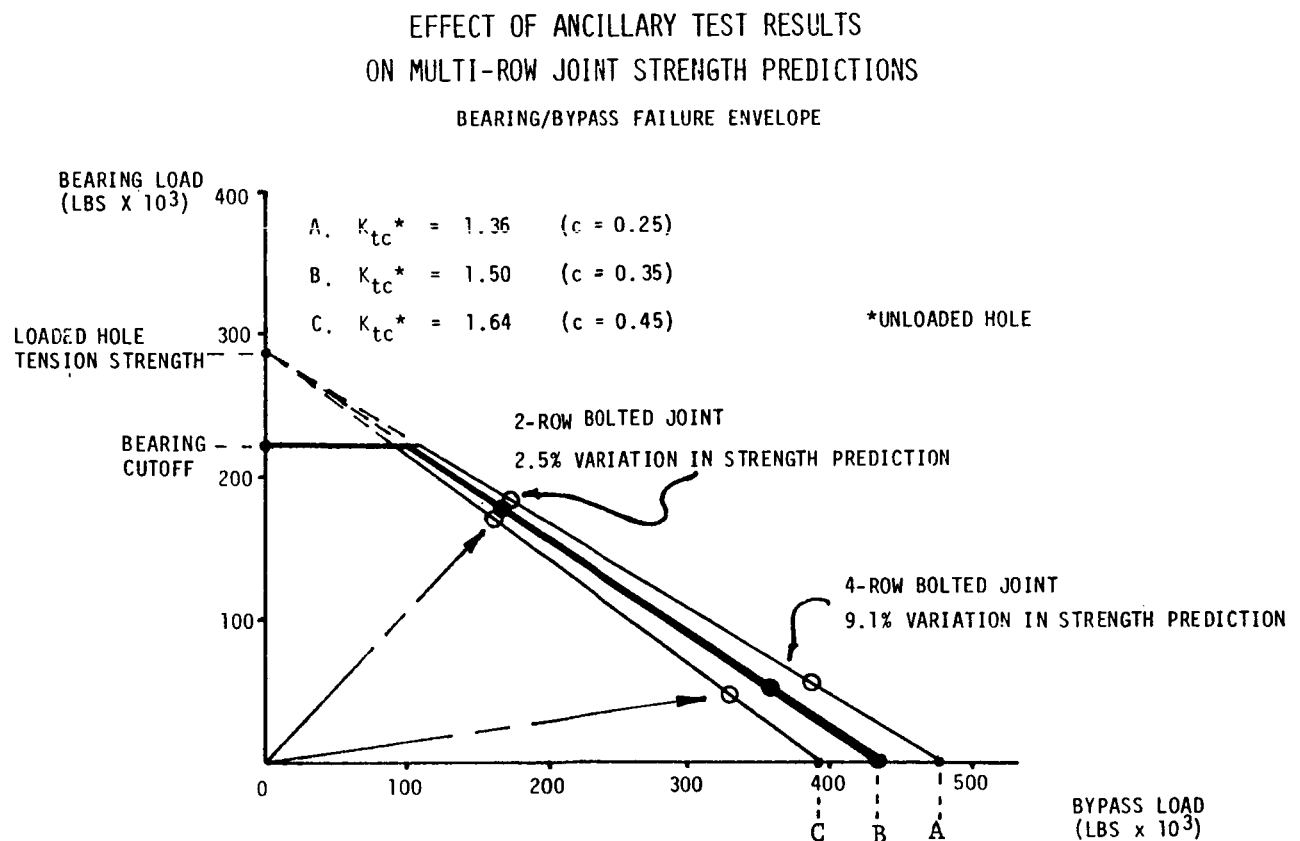


FIGURE 42. EFFECT OF ANCILLARY TEST RESULTS ON MULTIROW JOINT STRENGTH PREDICTIONS

hole strengths can have a significant effect on ultimate load predictions for combined bearing and bypass loads. Points A, B, and C represent three different bypass (unloaded hole) strengths resulting from variations in the predicted composite stress concentration factor (k_{tc}). With all other input being equal, the induced variations in multirow strength predictions are shown for a typical two-row and four-row joint. An important observation to be made from Figure 42 is that the error in predicted joint strength increases with additional rows of bolts. This occurs because as rows of fasteners are added, the failure is designed to take place at a low-bearing, high-bypass location.

The figure clearly shows that this type of failure condition (as in a 4-row joint) is much more sensitive to predicted unloaded hole strengths than a 2-row joint case, where the bearing load is nearly equal to the bypass load.

Similar studies were conducted to determine the sensitivity of multirow joint strength predictions to variations in load-deflection characteristics. The elastic springs rates were measured experimentally for all of the loaded hole ancillary tests, and an apparently high level of scatter among identical specimens was observed. Various analytical solutions for the ultimate loads of joints in the configurations of the JT4 and JT8 specimens were performed and the elastic bolt flexibilities were varied among solutions within the range of scatter encountered in our ancillary test program. Variations in predicted joint strength were about 6 percent from the average of the JT4 specimen, and about 2 percent for the JT8 specimen.

The principal message from these studies is that the importance of developing accurate, realistic input data for the A4EJ program should not be overlooked. The analyst must have a complete understanding of the empirical data on which the multirow solutions will be based before attempting more complex analyses. If several parameters are susceptible to substantial variation, the analytical solutions must reflect this if a conservative solution is desired.

6.0 PRELIMINARY SUBCOMPONENT JOINT STRENGTH ANALYSIS

Preliminary evaluations of various joint concepts and geometries were performed using the A4EJ computer program before final decisions were made for subcomponent joint designs. Most of this work was done prior to the completion of ancillary testing. Hence, the empirical base (on which A4EJ heavily relies) was limited to data from prior test programs of limited scope and other material systems. Nevertheless, these efforts demonstrated the effectiveness of the A4EJ program as a preliminary design tool.

In order to determine the most efficient design concepts, studies were made to evaluate the effect of joint configuration on bolt load distribution and overall performance. The results of one such study is presented in Figure 43 examining four basic joint concepts. Despite a natural inclination to expect the scarf joint (Configuration A) to be the most efficient, it was actually shown to be the

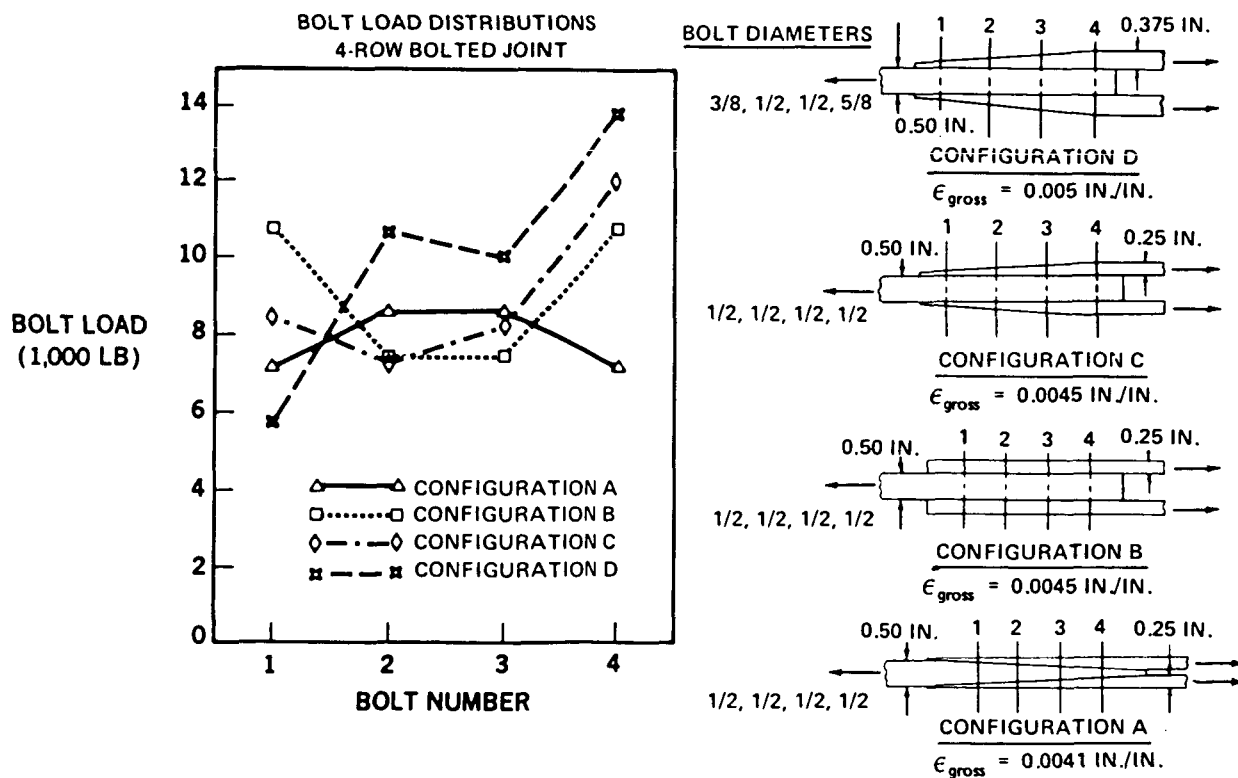


FIGURE 43. EFFECT OF JOINT CONFIGURATION ON BOLT LOAD DISTRIBUTION

weakest, as well as the most difficult to manufacture and assemble. That conclusion should also be true for metal alloy constructions. The scarf joint failed basically because the thickness of the skin was reduced below nominal before the first fastener station was reached. (Obviously, one could counter that loss of area by a local buildup in the vicinity of the joint, but all of the concepts could be improved by the stress reduction associated with local reinforcement of the joint area.) It should be noted that the outermost rows of bolts in the scarf joints transfer less load than is carried by the interior bolts. That is caused by the reduced stiffness associated with the local thinning of the skin and splice plates.

The joint with uniformly thick splice plates (Configuration B, Figure 43) was predicted to perform surprisingly well, and actually did in subsequent sub-component joint tests. The combination of a uniform skin and reinforced tapered splice plates was predicted to be the most efficient joint design. Structural tests substantiated this result, despite premature failures as a result of delaminations in tapered splice members. The development of an improved tapered splice design and fabrication method should eliminate this phenomenon and further verify the predicted superiority of this design. Nevertheless, in consideration of the interlaminar weaknesses associated with tapered members, the simple uniform joint should be looked upon as one of the two most viable candidate designs for fibrous composite construction. Certainly, the absence of critical interlaminar stresses, as in metallic construction, should make the joint with uniform skin and tapered splice plates the best candidate.

The use of tapered splice plates without an increase in thickness at bolt row Number 4 (greater than one-half the skin thickness) obviously cannot represent an improvement over the strength with uniform splices since tapering transfers more load to the most critical fasteners, nearest to the middle of the splice plates where the skins butt together. A comparison of gross-section strains for Configurations B and C in Figure 43 illustrates this phenomenon. A relative increase in thickness of the tapered splice plates is needed not only because of the extra load transferred to those bolts but also because the splice plate joint allowables are weaker than those of the skin when the skin is sandwiched in double shear.

The superiority of the thickened tapered splice members of Configuration D in combination with a uniform skin can be explained easily. The greatest strength is obtained by maximizing the bypass load at the outermost row of fasteners -- that is, the first row of fasteners in the skin (Row 1 in Figure 43) -- and this involves decreasing the bearing load at that location in order to maximize the bypass load, which represents the sum of all of the other bolt loads for Rows 2, 3 and 4. This design philosophy is reflected in Figure 44, which shows that the only way a multirow joint can be more efficient than the optimum single-row joint is by minimizing the bearing stress at the critical row of fasteners and further separating the bolts (that is, increasing the w/d ratio). The sequence of iterations in optimizing the design is governed by maximizing the total load (or gross-section strain) in the skin at the first row of fasteners (Row 1) while not causing a premature failure in either the skin or splice at the last row of fasteners (Row 4). Since there is no bypass load in the skin at the last row of fasteners,

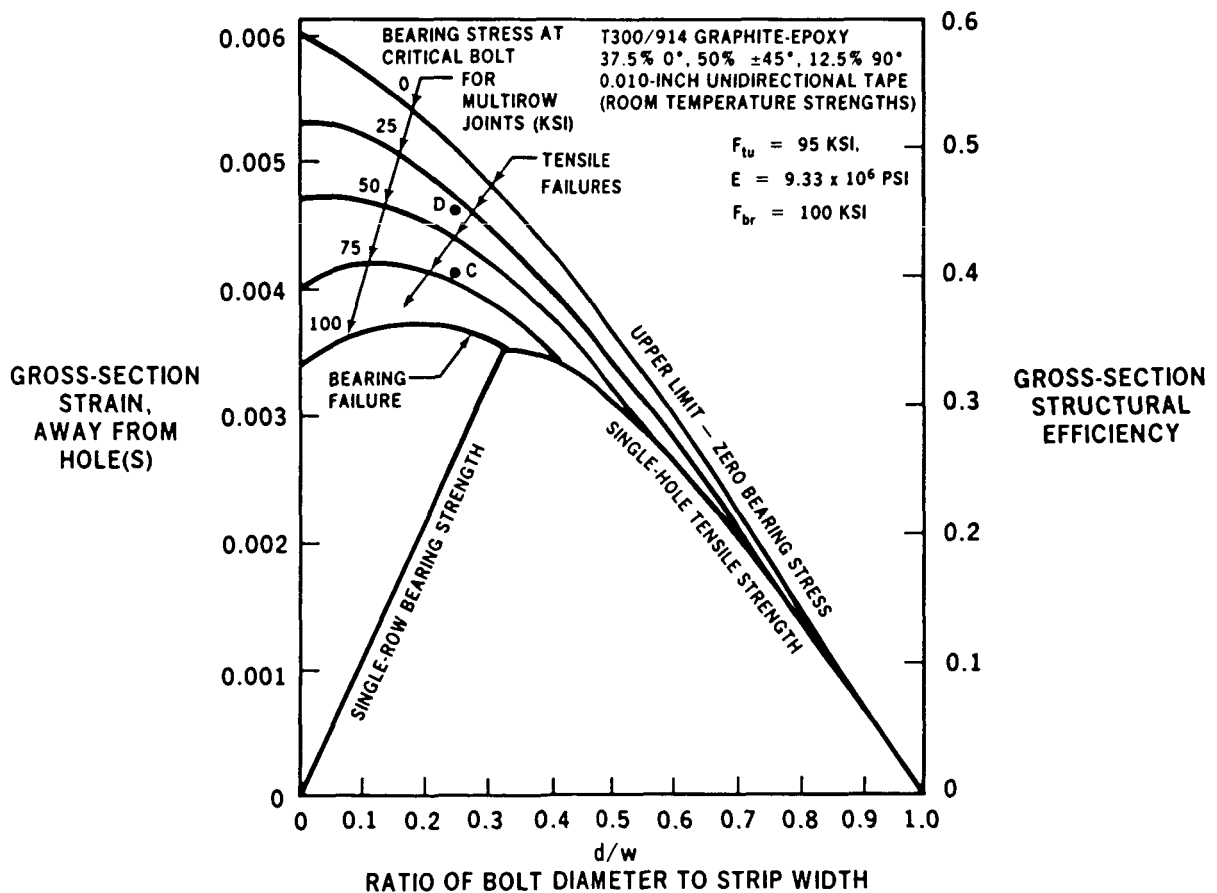


FIGURE 44. STRESS CONCENTRATION INTERACTIONS IN MULTIROW BOLTED COMPOSITE JOINTS

it is desirable to maximize the load transfer there to relieve the load on the first row. Only local reinforcement is needed in the splice plates to tolerate the combination of maximum bearing and bypass loads at Row 4. A larger diameter fastener for the last row of bolts or a smaller one for the first row, where the splices are thinnest, will often be of assistance in this optimization process. Any small extra weight in the splices or fasteners is worth incurring to maximize the efficiency of the large, heavy skins. It is wrong to evaluate splice efficiencies only on the basis of minimizing the weight of the splices and fasteners.

As previously stated, the final configurations of subcomponent joint specimens were based on A4EJ solutions using input data from prior test programs. After the completion of the ancillary test program, the subcomponent joint designs were re-analyzed with more appropriate input data from the single hole tests. In some cases, the difference in mechanical properties and notched strength levels between the Ciba-Geigy 914/T300 material and other materials for which data was available indicated that the subcomponent design proportions would not make the most efficient use of the material. Such an analysis is displayed in Figure 45 where the initial design of the 8-bolt tension joint was re-analyzed

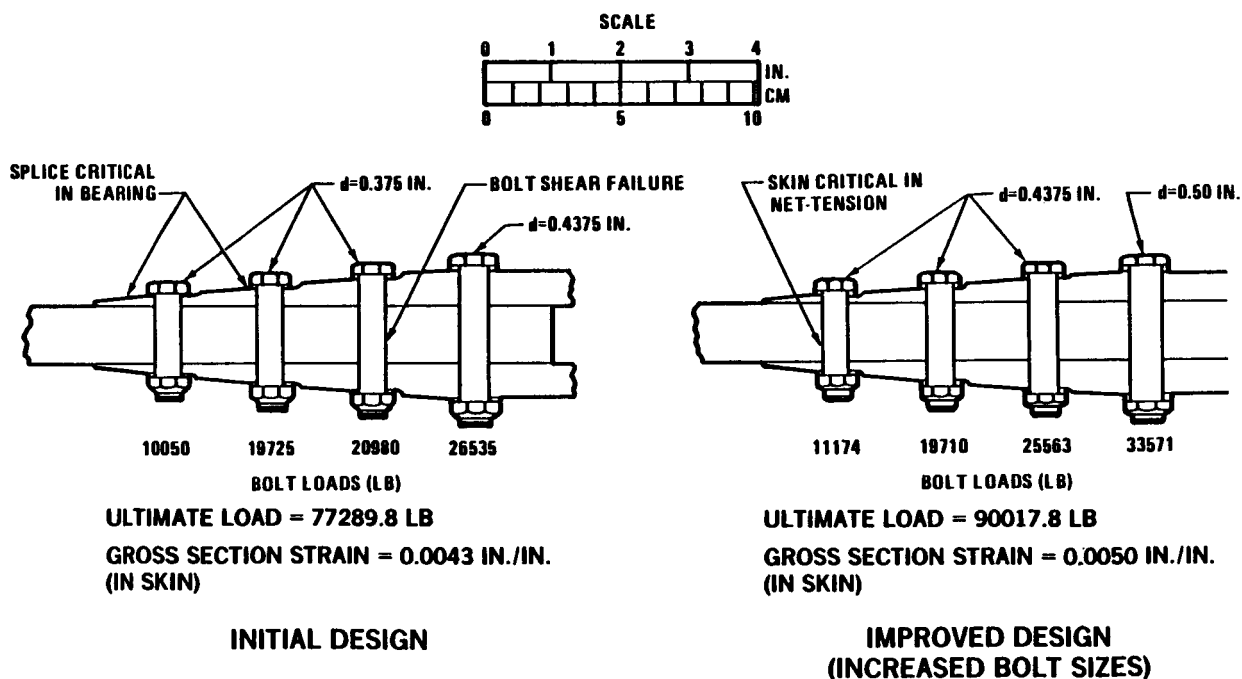


FIGURE 45. USE OF A4EJ ANALYSIS TO IMPROVE BOLTED JOINT DESIGN

using updated input data. The results showed this configuration to be bearing and bolt critical, and that the central skin member was not being used efficiently. This joint was then re-analyzed with a 1/16 inch increase in bolt diameters, the results of which are shown to the right side of Figure 45. A 16 percent increase in joint strength was predicted for this modification.

Such comparative analyses were performed for many joint configurations. One of the 8-bolt joint specimens discussed above was reworked to the sizing shown to the right of Figure 45, but the premature delamination failure of the tapered splice members prevented the specimen from approaching its potential strength (refer to Figure 17). In any case, this exercise demonstrated the importance of using suitable single-hole data to form the empirical base from which A4EJ multirow joint solutions are performed.

7.0 ANALYSIS/TEST CORRELATION

Subcomponent joint analyses were performed for all specimen configurations in advance of structural tests. In some cases, where a new or unanticipated failure mode was encountered, the analytical solutions were revised to account for the variation in joint performance. Predictions of joint ultimate load and strain levels were made using the A4EJ program with input data generated from the ancillary test results and associated semi-empirical methods. Appendix B contains the analysis results for the four basic configurations of subcomponent joint tests.

The following sections discuss the correlation between the analysis and test results for the entire series of tests. Ultimate load comparisons are made despite the premature failures of several specimens due to unexpected modes of failure. For those specimens equipped with strain gages along the length of the joint, comparisons are made between the tested and predicted bolt load distributions throughout the test.

In general, good correlation is shown between the various analysis predictions and test results. The results of this study have indicated that accurate prediction of multirow bolted composite joints are possible, although there is still much to be learned about the performance of multirow bolted joints in composites and the extent that each of the various parameters contribute to that performance. It should be noted that most of the tested weaknesses were found to be in the splice plates, which have lower allowables than the skins with better clamp-up, and in excessive bending of many of the bolts. In the case of tension loadings, the splice plate weaknesses should be eliminated with improved design and manufacturing techniques. For compression loading it appears that the strength and performance of external splice members will usually determine the overall joint compression strength. One key to structurally efficient bolted joints in fibrous composites is a low working stress in bearing which permits maximization of the bypass stress and hence the total stresses in the joint. Another is to use stiff bolts having a sufficient diameter to not bend under the applied loads.

7.1 4-BOLT TENSION AND COMPRESSION

The 4-bolt joint was the simplest configuration of the subcomponent specimens and was accordingly the simplest to analyze. In a two-row joint where the splice thickness equals one-half the thickness of the central blade, each row of bolts will carry one-half the total load. Since the splice plates in our test were reinforced with respect to the skin, the slight stiffness imbalance forces the outer rows of bolts to carry more than the inner rows. The results of the A4EJ solution in Appendix B confirm this phenomenon.

The most instructive way to examine the correlation between test results and analysis solutions is through the use of the bearing-bypass failure envelope for the critical location in the joint. These curves are plotted in Figure 46 for the critical positions in the 4-bolt subcomponent joint under tension and compression loading. The analytically predicted strengths are indicated along with the actual failures of joint test specimens.

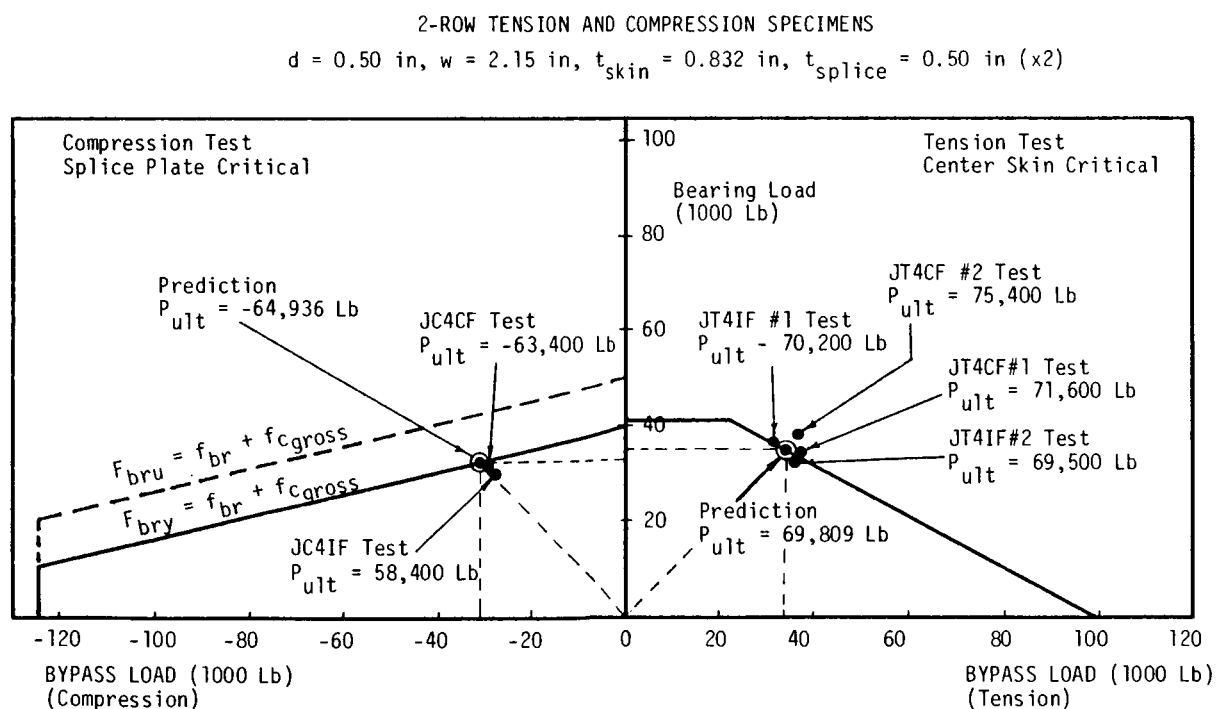


FIGURE 46. 4-BOLT JOINT BEARING-BYPASS FAILURE ENVELOPES

For tension loading, a net-section failure was predicted in the skin at the outer row of bolts with an ultimate load of 69,809 pounds and a gross section strain of 0.0042. Note that the analysis does predict that slightly more bearing load than bypass load occurs at the critical fastener location which is to be expected, as discussed above. It would appear from Figure 46 that there was very good correlation between the analysis predictions and test results, but the cluster of test results plotted close to the predicted strength were actually fastener failures resulting from the excessive bolt bending suffered by these specimens. Only the tested failure at 74,500 pounds (gross section strain of 0.005) was a net-tension failure as predicted.

A number of factors may have contributed to this higher-than-predicted strength. There may be some inherent conservatism in the predicted stress concentration factors because of the differences between the test coupons and actual structure as previously mentioned. By changing to large tension nuts as opposed to shear nuts on one JT4CF specimen, the bolt failure mode was suppressed long enough to allow the tension failure to occur at a higher strength. Nevertheless, the specimen did experience severe bolt bending (refer to Figure 14) which may have favorably modified the bolt load distribution, thus permitting a higher failure load.

The 4-bolt joint analysis for compression loading was revised after-the-fact to concur with the latest version of the bearing-bypass interactions for unsupported joint members. The concept involves compression failures in external splice members induced by the initial delaminations occurring at bolt holes loaded to the bearing yield stress of the laminate. The principal behind this is explained in the ensuing discussion of the 12-bolt joint.

The predicted compression failure load of 64,937 pounds in Figure 46 corresponds to a compression failure of the splice plates at the inner row of fasteners. A comparison of this analysis result with actual test cases is academic because of the great difference in failure modes. Compression failures of the larger multirow joints are more readily comparable to the analysis solutions.

7.2 8-BOLT TENSION AND COMPRESSION

All of the tested failures of the 8-bolt tension joints were caused by the premature delaminations of the splice members as described earlier. Because this mode of failure was not anticipated, a direct comparison of tested and predicted failure loads must be examined with due consideration to the differences in failure mode. The bearing-bypass failure envelopes for the predicted critical locations under tensile and compressive loads are presented in Figure 47. For the tension joint, none of the test specimens reached their analytically predicted strengths. The analysis presented on the left side of Figure 45 describes the kind of performance expected from this joint. Despite the external splice delaminations, the tested joints did show substantial bearing deformation and bolt bending as indicated by Figure 18. In fact, the ultimate load prediction was made with some intrinsic uncertainties because of the potentially irregular or inconsistent performance associated with so much plastic (nonlinear) behavior. The improved design with an increase in bolt size (JT8CF-515) did not show an improvement over the specimens tested in the original configuration (despite the considerable reduction in nonlinear behavior) because of the splice delamination phenomenon.

4-ROW TENSION AND COMPRESSION SPECIMENS

$d_{1-3} = 0.375$ in, $d_4 = 0.4375$ in, $w = 2.15$ in, $t_{skin} = 0.832$ in, $t_{splice} = 0.50$ in (12)

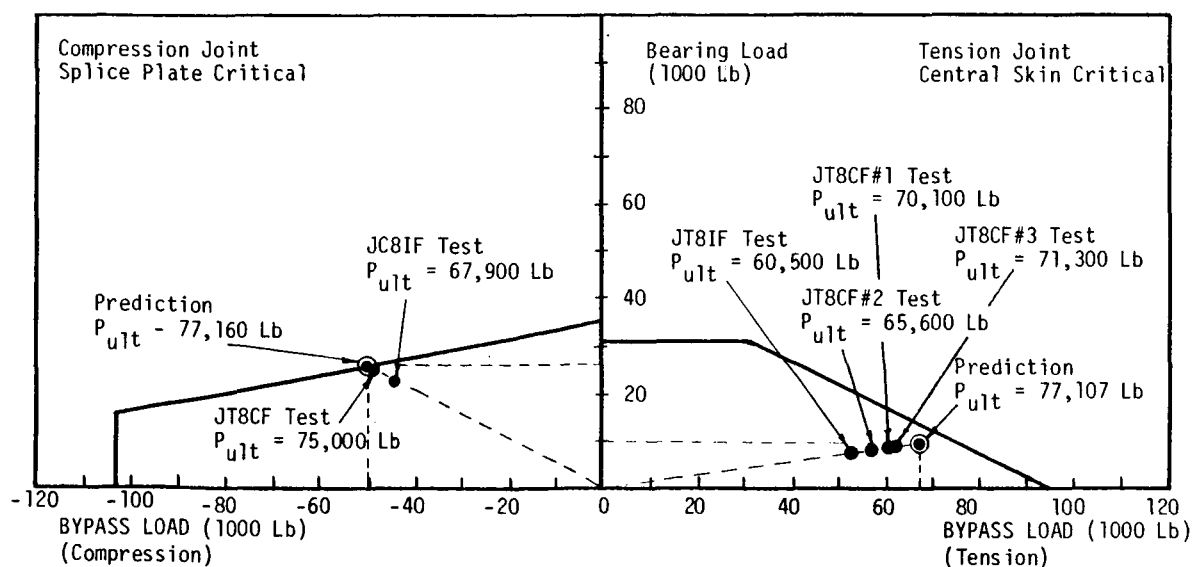


FIGURE 47. 8-BOLT JOINT, BEARING-BYPASS FAILURE ENVELOPES

The JC8CF and JC8IF compression joint strengths are plotted with the analysis solution to the left in Figure 47. The accuracy of the prediction is uncertain again because of the extensive nonlinear behavior and the introduction of a relatively new mode of failure in compression. In this case, the joint tests exceed the predicted strength when limited by the diagonal line of Figure 47 which represents a constant bearing yield stress condition. Radical changes in the bolt load distribution with such extensive nonlinear behavior may have contributed to these differences. It will be shown that such analysis solutions were found to be more accurate for the larger joints where much less plastic deformation took place in the bolts or around the fastener holes in the joint members.

Three of the JT8 specimens were strain gaged along the length and on either side of each member (Figure 48). Readings were taken during the test at specified increments of applied load. These strain gage readings permit a detailed comparison of the test results with our analysis predictions in terms of the bolt load distribution throughout the test.

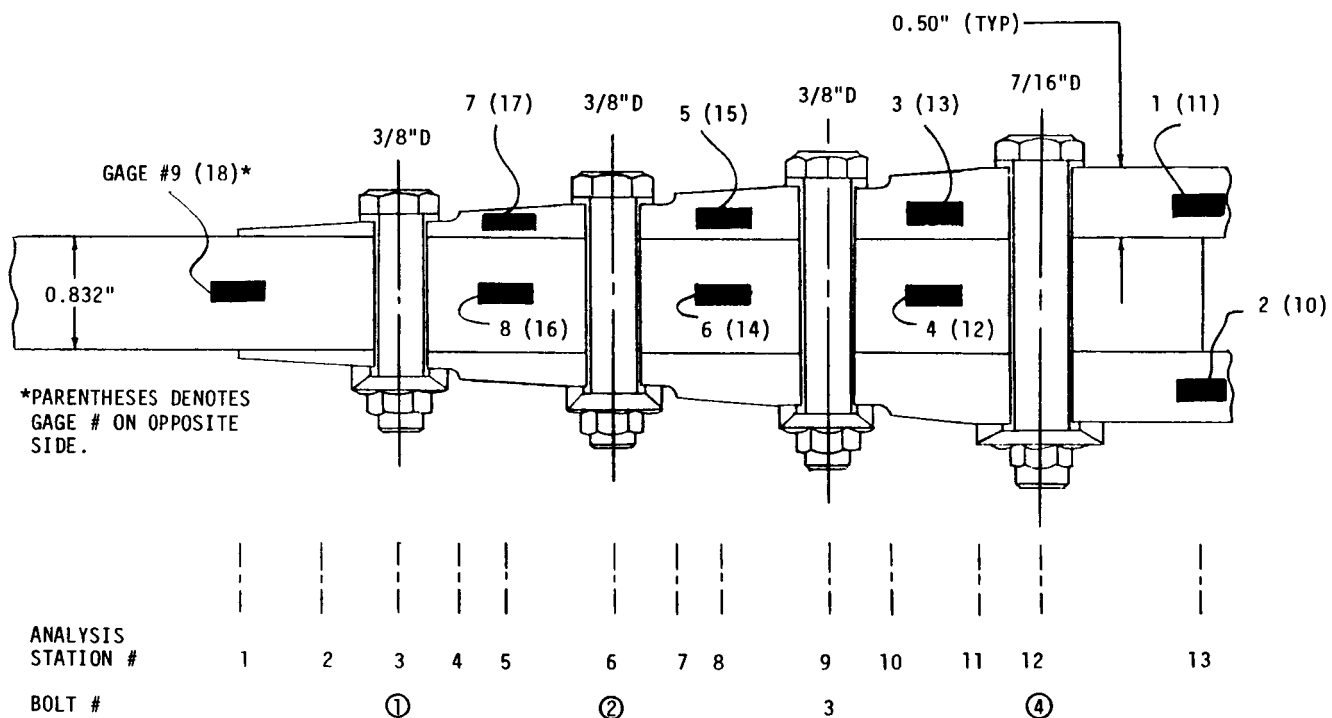


FIGURE 48. TAPERED JOINT - STRAIN GAGE LOCATIONS

The A4EJ computer program is capable of solving for the joint internal loads for a given applied load, as well as solving for the joint ultimate load. An iterative solution was performed at each applied load level that a reading was taken. This analysis has been compared to the test results from one of the 8-bolt tension tests. The comparison was made up to the point at which the surface delaminations of the splice members were believed to be affecting the strain gage readings.

Some data reduction of the raw strain gauge data was required to facilitate the comparison. From the strain readings in the gross section of each member, Young's modulus was calculated for each load increment. The load level at each gage was then calculated using the strain readings, Young's modulus, and the gross area at the center of the gage. The load levels were then adjusted to account for eccentricities and variations in the stress distributions across the width in the gross-sections between the bolts. This adjustment was made equally to the readings from both members such that the sum of the skin and splice plate loads must equal the joint applied load at any given location along the joint.

The analysis shows good correlation with the test results for the amount of load transferred at each bolt throughout the test as shown in Figure 49. Slight differences in the predicted bearing yield point do not have a significantly adverse effect on the correlation between test and theory. Similar comparisons between tested and predicted bolt load distributions will be presented for the larger 24-bolt joint.

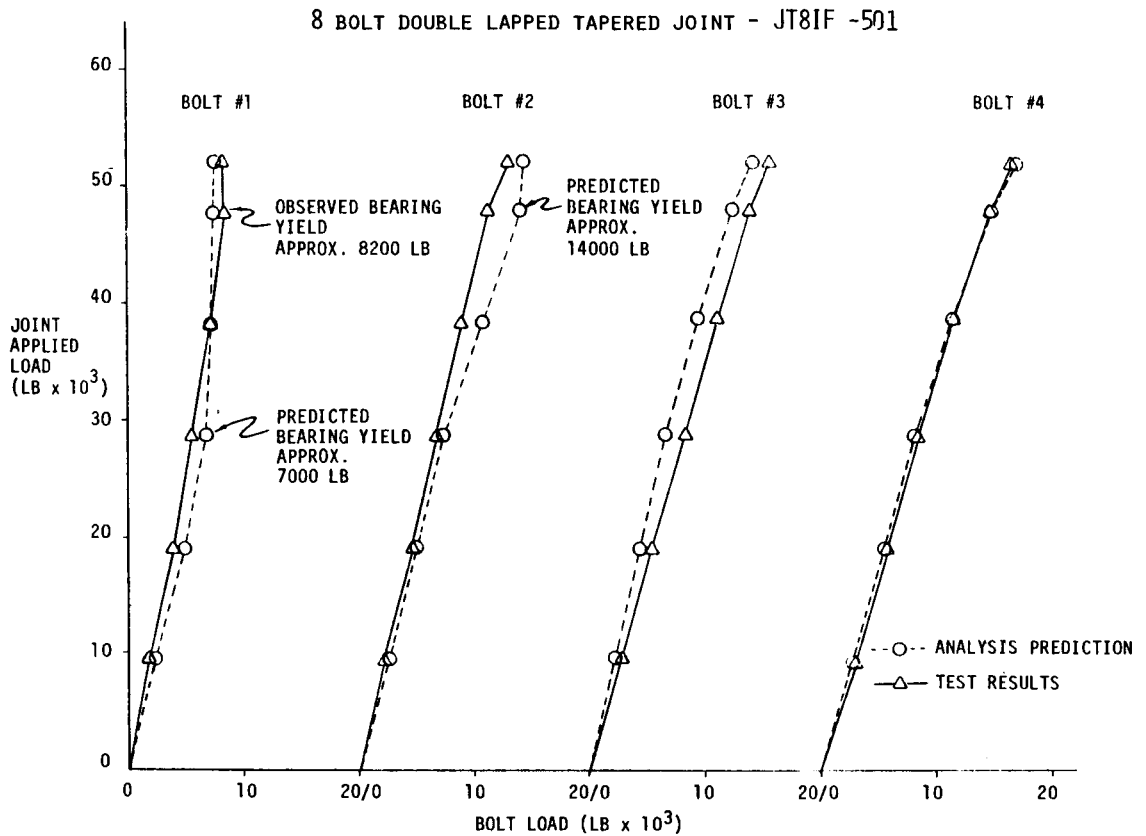


FIGURE 49. 8-BOLT JOINT LOAD DISTRIBUTION - TEST VS ANALYSIS

7.3 12-BOLT TENSION

The 12-bolt joint was essentially a scaled up version of the 4-bolt specimen. As in the 4-bolt joint, the total thickness of the splice plates exceeded that of the skin, so that more load would be transferred at the outermost row of fasteners and the critical member would therefore be the skin and not a splice member.

Both the test result for the JT12CF specimen and the analysis predictions confirm this. The joint strength at the critical location is limited by the bearing-bypass envelope shown in Figure 50, which also shows the excellent agreement between the test result and the predicted ultimate load. A tension-through-the-hole failure had been predicted, and that is consistent with the

2-ROW, 3-COLUMN TENSION AND COMPRESSION SPECIMENS
 $d = 0.75$ IN., $w = 9.0$ IN., $t_{\text{SKIN}} = 1.0$ IN., $t_{\text{SPlice}} = 0.67$ IN. (x 2)

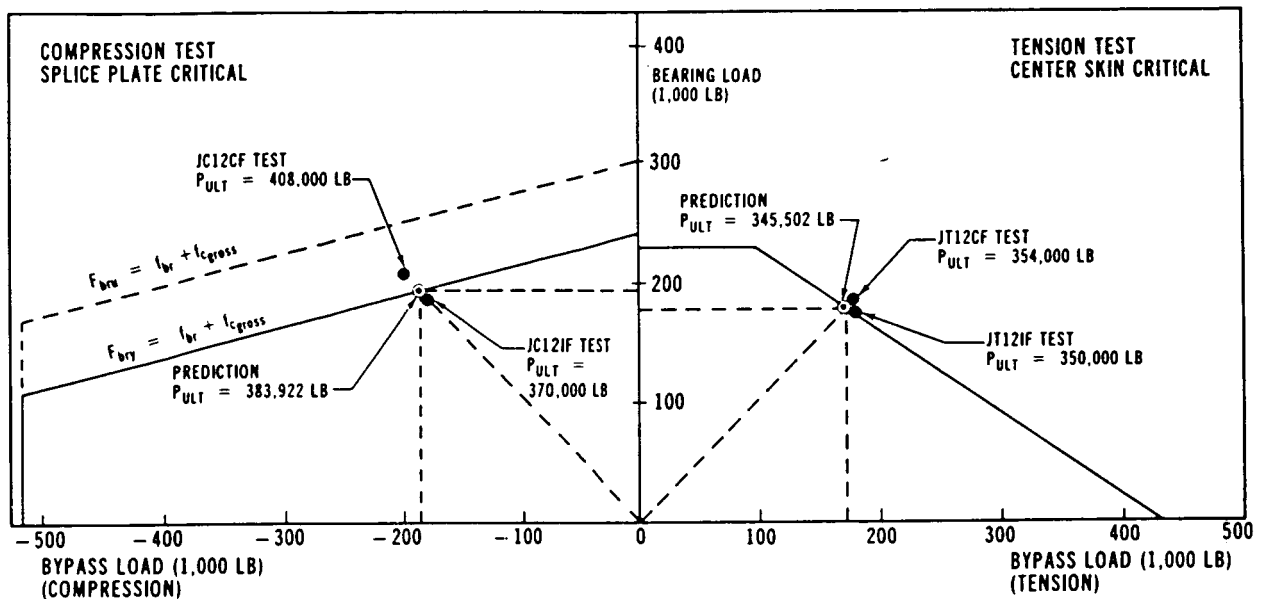


FIGURE 50. 12-BOLT JOINT, BEARING BYPASS FAILURE ENVELOPES

appearance of the failed specimen shown in Figure 19, with a clean textbook fracture. It should also be noted that the bearing load at the critical bolt row is slightly greater than the bypass load which is reacted at the other row of bolts. The bearing stress cutoff in Figure 50 corresponds to a failure stress of 100 ksi. It probably should have been somewhat higher for a bearing strength of 120 ksi in the sandwiched member rather than the 100 ksi which would remain applicable for the more severely load splice plates. Nevertheless, that refinement would not alter the sloping line for the tension-through-the-hole failures and would therefore not affect the predicted failure load. The failure strain of 0.0042 is impressive for such a simple joint geometry, but Figure 44 indicates that still higher results should be attainable for more efficient joint geometries.

The geometrically similar JT12IF specimen was tested with interference fit sleeved titanium bolts instead of the solid titanium bolts used in the clearance fit specimen. This test did not achieve its purpose because the use of the annealed sleeves in combination with smaller titanium bolts resulted in gross bolt yielding, and would not accept load beyond 350,000 pounds. It had been

anticipated that the use of interference-fit fasteners should have increased the joint strengths because of the improved load-sharing between the bolts. However, these benefits were nullified by the recurrent bolt bending failures.

7.4 12-BOLT COMPRESSION

Testing of similar multirow joints in compression established that these joints were stronger than when loaded under tension. This testing also showed that the allowable ultimate compressive bearing stresses may be severely restricted in the presence of high compressive bypass loads.

Good correlation between test and theory was found for the JC12CF and JC12IF specimens with two rows of 3/4-inch bolts. These specimens had uniform splice plates and three columns of bolts in each row, having the same geometry as the tensile test specimens described above. The test results of 408,000 and 370,000 pounds, respectively, closely agreed with the 383,922 pounds determined by analysis. These results are plotted on the left side of Figure 49, with the strength limited by the combination of bearing and bypass stresses.

$$F_{bry} = f_{brg} + f_{c_{gross}}$$

The observed failure was by delamination and compression failure of the splice plates between the innermost bolts, initiated immediately in front of the bolts, where the bearing and bypass loads combined (see Figure 27). The strength prediction of 357,000 pounds (39,667 psi) for this 9-inch-wide and 1-inch-thick skin laminate had been made on the basis of combined stress allowable of 100 ksi for F_{brg} and the critical location had been anticipated to be in the skin at the outermost rows of fasteners. Because of the better clamp-up there, the joint was reanalyzed with an increased allowable of 120 ksi. The splice plate bearing allowables were accordingly reduced to 80 ksi in consideration of the observed bearing yield stress levels in splice members during ancillary testing. The analysis then agreed with the test, in regard to both the failing load and the location of failure.

The failure of these specimens, JC12CF and JC12IF, suggests the existence of a new failure mode. The initial delaminations of a pin-loaded hole occur at about 60 ksi in bearing and, in the absence of compressive bypass loads, do not spread catastrophically. However, unless there is adequate clamp-up, as in the middle of a sandwich, those initial delaminations could interact with any compressive bypass stresses and spread catastrophically. This phenomenon was demonstrated by the performance of the two 12-bolt specimens. The lower strength of the JC12IF specimen relative to the JC12CF joint test reinforces this interpretation since the interference fit bolts bent at a lower load, thus decreasing the joint applied load at which the bearing yield stress and associated compression failure is reached.

7.5 24-BOLT TENSION

This 24-bolt specimen had tapered splice plates with four rows of bolts at each end, in three columns. The total width was 6.0 inches and the thickness of the skin was again 1.0 inch. The maximum and minimum splice plate thicknesses were 0.67 inch and 0.08 inch, respectively. This specimen used 5/8-inch-diameter bolts for the last row in the skin, with the objective of stiffening them up to accept more load - the reinforced splice plates were not predicted to be critical - and to decrease the bearing stresses there in all members. All the remaining bolts were of 1/2 inch diameter.

The failure load of 259,000 pounds for JT24CF specimen corresponds to a gross-section strain of 0.0047 inch in the skin at the first row of bolts. The JT24IF specimen reached a slightly higher load of 265,000 pounds with a gross-section strain of 0.0049.

Actually, a slightly higher strength of 286,055 pounds, or a gross section strain of 0.0051, had been predicted. The test failure was, in fact, triggered by delaminations starting on the outside surface of the tapered splice plates, resulting in premature failure as described in the discussion of test results.

Several of the 24-bolt subcomponent joint specimens, including JT24CF, were equipped with 18 strain gages mounted along the length of the joint on both sides of the central skin member and one splice member in the same manner as the 8-bolt joints. These gages were located midway between the bolt rows. Additional gages were mounted away from the bolts in all three members to verify the lack of bending deformations. Strain readings taken at pre-determined increments where loads were applied to joints were used to calculate the bolt load distribution through the test. Analyses using the A4EJ program were run at the same load increments to solve for the joint internal loads in addition to the ultimate load solutions.

A comparison of the test and analysis results for this four-row, three-column joint is presented in Figure 51. The predicted loads were taken directly from the A4EJ solutions at each applied load level. The test data needed further interpretation because of the nonuniform strains across the widths of the specimen. All readings at any one station were adjusted by the same

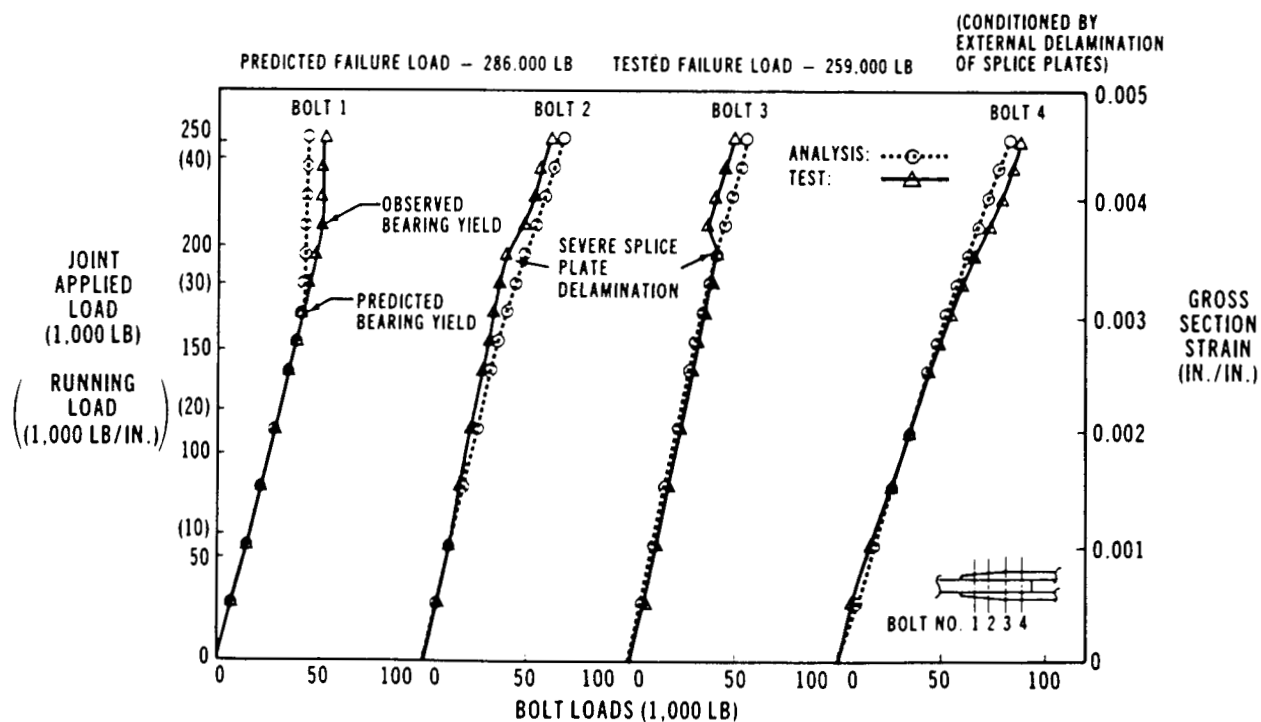


FIGURE 51. 24-BOLT JOINT LOAD DISTRIBUTION - TEST VS ANALYSIS

factor so that the sum of skin and splice plate loads would equal the joint-applied loads at any location along the joint. The transition from linear to nonlinear behavior due to bearing yield at the thin end of the splice plates is clearly observed at bolt row No. 1 in Figure 51. The observed higher bearing yield is possibly due to a much greater diameter-to-thickness ratio for these particular holes, in effect giving more clamp-up than in the tests for untapered specimens. In addition, the effects of the premature delaminations of the splice plate outer plies are also visible as sudden variations in load distribution at a joint applied load of approximately 200,000 pounds.

The bearing-bypass failure envelopes for tensile and compressive loading are presented along with the tested strengths in Figure 52 as a point of reference. It is firmly believed that a tension joint of this configuration would reach or exceed the predicted strength level with an effectively modified splice plate design.

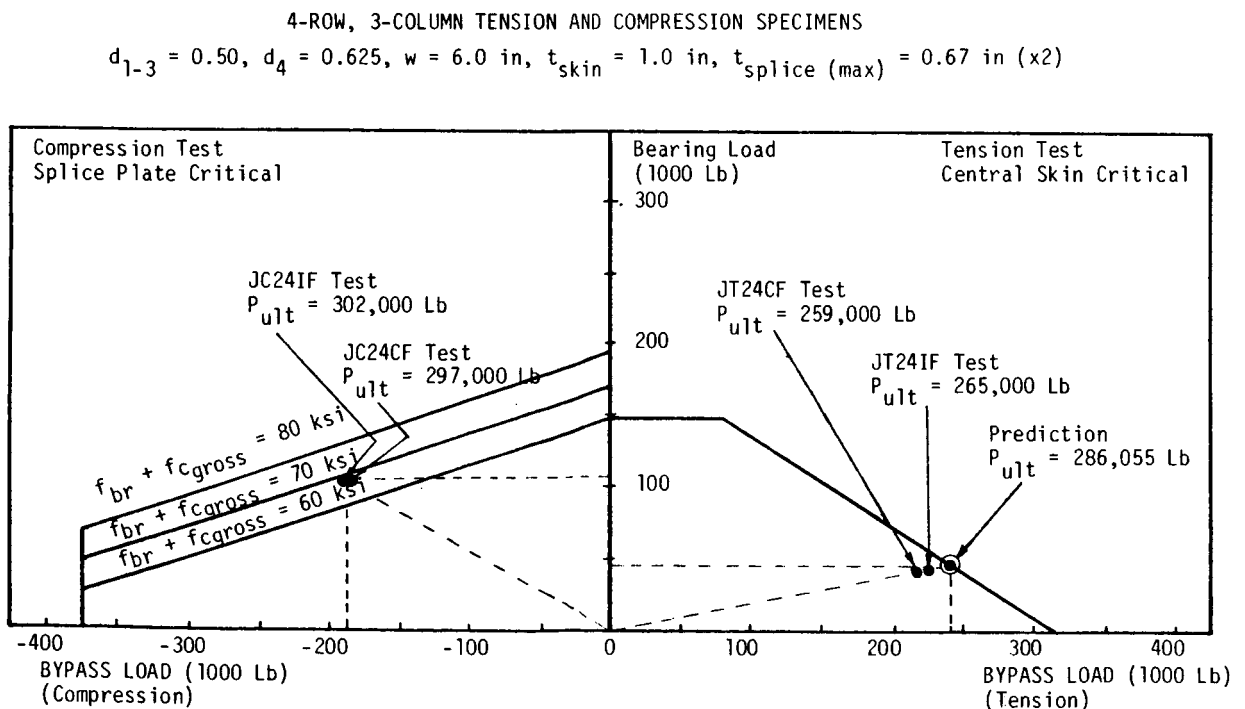


FIGURE 52. 24-BOLT JOINT, BEARING-BYPASS FAILURE ENVELOPES

7.6 24-BOLT COMPRESSION

The same phenomenon that was associated with the 12-bolt compression failures is believed to have triggered the failure in the compressive tests on the 24-bolt multirow joints with tapered splice plates. These specimens, having four rows of bolts in three columns, were identical to the corresponding tensile specimens described above. Specimens JC24CF and JC24IF failed by massive delaminations of the central region of the splices, as shown in Figure 29. The specimens were stabilized against overall buckling, so the failure is believed to have been triggered by the combination of high bearing and bypass stresses in compression. The failure of both specimens occurred at gross-section strains of 0.0062 in the skin outside the joint, indicating that the tensile strength limits are more severe, at about 0.0050. These high compressive strains, without failure in the skin, were achieved by the combination of low bearing stresses (about 35 ksi) in the skin and good clamp-up between the splice plates. The failing loads of the splice plates, 297,000 and 302,000 pounds, are between the 277,875 and 321,343 pounds derived by analysis for ultimate combined bearing stresses of 60 and 70 ksi, respectively, in the splice plates.

The joint compression strength is limited by the diagonal line of Figure 52, representing a state of constant bearing yield stress. The point of bearing yield has been shown to decrease (or, occur at a lower load) with an increase in the degree of bolt bending. Since the onset of this phenomenon is difficult to predict, so then is the joint compression failures which are believed to be triggered by the initial delaminations induced by bolt bearing loads.

8.0 SPECIMEN INSPECTION AFTER TESTING

Several of the failed subcomponent joint specimens were disassembled and thoroughly inspected in an attempt to reveal any phenomena that might enhance our understanding of the joint behavior and failure modes. This procedure was also used to identify those specimens (or parts of specimens) which were sufficiently undamaged to be utilized in future tests.

Prior to removal of the bolts, most of the central blade members appeared relatively undamaged, except for those specimens which failed in net-tension through the skin. After disassembly, several center members did show some local delaminations around the fastener holes, but the actual cause of this damage is unclear. Several of these specimens experienced substantial bending of the bolts, and an excessive amount of force was required to remove them from the specimens. It is uncertain as to how much of the damage to the holes was inflicted during testing or during the disassembly procedure. Some of the blades were also found to have several edge delaminations along the length of the joint which became visible after the nuts were loosened and the clamp-up forces were removed. Damage of this sort was more pronounced in the interference fit specimens, although one unfailed central blade from a clearance fit specimen also suffered a severe edge delamination.

Five blade members from JT12 and JT24 specimens that visually appeared undamaged were C-scanned, the results of which are shown in Figures 53 through 57. The JT12CF specimen failed in net-tension through the outer row of fasteners in one blade member. The other side, which remained intact, was C-scanned as shown in Figure 53. Damage of some sort is indicated by the white areas, although it cannot be discerned from a C-scan whether the damage represents the delamination of a single ply or an interspersed of smaller delaminations distributed through the thickness. The outer row of bolts (lower row, Figure 53) shows damage across the width where the high bearing-bypass load interaction took place. This specimen actually failed at that location in the other blade (not shown), so it is reasonable to assume that the member in Figure 53 was quite close to failure as well. The spikes or peaks at the edges of the holes

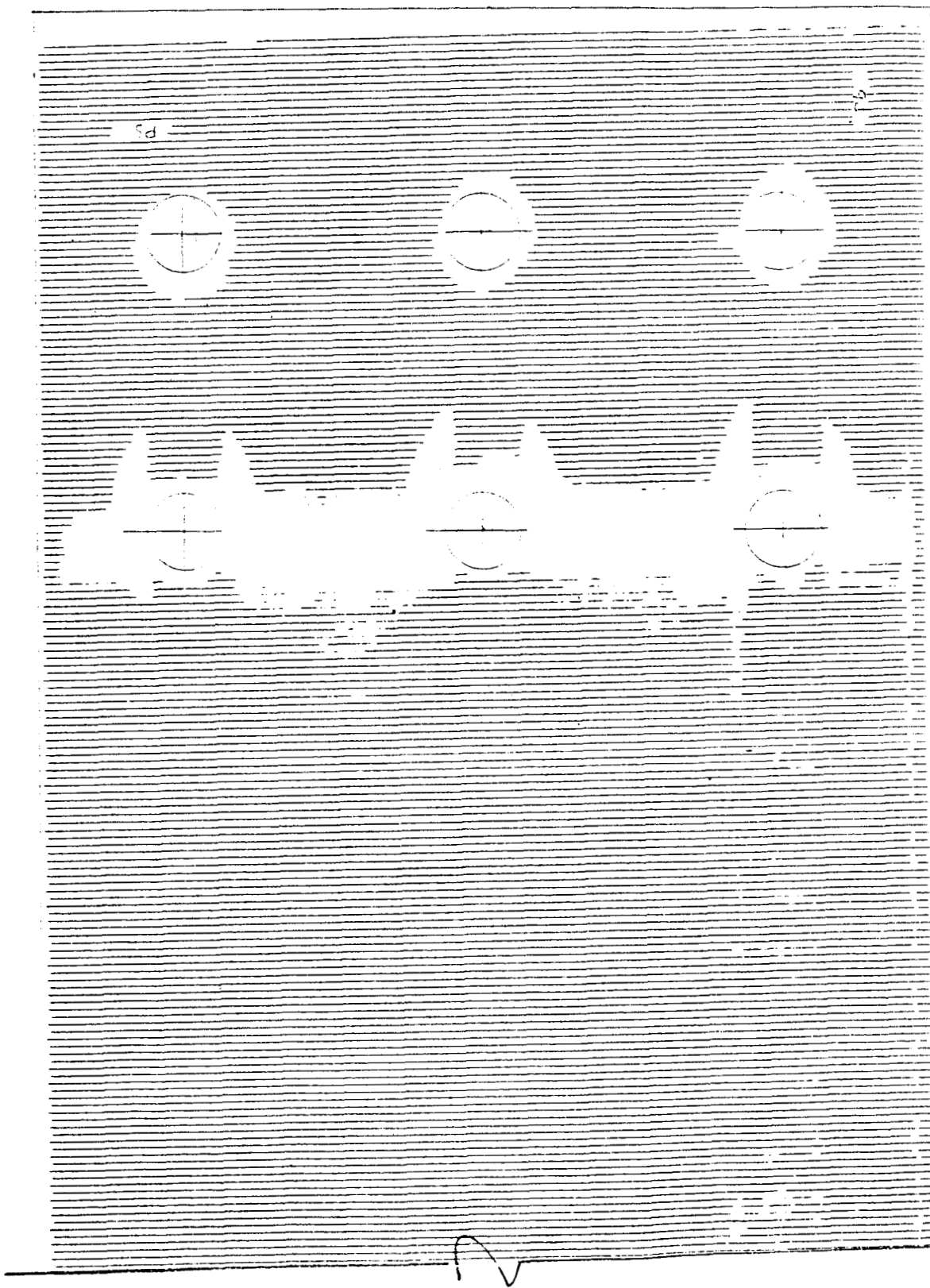


FIGURE 53. JT12CF BLADE "A" C-SCAN

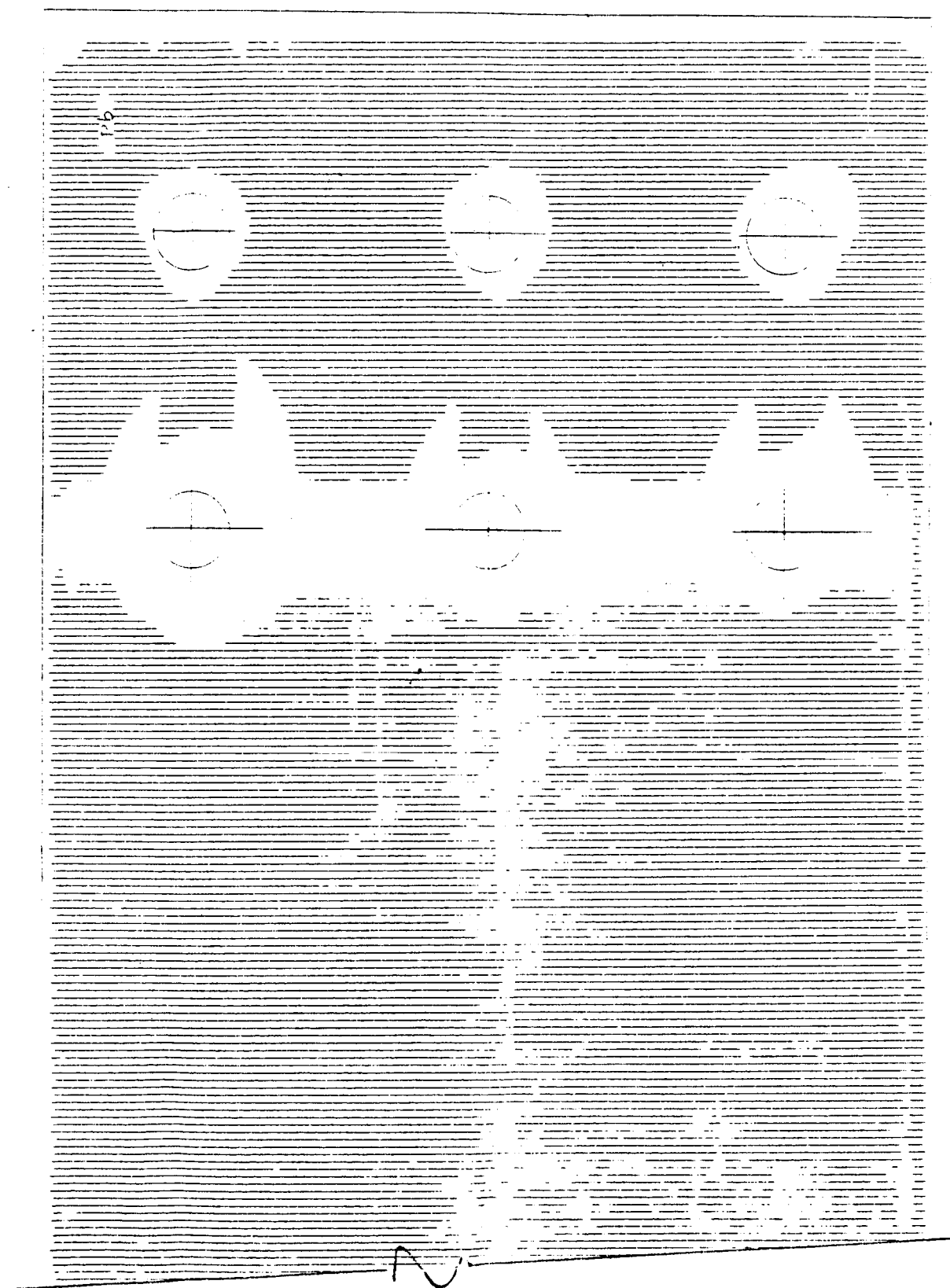


FIGURE 54. JT12IF BLADE "A" C-SCAN

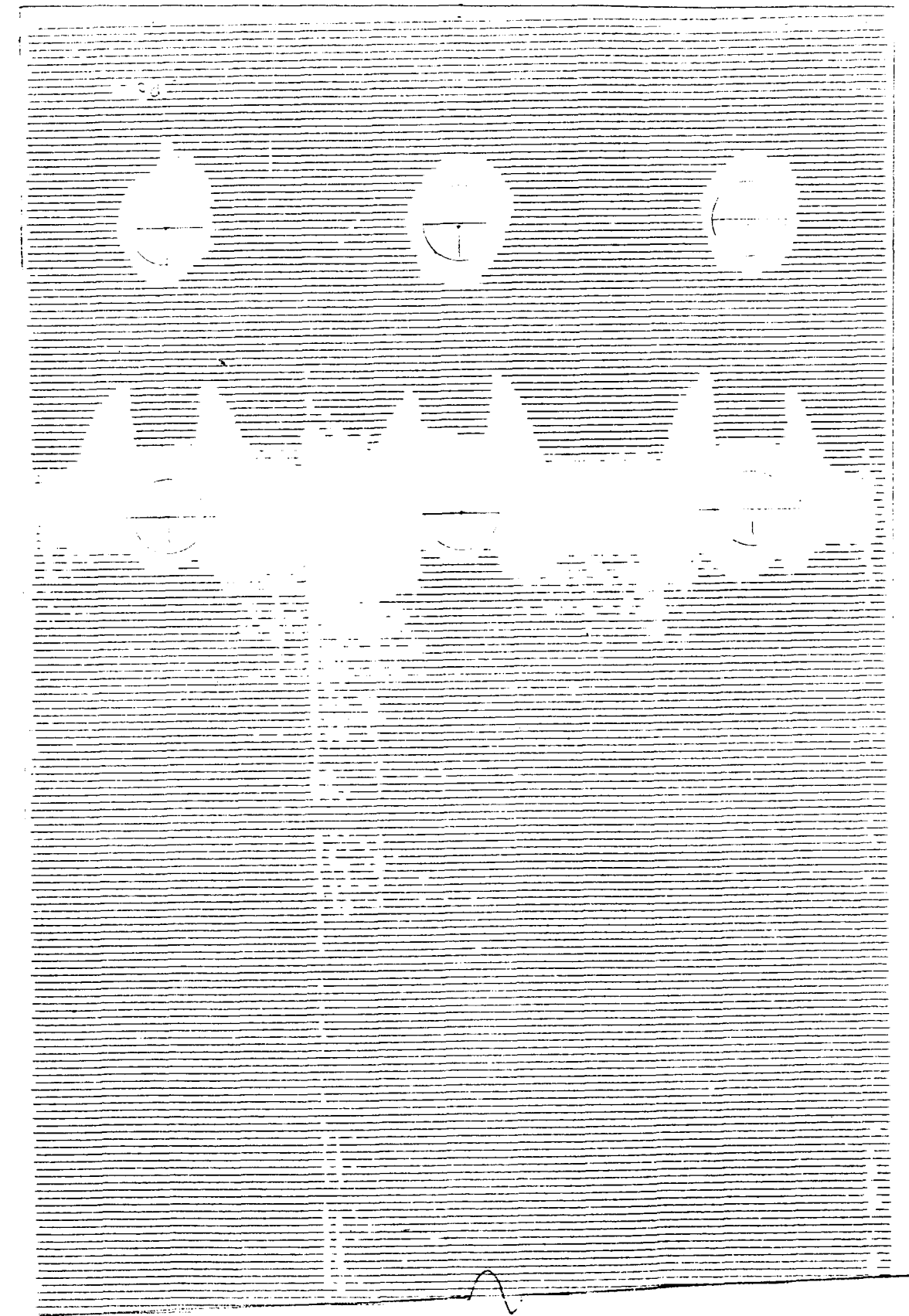


FIGURE 55. JT12IF BLADE "B" C-SCAN

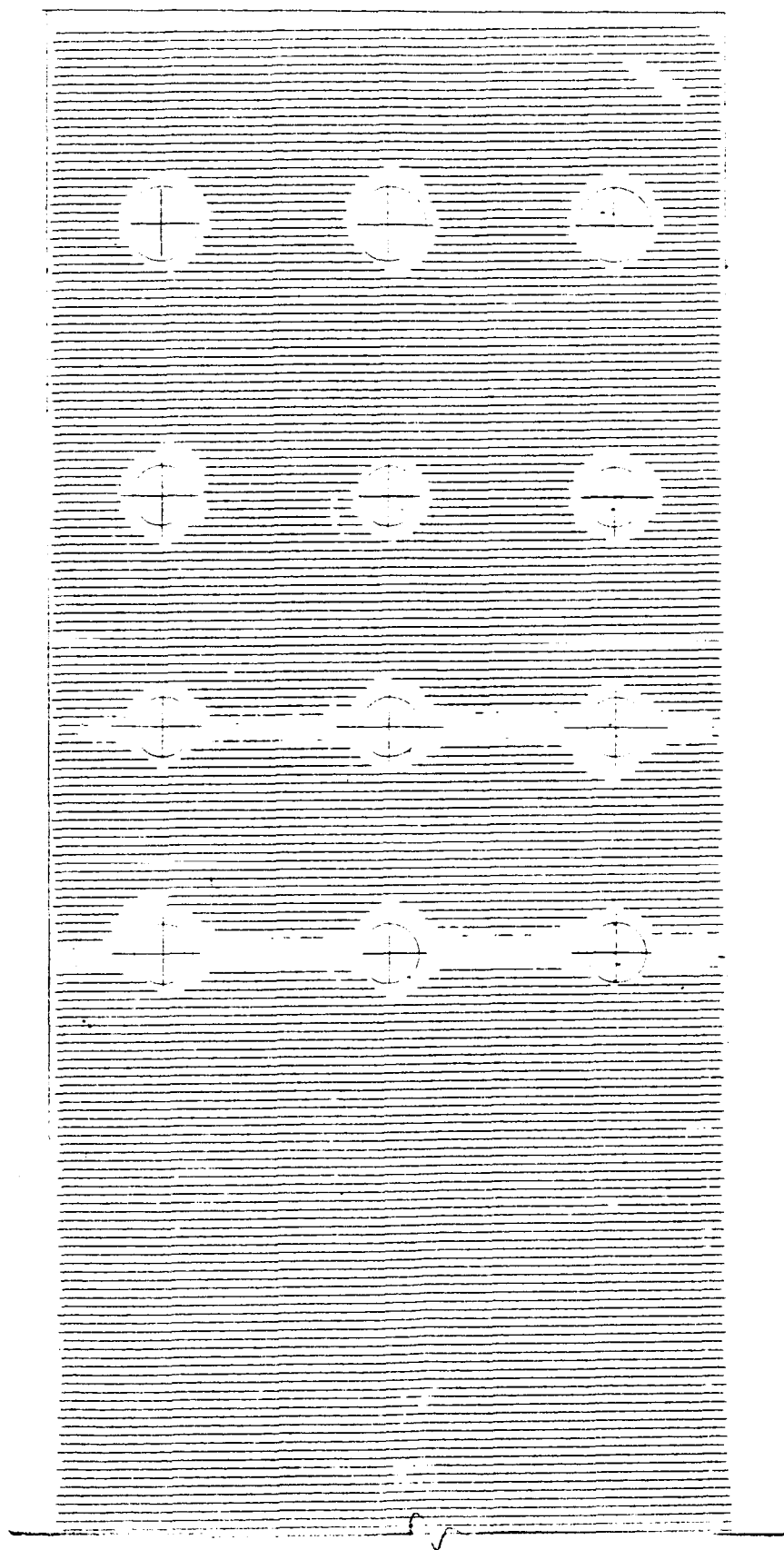


FIGURE 56. JT24CF BLADE "A" C-SCAN

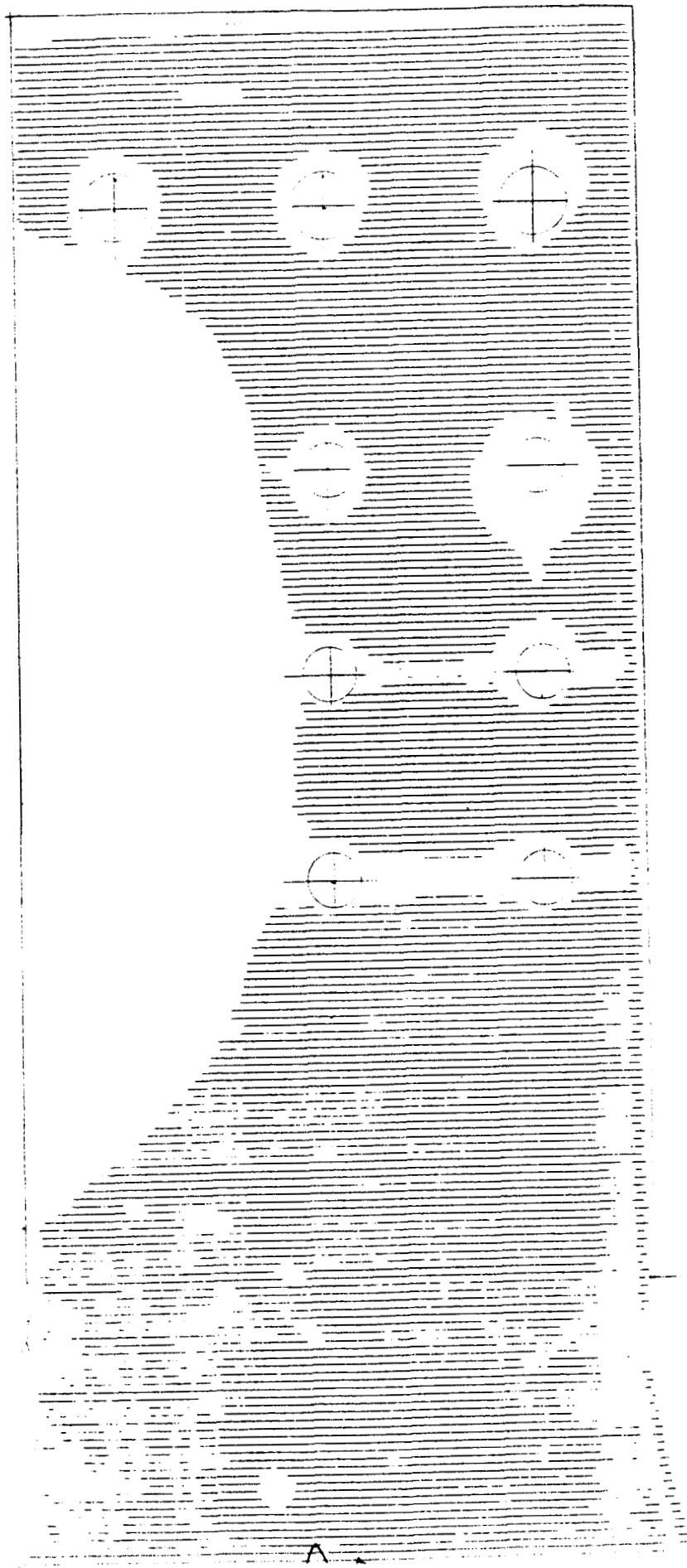


FIGURE 57. JT24CF BLADE "B" C-SCAN

typically represent shearing within 0-degree plies which is caused by the bypass tension stress field interacting with the local compression field on the bearing side of the fastener. It is believed that most of this damage is distributed through the thickness.

The source of delaminations around the other fastener holes is also subject to speculation. Certainly the high bearing loads sustained by these joints may have brought about some damage although the possibility of delaminations resulting from fastener removal or from the drilling operations must also be considered. The specimens were not C-scanned in advance of testing.

The results of C-scans performed on the blades of the JT12IF specimens are shown in Figures 54 and 55. This specimen reached its ultimate load when the fasteners yielded in bending, though the C-scans look much the same as the JT12CF results. Slightly more damage is evident around the fastener holes, probably caused by the more severely bent bolts either during the test or as the bolts were removed.

The two blade members from the JT24CF specimens were C-scanned with the results shown in Figure 56 and 57. Once again, those fastener rows that were subjected to high levels of combined bearing-bypass loads show damage initiated across the entire width of the specimen. Figure 57 shows substantially more damage around the bolt holes than shown for the other blade, and a large section reaching from the side edge nearly to the centerline is delaminated. Although the difficult process of removing the bent bolts may have contributed to this damage, the possibility exists that the specimen simply delaminated under high tensile load. Indeed, several blades from the JT24 test series displayed similar delaminations throughout the thickness. The more extensive delaminations suffered by the interference fit specimens suggests that the bolt bending phenomenon may have contributed to the problem. In any case, the onset of such damage in what were seemingly undamaged parts indicates that more attention to this phenomenon is warranted in future tests.

9.0 CONCLUSIONS

The prime conclusion to be drawn from this investigation is that it is possible to make reliable strength predictions for large multirow bolted joints in fibrous composite laminates. Not all geometries or load conditions have been covered yet, and the testing during this investigation has revealed new failure modes, particularly for compressive loading. With efficient joint design, gross-section strains in the basic skin laminates can reach 0.005, which represents a considerable improvement over the prior state of the art, even for only room-temperature tests.

The most efficient joints have uniform unreinforced skins to maximize the quality of the laminates and to permit straightforward and bolted repairs in service, in combination with reinforced tapered splice plates. Other joint geometries have been shown to be less efficient, both by analysis and test.

The key to obtaining high operating strains in bolted joints in fibrous composite laminates is in restricting the bolt bearing stresses in the most critically loaded locations. The ability to do this depends on the availability of a good load-sharing analysis, such as the A4EJ program, and sufficient test data to provide the input. The nonlinear capability of the program, permitting some bolts to fail in bearing but still carry loads while others accept more, is believed to be necessary for accurate ultimate strength predictions.

The failure of most efficiently designed multirow bolted joints is governed by bearing-bypass load interactions in tension and compression and cannot be explained adequately on the basis of separate bearing and net-section allowables. There is also a strong influence from the presence or absence of through-the-thickness clamp-up for both tensile and compressive loads.

The joint strengths attainable are sensitive to the joint geometry as well as to the fiber and resin employed, although they are insensitive to other minor changes in fiber pattern throughout the optimum design region, which includes the quasi-isotropic layup. For HTS carbon-epoxy laminates, the optimum w/d ratio is on the order of 3 for single-row joints and is more likely to be in the range of 4 to 5 for multirow joints.

The strength of bolted joints in composite laminates is limited by the brittleness of the 350°F cured epoxy resins. It is therefore vital to intersperse the plies as much as possible and not to stack parallel plies together. This program did not attempt to resolve whether 0.010-inch or 0.005-inch tapes are superior - all that can be said is that the analyses have been confirmed for both thicknesses. The more widespread delaminations associated with the thicker plies appear to be of benefit with tensile loading and to be a tolerable weakness for compressive loading. However, other fiber-resin combinations could exhibit quite different behavior in this regard.

With close fit holes (0.002-.003 inch clearance) in the thick materials and ply patterns used in this program, spectrum fatigue bearing loads tested to two flight service lifetimes do not seem to be a problem for lightly clamped sandwiched laminates working up to 45-67 percent ultimate bearing stress, where F_{bru} is 120 ksi. The fatigue specimens were not tested in the presence of the bearing/bypass interaction. Significant and early hole wear resulted from spectrum fatigue peak stresses at 90 percent F_{bru} .

The high gross-section strains exhibited by the bolted joints tested here indicate that highly loaded primary composite structures are feasible, but require more careful design than is customary for ductile metal alloys.

10.0 REFERENCES

1. Hart-Smith, L. J., "Bolted Joints in Graphite-Epoxy Composites," NASA Langley Contract Report NASA CR-144899, January 1976.
2. Hart-Smith, L. J., "Design Methodology for Bonded-Bolted Composite Joints," USAF Contract Report AFWAL-TR-81-3154, Vol. I, February 1982. (Available from DTIC as AD A117 342.)
3. Tate, M. B., and Rosenfeld, S. J., "Preliminary Investigation of the Loads Carried by Individual Bolts in Bolted Joints," NACA TN 1051, May 1946.
4. Hart-Smith, L. J., "Mechanically-Fastened Joints for Advanced Composites - Phenomenological Considerations and Simple Analyses." Fibrous Composites in Structural Design, Edward M. Lenoe, Donald W. Oplinger, and John J. Burke, eds., Plenum Press, C. 1980, pp. 543-574.
5. Nelson, W. D., Bunin, B. L., and Hart-Smith, L. J., "Critical Joints in Large Composite Aircraft Structure." NASA CR-3710, 1983.

APPENDIX A
SUBCOMPONENT TEST DATA

- Strain Gage Readings
- Load vs Head Travel Curves

TENSION TEST DATA

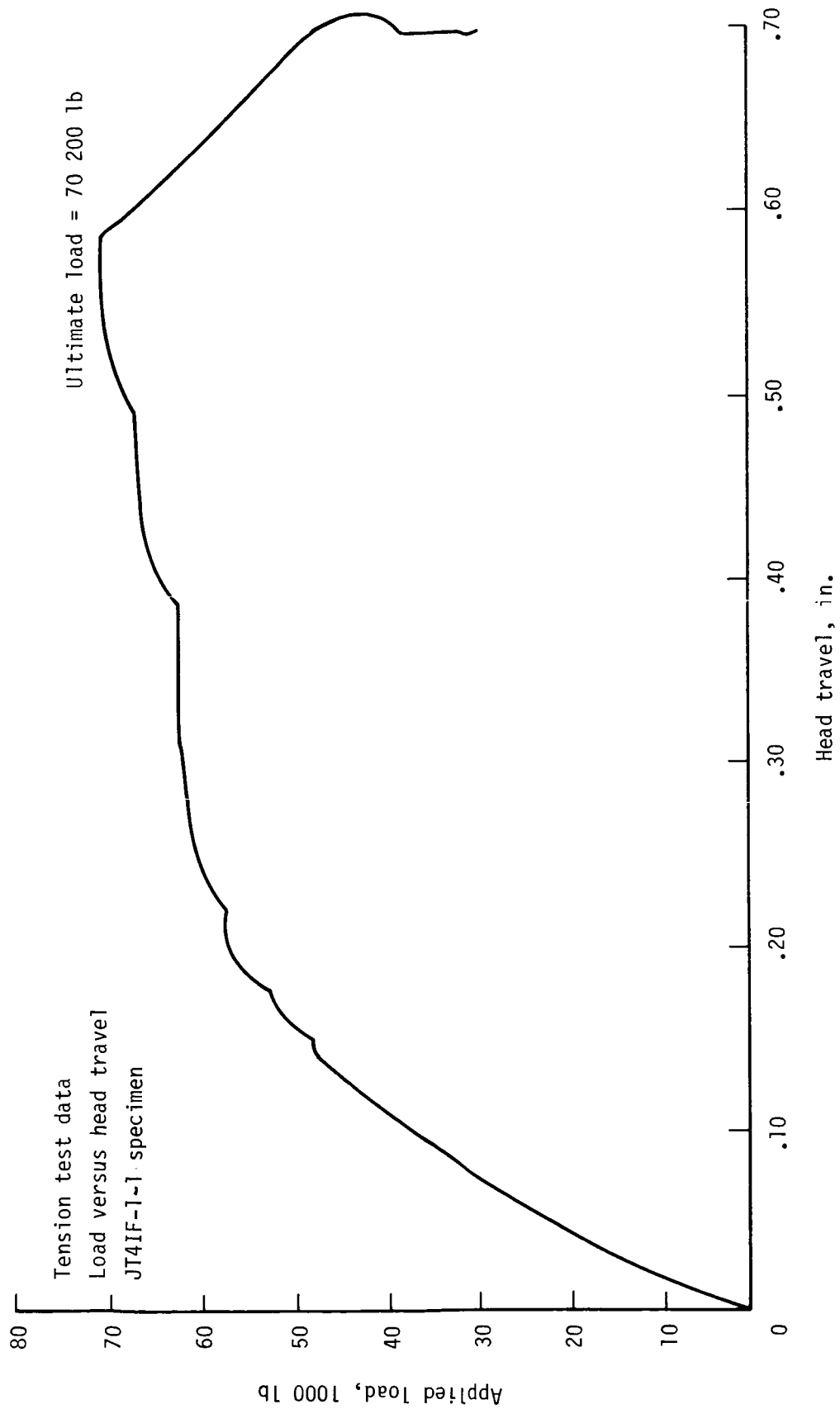
JT4IF-1-1 SPECIMEN

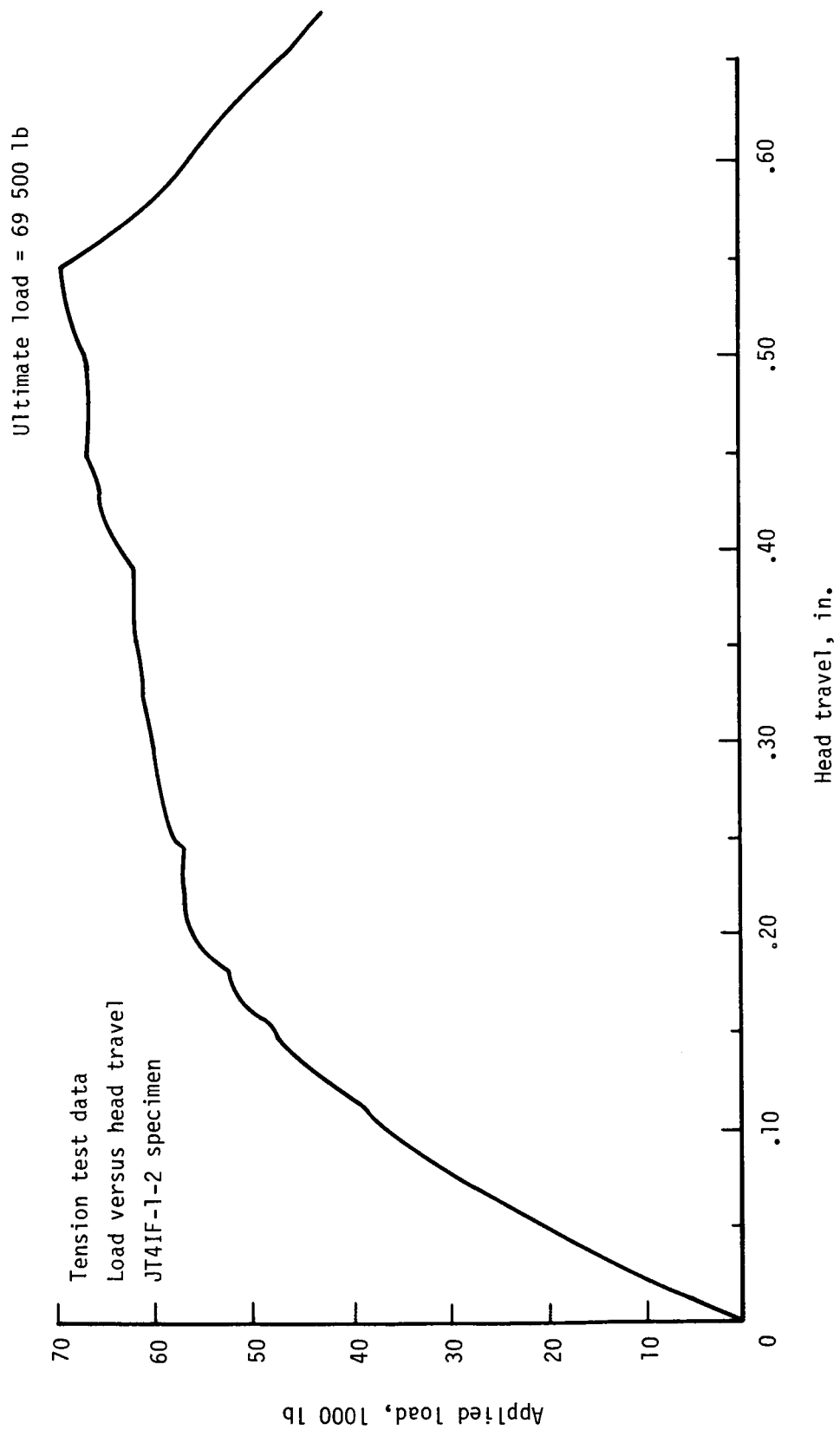
Applied Load (lb)	Strain Readings (μ)			
	Gage 1	Gage 2	Gage 3	Gage 4
0	0	0	0	0
9,540	424	452	444	440
19,080	893	933	923	929
28,620	1385	1429	1426	1433
38,160	1882	1943	1937	1952
47,700	2363	2441	2433	2452
52,470	2605	2692	2686	2691
57,240	2823	2904	2965	2900
62,010	3166	3195	3312	3202
66,780	3392	3469	3525	3496
70,200	Ultimate Load			

TENSION TEST DATA

JT4IF-1-2 SPECIMEN

Applied Load (lb)	Strain Readings (μ)			
	Gage 1	Gage 2	Gage 3	Gage 4
0	0	0	0	0
9,540	532	517	421	413
19,080	1060	1072	844	875
28,620	1593	1627	1288	1346
38,160	2136	2184	1760	1824
47,700	2678	2722	2249	2297
52,470	2968	2952	2488	2540
57,240	3245	3152	2746	2797
62,010	3610	3345	3138	3029
66,780	3888	3560	3364	3288
69,500	Ultimate Load			





TENSION TEST DATA

JT4CF-503-1 SPECIMEN

Applied Load (lb)	Strain Readings (μ)			
	Gage 1	Gage 2	Gage 3	Gage 4
0	0	0	0	0
9,540	405	600	619	464
19,080	878	1192	1208	955
28,620	1388	1778	1795	1488
38,160	1865	2289	2289	1964
47,700	2403	2777	2810	2488
52,470	2665	2976	3017	2713
57,240	2963	3178	3230	2970
62,010	3342	3333	3355	3340
66,780	3889	3421	3678	3579
71,600	Ultimate Load			

TENSION TEST DATA

JT4CF-503-2 SPECIMEN

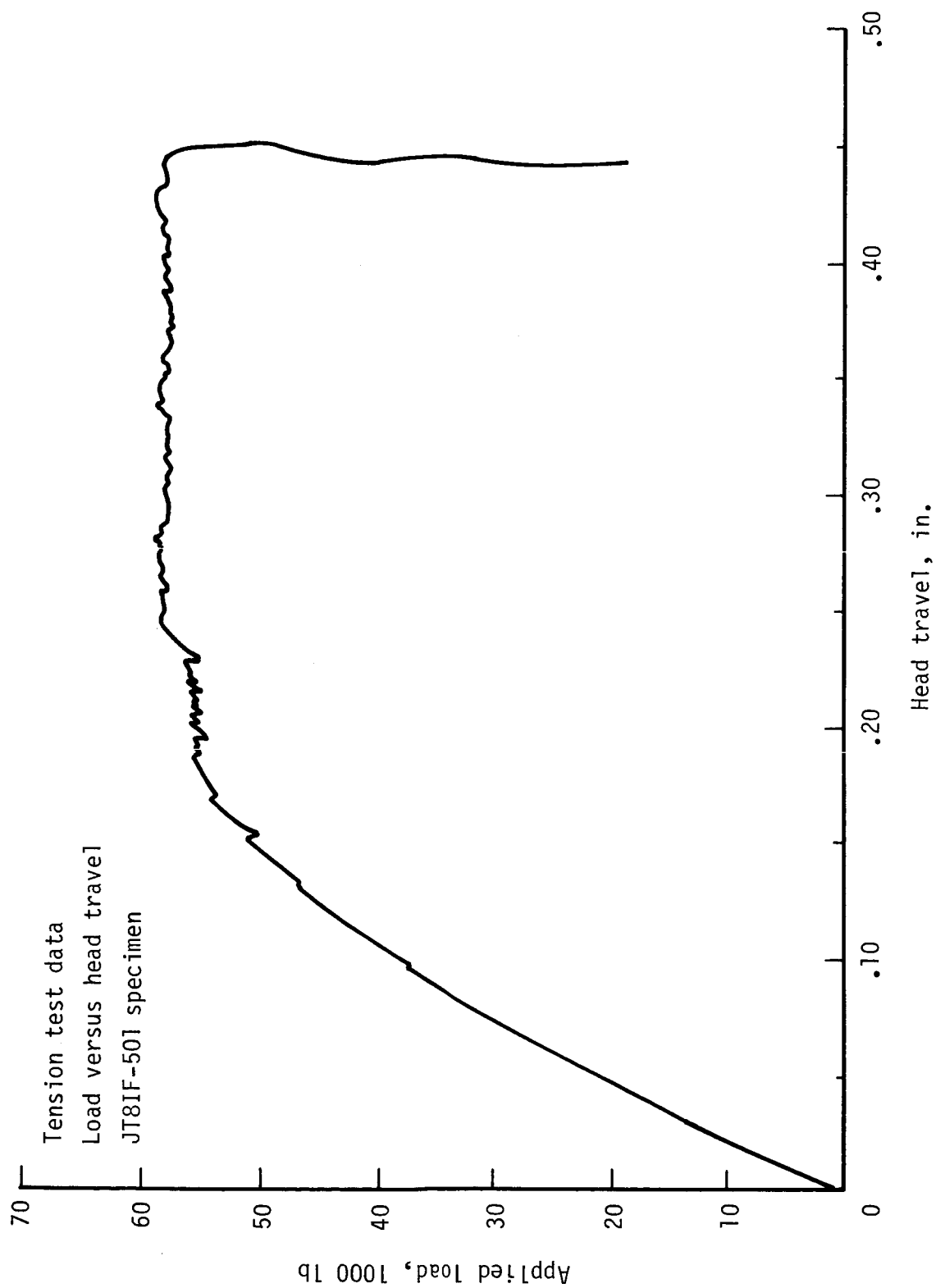
Applied Load (lb)	Strain Readings (μ)			
	Gage 1	Gage 2	Gage 3	Gage 4
0	0	0	0	0
9,540	497	525	603	538
19,080	1004	1038	1167	1065
28,620	1499	1559	1719	1576
38,160	1985	2072	2259	2077
47,700	2462	2575	2773	2568
52,470	2661	2848	3000	2833
57,240	2867	3108	3284	3066
62,010	3140	3341	3581	3394
66,780	3395	3617	3927	3679
71,600	3597	3901	4198	4018
75,400	Ultimate Load			

TENSION TEST DATA

JT8IF-501 SPECIMEN

Strain Readings (μ)

Load (lb)	1	2	3	4	5	6	7	8	9	10	11	12	13	14	15	16	17	18
0	0	0	0	0	0	0	0	0	0	0	0	0	0	0	0	0	0	0
9,540	454	447	370	166	274	337	211	438	555	418	416	196	348	358	282	483	162	575
19,080	914	902	757	338	590	678	429	890	1122	852	854	366	733	716	595	967	343	1155
28,620	1405	1370	1173	525	929	1040	676	1360	1690	1298	1316	538	1144	1092	909	1461	544	1732
38,160	1951	1880	1647	743	1319	1448	1915	1870	2283	1776	1826	746	1592	1518	1224	1992	736	2318
47,700	2533	2383	2159	982	1722	1900	1140	2400	2859	2234	2370	993	2069	1983	1544	2546	895	2898
52,470	2904	2654	2474	1104	1946	2141	1262	3130	3136	2458	2686	1122	2314	2216	1706	2820	928	3178
57,200	3557	3395	-	1372	1865	2588	909	3017	3439	3592	3544	1334	2907	2626	2425	3206	855	3504
60,500	Ultimate Load																	



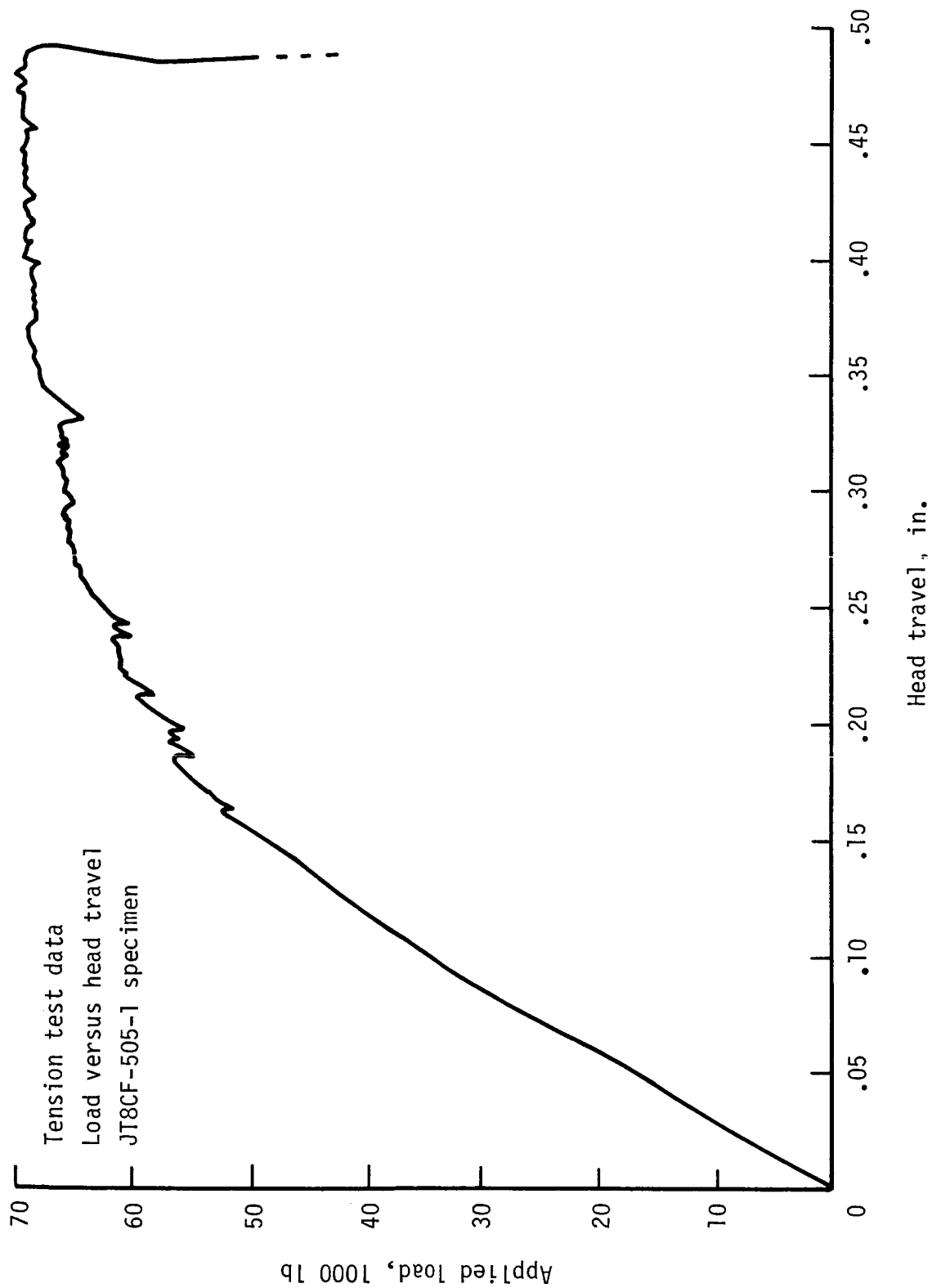
TENSION TEST DATA

JT8CF-505-1 SPECIMEN

Strain Readings (μ)

Load (lb)	1	2	3	4	5	6	7	8	9	10	11	12	13	14	15	16	17	18
0	0	0	0	0	0	0	0	0	0	0	0	0	0	0	0	0	0	0
9,540	575	578	556	249	404	421	262	571	596	550	547	187	514	353	455	545	303	565
19,080	1124	1128	1086	546	802	897	530	1165	1177	1081	1090	441	1003	776	838	1109	579	1131
28,620	1650	1658	1605	821	1201	1355	802	1737	1743	1582	1608	692	1492	1192	1217	1657	846	1679
38,160	2173	2197	2131	1090	1606	1817	1084	2314	2313	2085	2132	951	1992	1626	1600	2221	1112	2236
47,700	2686	2712	2641	1395	1970	2314	1292	2901	2868	2560	2648	1226	2490	2092	1945	2791	1332	2777
52,470	2934	2975	2872	1540	2113	2553	1330	3176	3128	2786	2874	1355	2717	2304	2385	3054	1398	3012
54,800	3050	3207	3019	1621	2153	2730	1241	3384	3311	2890	3070	1449	2926	2473	2182	3230	1389	3195
57,200	3920	3352	3154	1700	2225	2853	1281	3522	3445	3037	4050	1510	3022	2571	2238	3352	1432	3316
	-	-	-	-	-	-	-	-	-	-	-	-	-	-	-	-	-	-
62,000	4391	3696	3465	1913	2402	3154	1376	3846	3718	3344	4466	1668	3303	2800	2410	3616	1554	3536
65,000	5491	4090	4550	2073	2556	3453	1303	4124	3906	3668	4932	1822	4567	3091	2486	3880	1434	3715
70,100						-	-	-	-	-	-	-	-	-	-	-	-	-
	Ultimate Load																	

Ultimate load = 70 100 lb

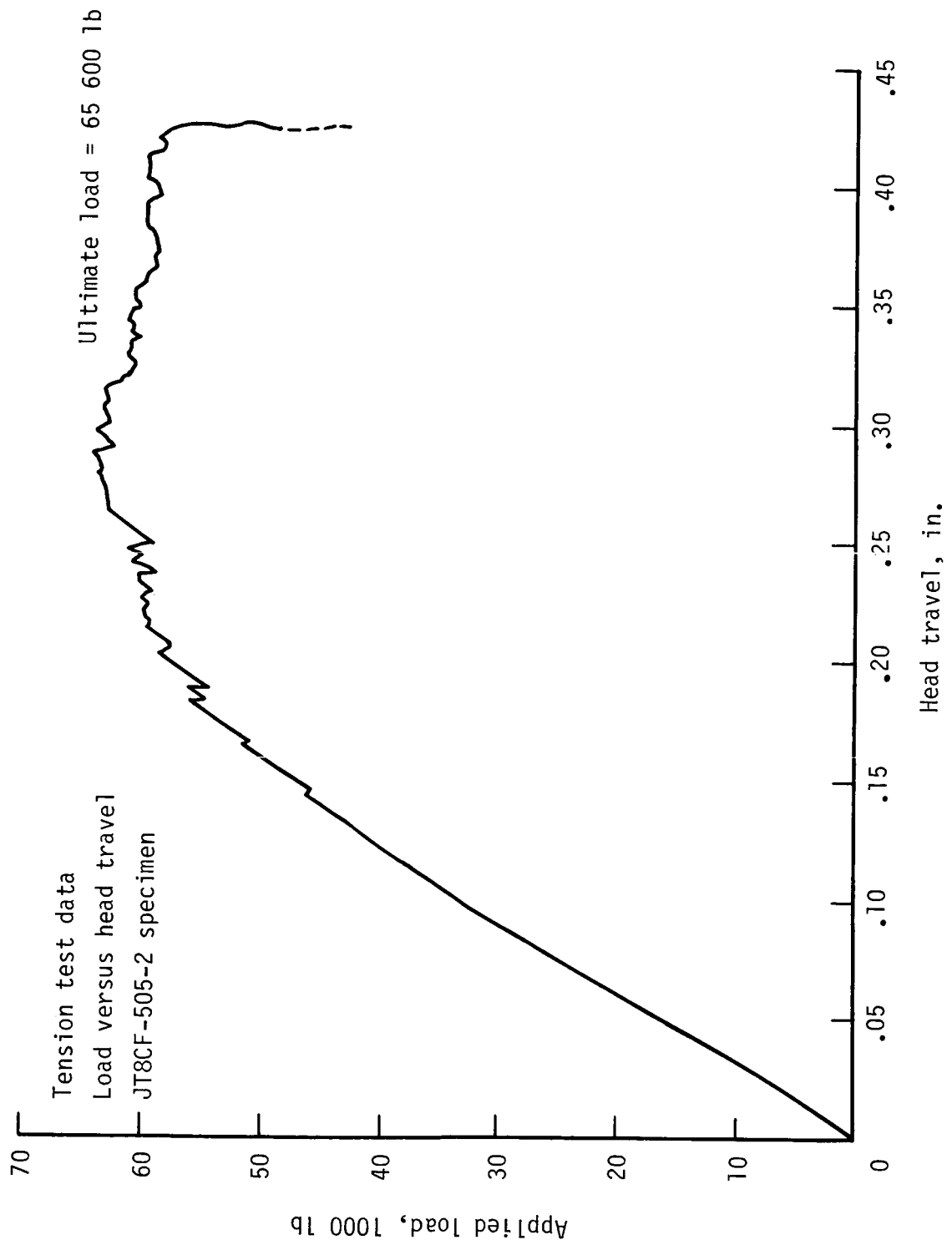


TENSION TEST DATA

JT8CF-505-2 SPECIMEN

Strain Readings (μ)

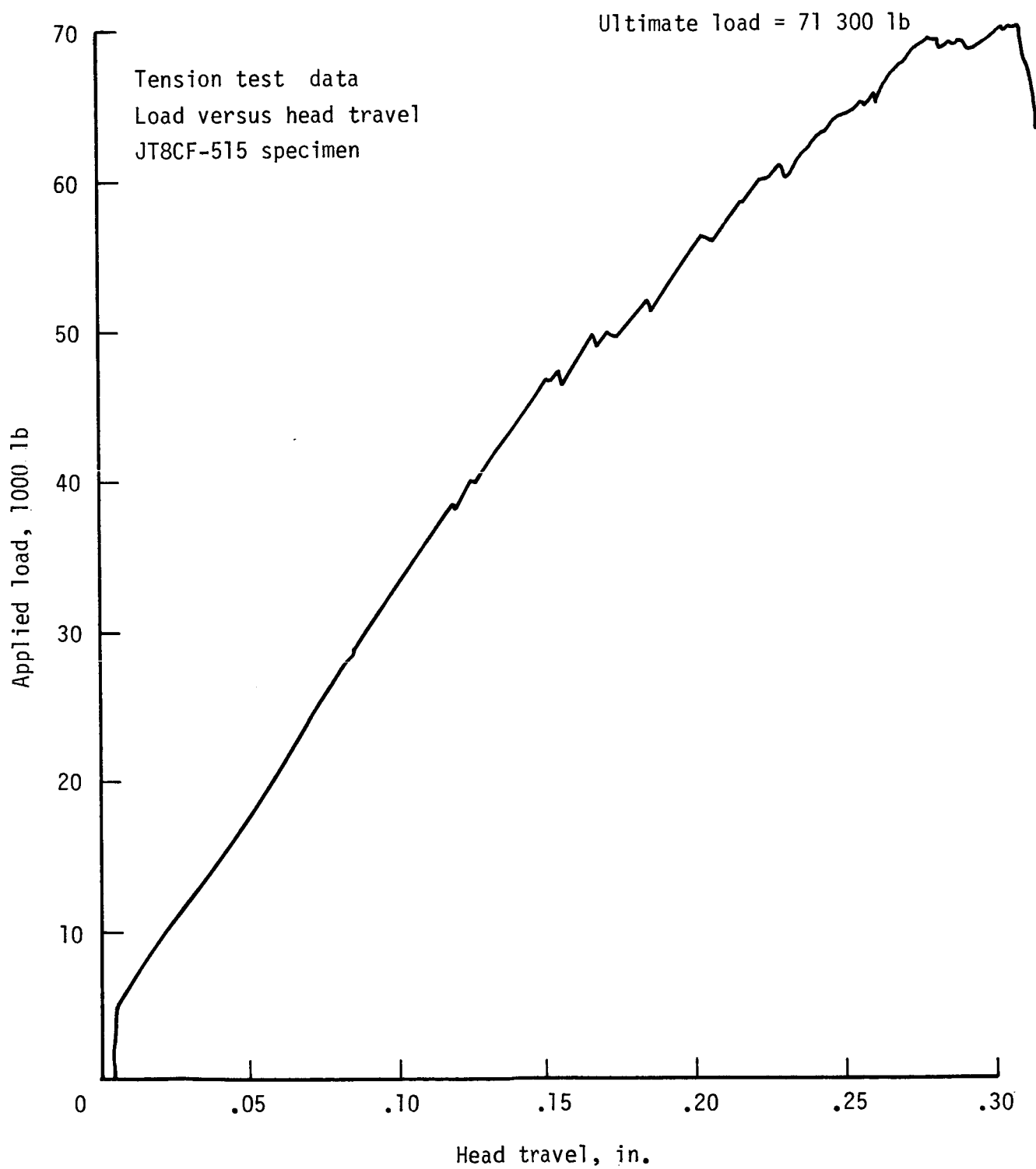
Load (lb)	1	2	3	4	5	6	7	8	9	10	11	12	13	14	15	16	17	18
0	0	0	0	0	0	0	0	0	0	0	0	0	0	0	0	0	0	0
9,540	587	546	573	229	475	404	313	545	597	523	554	240	502	416	418	570	315	601
19,080	1145	1093	1105	477	902	845	595	1113	1197	1048	1035	509	1013	845	820	1155	609	1203
28,620	1697	1625	1629	720	1322	1273	879	1679	1793	1565	1608	774	1521	1273	1222	1744	874	1790
38,160	2244	2166	2155	974	1726	1718	1147	2247	2389	2076	2127	1043	2026	1712	1605	2386	1154	2381
47,700	2749	2680	2628	1247	2040	2204	1306	2814	1364	2563	2613	1342	2484	2203	1897	3144	1280	2950
52,470	3025	2947	2888	1394	2229	2466	1421	3115	3257	2821	2870	1500	2730	2463	2045	3529	1336	3247
55,800	3144	3236	3033	1530	2305	2707	1380	3380	3520	3063	3092	1652	2874	2710	2099	3817	1330	3501
60,400	3642	3615	3475	1713	2444	3020	1239	3705	3812	3578	3605	1905	3261	3073	2149	4512	1341	3826
65,600	Ultimate Load																	



TENSION TEST DATA

JT8CF-515 SPECIMEN

Applied Load (lb)	Strain Readings (μ)			
	Gage 1	Gage 2	Gage 3	Gage 4
0	0	0	0	0
9,540	723	629	641	437
19,080	1451	1244	1238	828
28,620	2155	1876	1895	1204
38,160	2842	2504	2447	1579
47,700	3485	3054	2954	1940
52,470	3579	3548	3215	2144
57,240	3890	3858	3478	2323
62,010	4220	4330	3805	2507
66,780	5405	4750	4119	2698
71,300	Ultimate Load			



TENSION TEST DATA

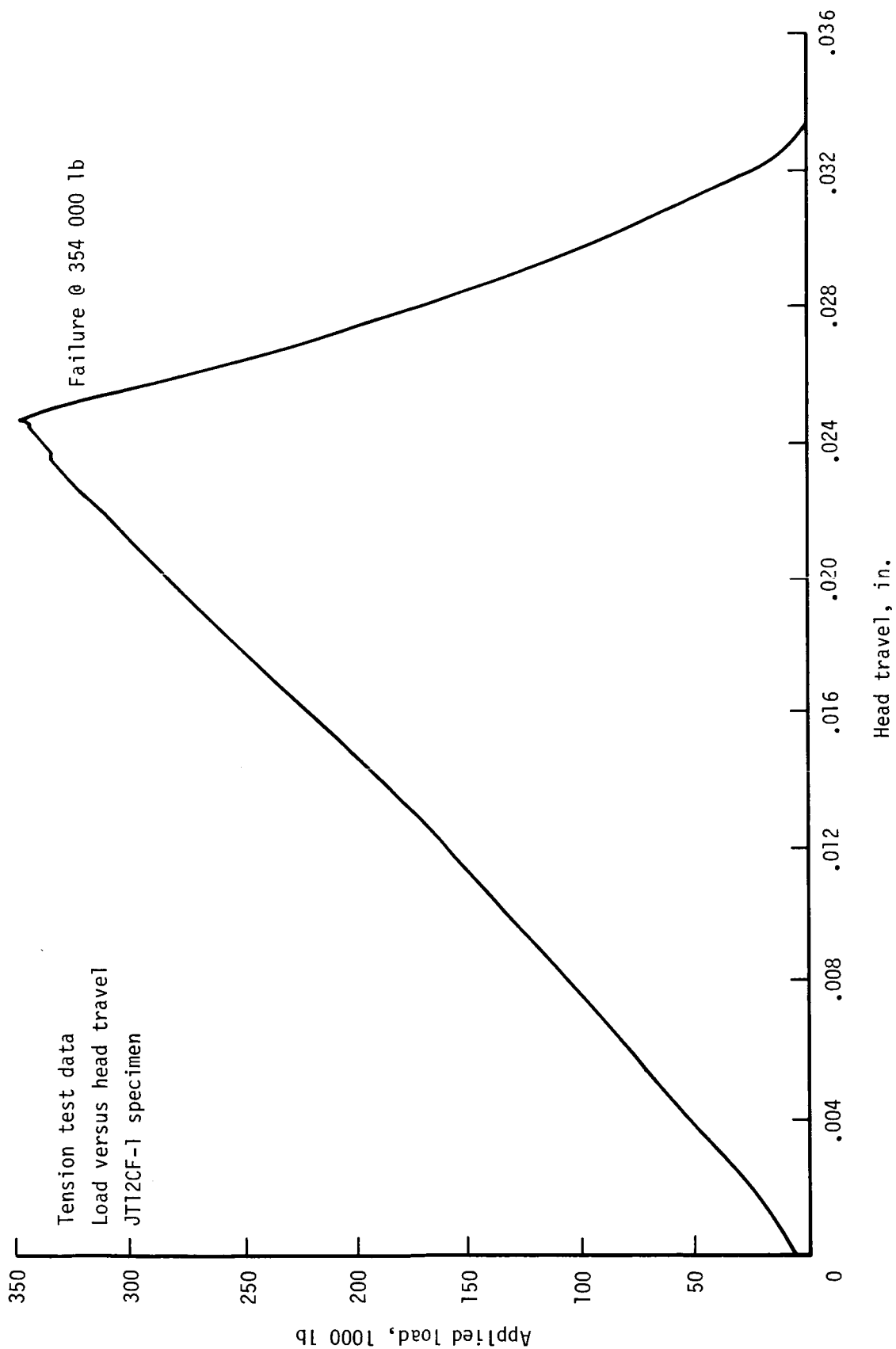
JT12CF-1 SPECIMEN

Applied Load (KIPS)	Strain Readings (μ)			
	Gage 1	Gage 2	Gage 3	Gage 4
0	0	0	0	0
48K	443	512	405	446
96K	885	948	832	879
140K	1274	1320	1221	1263
192K	1728	1748	1700	1727
240K	2157	2134	2136	2142
264K	2375	2321	2353	2337
288K	2601	2515	2570	2525
312K	2833	2699	2784	2712
336K	3070	2915	2999	2901
354K	Ultimate Load			

TENSION TEST DATA

JT12IF-501 SPECIMEN

Applied Load (KIPS)	Strain Readings (μ)			
	Gage 1	Gage 2	Gage 3	Gage 4
0	0	0	0	0
48K	400	415	348	364
96K	800	805	731	739
140K	1172	1162	1089	1082
192K	1629	1607	1552	1517
240K	2062	2024	1978	1922
264K	2270	2226	2180	2122
288K	2474	2450	2393	2325
312K	2689	2679	2626	2544
336K	2943	2843	2878	2816
350K	Ultimate Load			

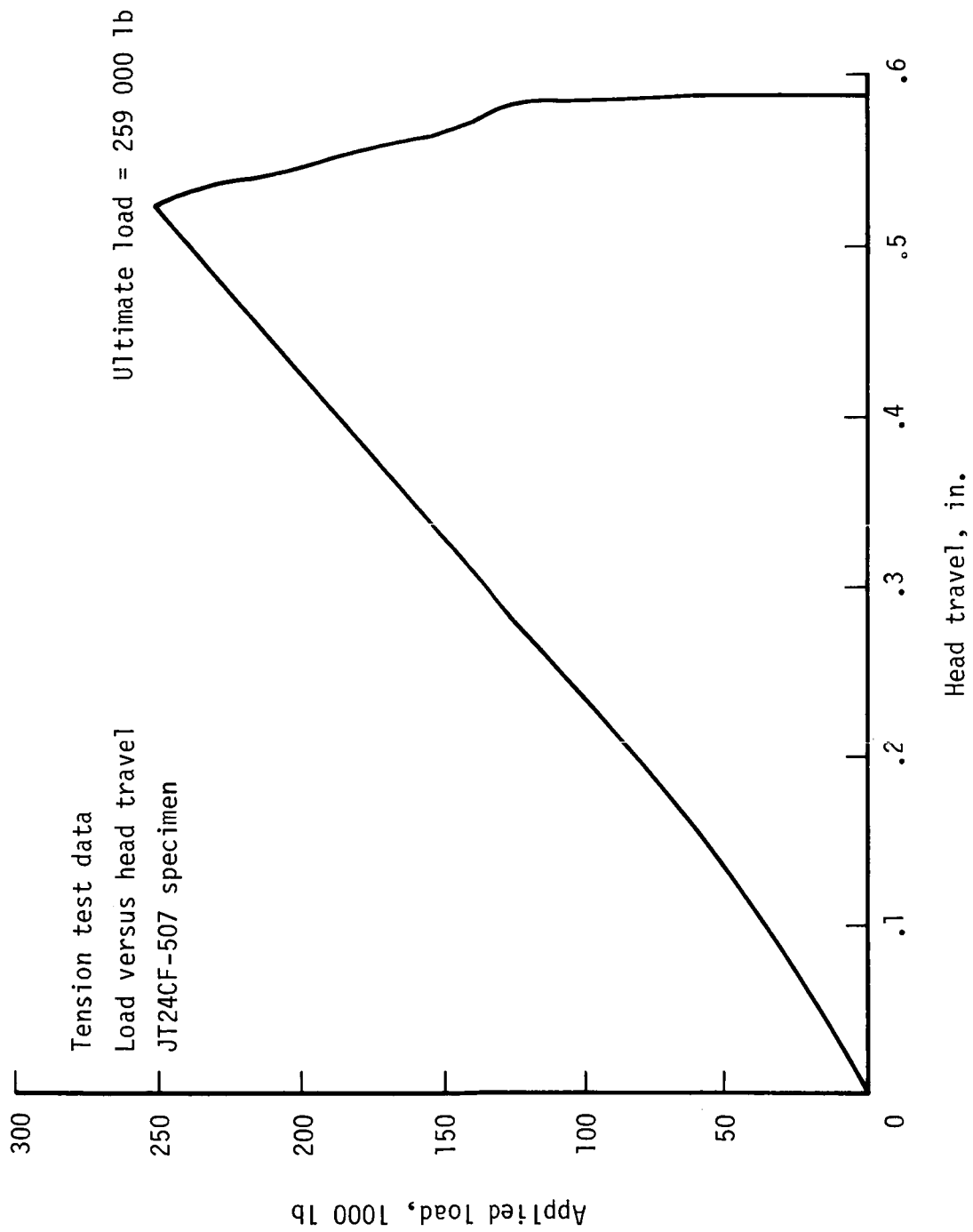


TENSION TEST DATA

JT24CF-507 SPECIMEN

Strain Readings (μ)

Load (KIPS)	1	2	3	4	5	6	7	8	9	10	11	12	13	14	15	16	17	18
0	0	0	0	0	0	0	0	0	0	0	0	0	0	0	0	0	0	0
28	464	466	531	151	490	350	346	537	548	361	356	379	123	328	264	245	411	431
56	927	922	979	461	939	827	738	1128	1115	776	789	832	346	738	659	564	955	941
84	1338	1332	1379	730	1342	1260	1081	1677	1638	1170	1189	1224	593	1082	1061	846	1486	1432
112	1722	1718	1753	982	1719	1671	1396	2199	2130	1545	1572	1596	835	1409	1455	1118	2000	1904
140	2112	2113	2133	1239	2103	2100	1702	2743	2637	1933	1968	1985	1084	1747	1867	1398	2532	2390
154	2317	2322	2333	1378	2298	2333	1830	3036	2904	2140	2177	2194	1220	1927	2091	1543	2820	2650
168	2516	2526	2558	1531	2512	2587	1964	3319	3164	2347	2379	2403	1361	2102	2342	1666	3121	2907
182	2746	2763	2749	1666	2701	2816	2080	3584	3402	2517	2566	2577	1498	2282	2590	1771	3403	3135
196	2972	2964	2927	1808	2853	3054	2163	3876	3671	2664	2784	2717	1650	2495	2856	1880	3692	3374
210	3138	3161	1005	1988	3582	3324	2263	4170	3911	2802	2956	2070	1845	2841	3119	1994	3963	3600
224	3393	3317	1310	2124	3763	3590	2312	4524	4205	3035	3117	2254	2055	2941	3422	1914	4301	3878
238	3657	3528	1485	2256	3974	3874	2385	4854	4478	3211	3324	2508	2209	3069	3708	1939	4619	4150
252	3839	3702	1424	2344	4087	4131	2419	5239	4752	3403	3500	2737	2319	3223	3984	1997	4945	4412
259	Ultimate Load																	



TENSION TEST DATA

JT24IF-509 SPECIMEN

Strain Readings (μ)

Load (KIPS)	1	2	3	4	5	6	7	8	9	10	11	12	13	14	15	16	17	18
0	0	0	0	0	0	0	0	0	0	0	0	0	0	0	0	0	0	0
28	386	448	176	355	310	560	423	260	340	324	380	168	316	285	330	376	259	511
56	784	840	346	685	615	1083	833	495	639	682	722	329	623	555	605	735	460	984
84	1190	1236	547	1051	949	1607	1283	769	979	1065	1079	517	981	853	909	1124	702	1468
112	1611	1651	791	1451	1343	2159	1804	1063	1353	1474	1460	752	1384	1224	1266	1603	994	1995
140	2015	2052	1037	1838	1755	2689	2340	1330	1717	1879	1845	995	1794	1629	1637	2128	1286	2522
154	2210	2240	1156	2016	1959	2938	2600	1413	1872	2072	2027	1110	1985	1830	1810	2385	1406	2772
168	2415	2438	1285	2200	2186	3201	2882	1448	2015	2276	2219	1238	2187	2054	1983	2664	1489	3036
182	2622	2640	1426	2388	2439	3475	3180	1480	2158	2490	2412	1380	2380	2316	2112	2975	1471	3310
196	2832	2845	1565	2590	2684	3764	3480	1554	2316	2710	2615	1518	2588	2564	2280	3280	1541	3588
210	3012	3009	1676	2734	2882	3980	3738	1582	2418	2869	2769	1627	2746	2769	2399	3542	1583	3805
224	3250	3185	1833	2880	3156	4277	4074	1630	2667	3115	2935	1788	2930	3076	2512	3918	1580	4112
238	3440	3210	1950	-	3314	4500	4520	1708	3148	3278	2973	1909	-	3273	2939	4230	1652	4307
252	3510	3511	2090	-	3612	4790	4956	1849	3407	3527	3222	2055	-	3612	3112	4745	1669	4635
265	Ultimate Load																	

COMPRESSION TEST DATA

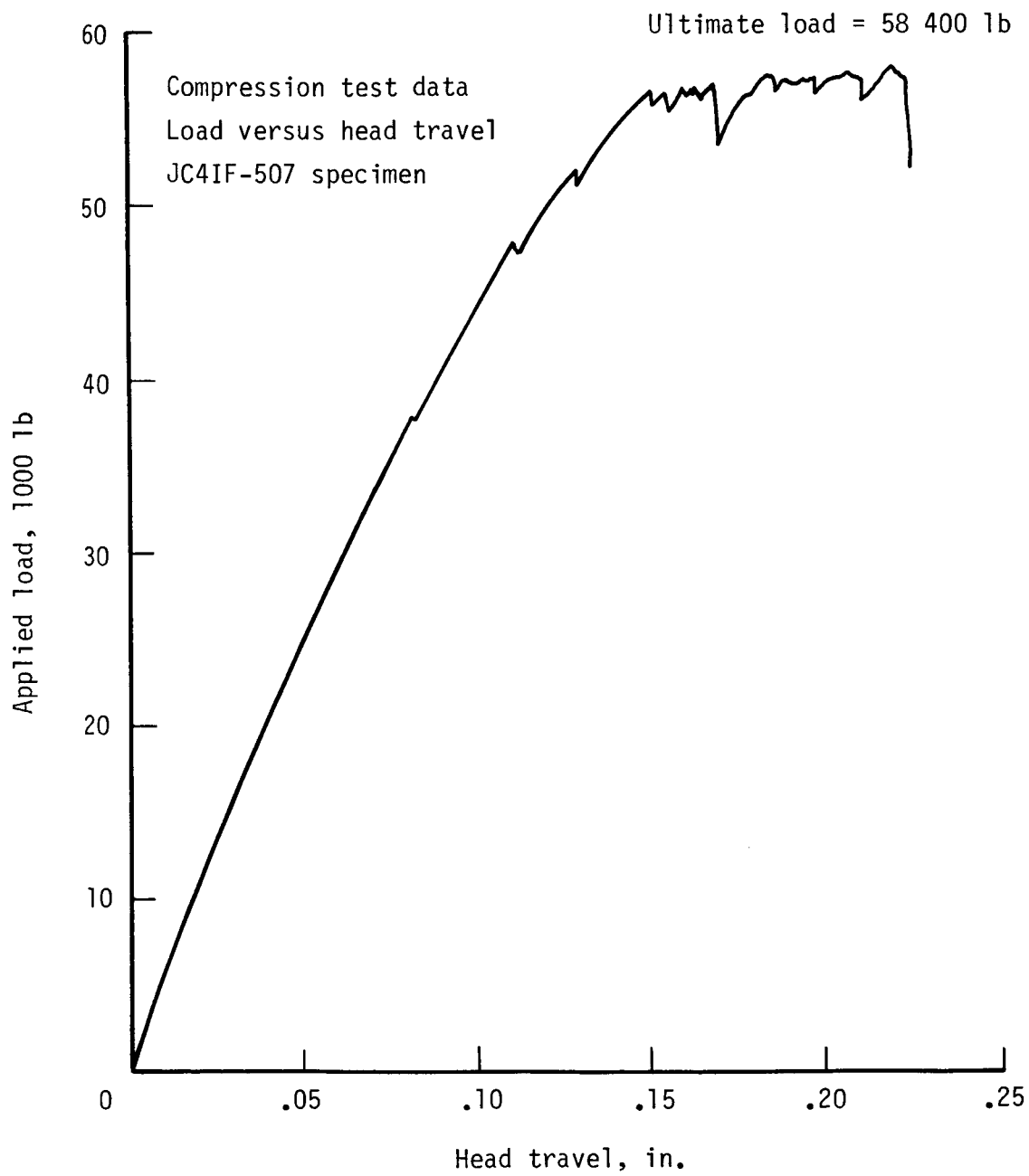
JC4CF-511 SPECIMEN

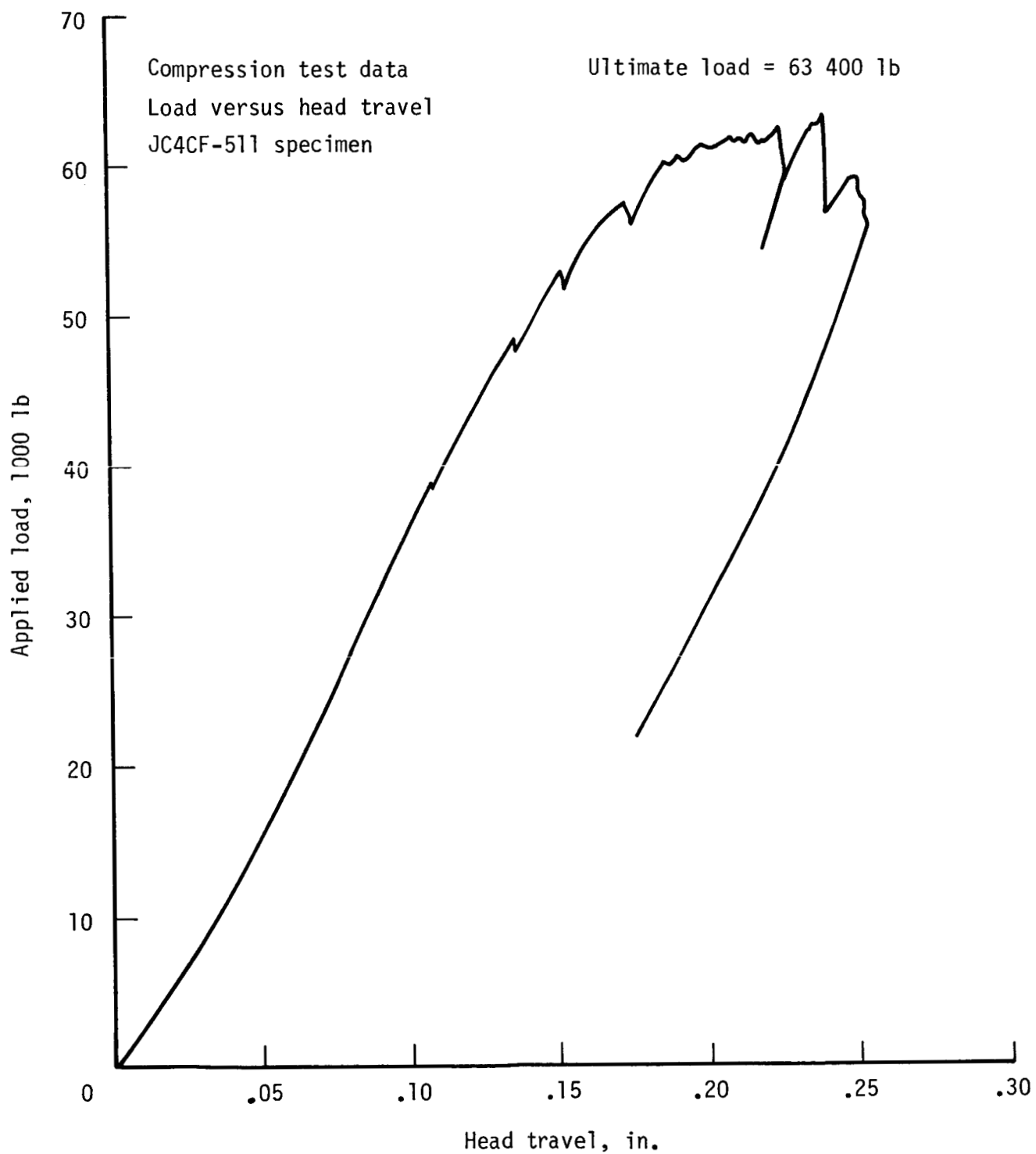
Applied Load (lb)	Strain Readings (μ)			
	Gage 1	Gage 2	Gage 3	Gage 4
0	0	0	0	0
9,540	-733	-718	-375	-355
19,080	1293	1287	858	845
28,620	1830	1850	1301	1309
38,160	2291	2256	1771	1817
47,700	2765	2705	2260	2305
52,470	3060	2992	2545	2627
57,240	3386	3266	2841	3003
62,010	4090	3690	3304	3587
63,400	Ultimate Load			

COMPRESSION TEST DATA

JC4IF-507 SPECIMEN

Applied Load (lb)	Strain Readings (μ)			
	Gage 1	Gage 2	Gage 3	Gage 4
9,540	542	544	642	602
19,080	1132	1120	1215	1176
28,620	1742	1719	1815	1770
38,160	2340	2332	2415	2361
47,700	2980	2977	3059	2999
52,470	3333	3290	3401	3030
57,240	3800	3750	3750	3830
58,400	Ultimate Load			





COMPRESSION TEST DATA

JC8IF-509 SPECIMEN

Strain Readings (μ)

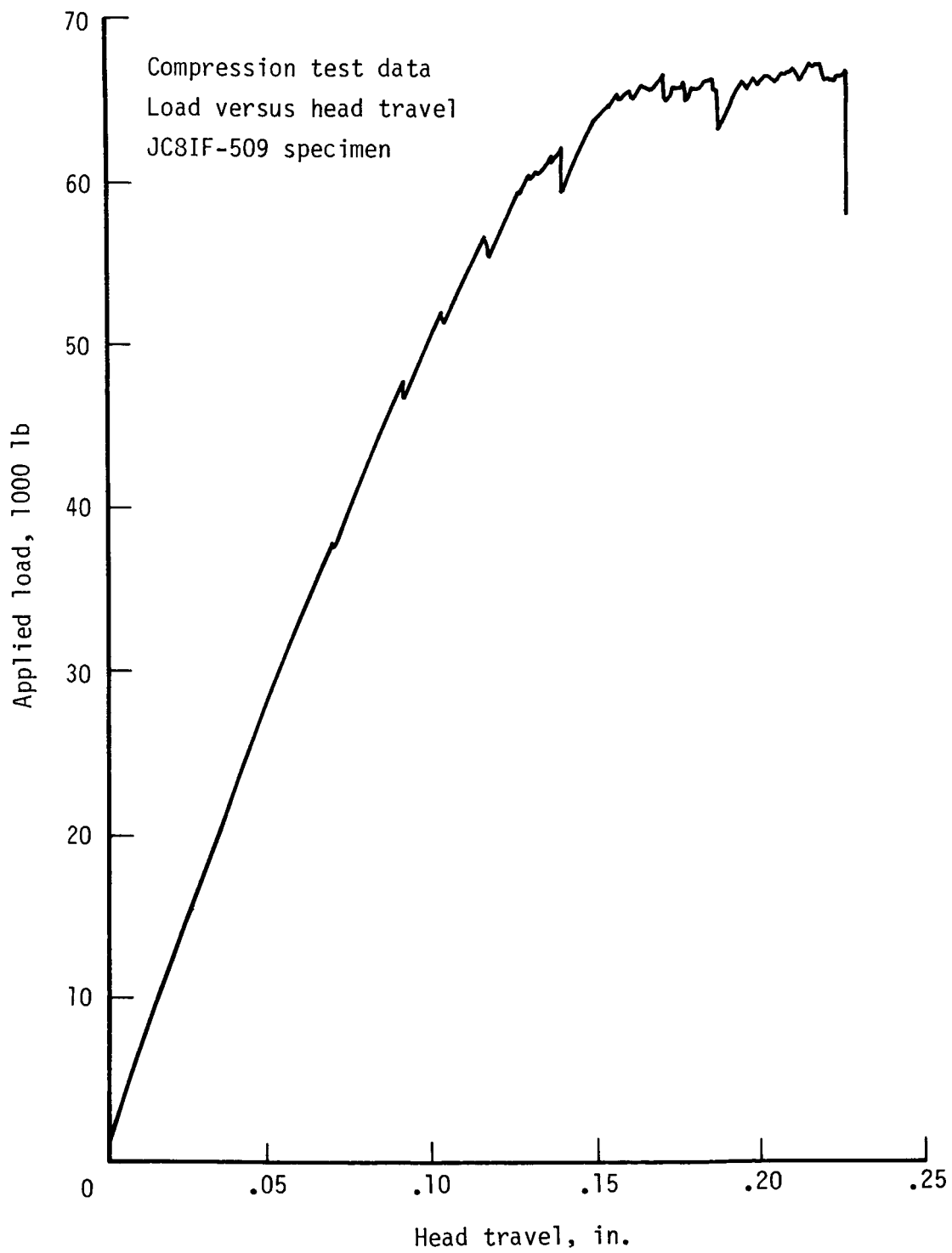
Load (lb)	1	2	3	4	5	6	7	8	9	10	11	12	13	14	15	16	17	18
0	0	0	0	0	0	0	0	0	0	0	0	0	0	0	0	0	0	0
9,540	433	486	414	140	382	346	272	285	614	397	405	125	349	296	299	409	162	491
19,080	890	956	846	260	696	671	416	930	1165	830	840	272	737	635	645	877	402	1067
28,620	1365	1446	1307	375	1065	995	631	1385	1722	1290	1291	423	1136	983	980	1351	615	1650
38,160	1876	1955	1802	490	1453	1333	845	1870	2308	1764	1775	585	1550	1349	1315	1850	816	2263
47,700	2405	2464	2315	606	1818	1662	1014	2350	2875	2252	2269	740	1956	1699	1617	2340	986	2867
52,470	2700	2750	2592	675	1998	1843	1105	2612	3182	2520	2540	825	2173	1892	1767	2610	1067	3190
57,240	3017	3029	2881	739	2176	2003	1200	2857	3465	2777	2839	902	2410	2070	1922	2862	1150	3490
62,010	3470	3450	3170	837	2205	2250	1197	3173	3783	3172	3210	1020	2588	2320	1920	3166	1308	3825
67,900	Ultimate Load																	

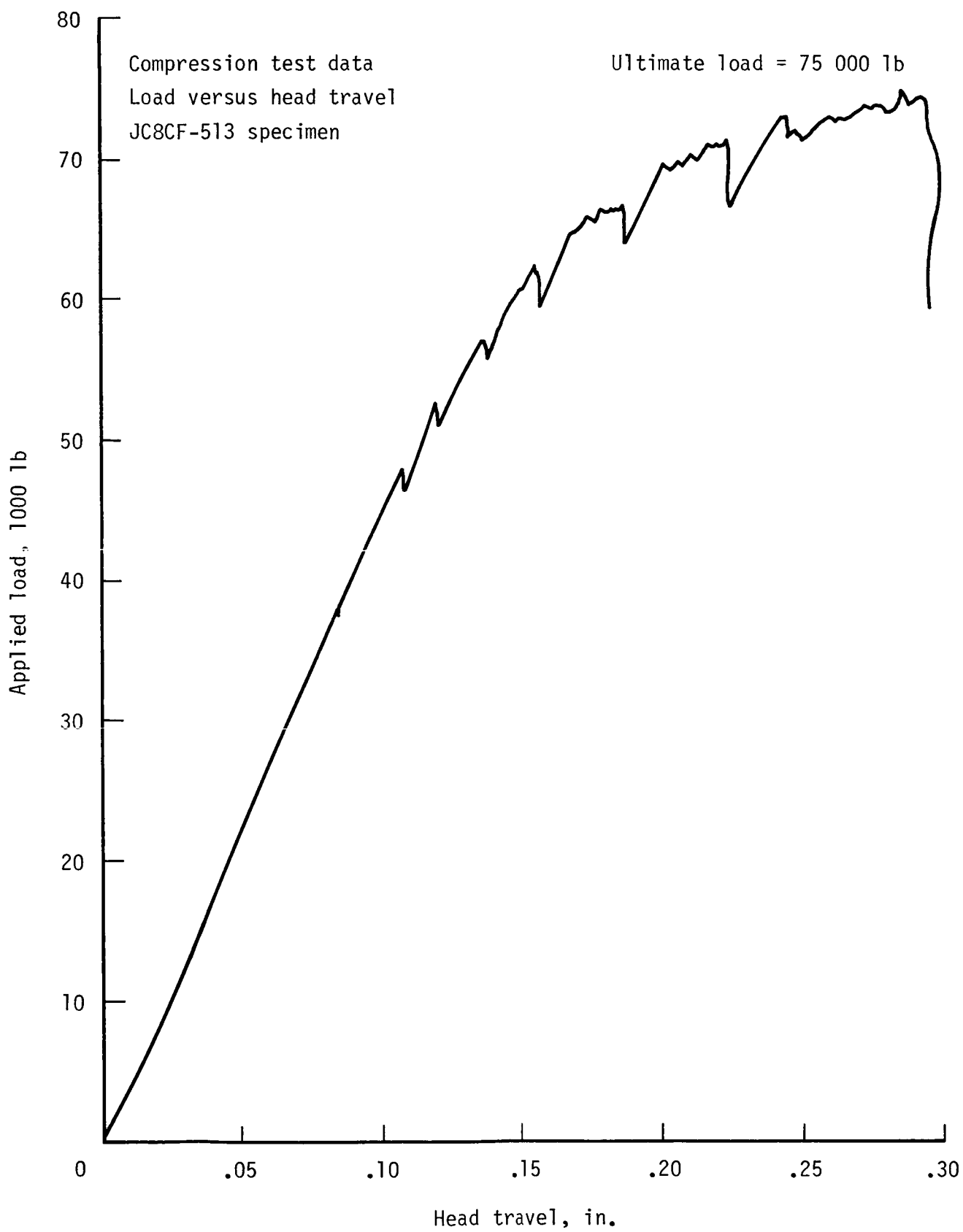
COMPRESSION TEST DATA

JC8CF-513 SPECIMEN

Strain Readings (μ)

Load (lb)	1	2	3	4	5	6	7	8	9	10	11	12	13	14	15	16	17	18
0	0	0	0	0	0	0	0	0	0	0	0	0	0	0	0	0	0	0
9,540	-500	-446	-400	-135	-270	-347	-137	-486	-548	-430	-424	-126	-360	-405	-320	-550	-142	-628
19,080	-982	-909	-812	-255	-240	-690	-259	-1006	-1170	-905	-875	-235	-720	-745	-553	-1038	-230	-1198
28,620	-1436	-1388	-1176	-383	-744	-1028	-360	-1533	-1786	-1385	-1335	-356	-1062	-1107	-748	-1550	-322	-1780
38,160	-1910	-1888	-1540	-523	-937	-1430	-448	-2088	-2430	-1893	-1825	-495	-1420	-1516	-948	-2110	-430	-2392
47,700	-2350	-2382	-1854	-672	-1195	-1816	-591	-2655	-3046	-2399	-2302	-658	-1745	-1948	-1154	-2691	-591	-2983
52,470	-2593	-2643	-2048	-751	-1352	-2012	-675	-2950	-3372	-2670	-2555	-742	-1922	-2160	-1316	-2973	-695	-3283
57,240	-2877	-2980	-2273	-844	-1519	-2242	-755	-3262	-3717	-2990	-2820	-837	-2131	-2380	-1492	-3270	-811	-3590
62,010	-3185	-3360	-2520	-932	-1675	-2441	-865	-3525	-4021	-3311	-3109	-925	-2375	-2595	-1680	-3530	-895	-3842
66,780	-3775	-3930	-2985	-1050	-1968	-2690	-1036	-3834	-4370	-3836	-3622	-1005	-2870	-2772	-1963	-3785	-992	-4135
71,550	-4445	-4885	-3519	-1102	-2235	-2850	-1105	-4000	-4548	-4569	-4255	-1050	-3365	-2932	-2125	-3972	-1090	-4335
75,000	Ultimate Load																	





COMPRESSION TEST DATAJC12IF-505 SPECIMEN

Applied Load (KIPS)	Strain Readings (μ)			
	Gage 1	Gage 2	Gage 3	Gage 4
0	0	0	0	0
48K	-309	-316	-377	-411
96K	715	699	737	795
140K	1056	1027	1071	1132
192K	1478	1427	1495	1561
240K	1892	1826	1889	1959
264K	2093	2010	2081	2156
288K	2314	2217	2287	2378
312K	2533	2436	2507	2605
336K	2798	2715	2765	2886
360K	3137	3014	3048	3201
370K	Ultimate Load			

COMPRESSION TEST DATAJC12CF-503 SPECIMEN

Applied Load (KIPS)	Strain Readings (μ)			
	Gage 1	Gage 2	Gage 3	Gage 4
0	0	0	0	0
48K	-321	-287	-410	-491
96K	702	665	815	919
140K	-	1008	1175	1297
192K	-	1432	1610	1751
240K	-	1833	2015	2165
264K	-	2038	2225	2380
288K	-	2241	2441	2590
312K	-	2460	2659	2809
336K	-	2701	2908	3036
360K	-	2884	3151	3298
384K	-	3173	3459	3575
408K	Ultimate Load			

COMPRESSION TEST DATA

JC24CF-511 SPECIMEN

Strain Readings (μ)

Load (KIPS)	1	2	3	4	5	6	7	8	9	10	11	12	13	14	15	16	17	18
0	0	0	0	0	0	0	0	0	0	0	0	0	0	0	0	0	0	0
28	368	341	77	341	174	323	248	145	439	450	426	329	225	314	495	194	687	916
56	766	730	214	701	510	629	717	300	1050	846	798	662	370	612	812	365	1149	1521
84	1150	1107	367	1065	852	926	1200	461	1609	1243	1163	1000	523	915	1134	541	1614	2065
112	1519	1477	532	1425	1221	1204	1722	621	2155	1635	1491	1324	689	1193	1488	698	2129	2577
140	1909	1862	712	1753	1623	1389	2297	780	2720	2036	1856	1631	870	1400	1861	880	2662	3127
154	2123	2078	813	1942	1843	1506	2610	870	3032	2250	2054	1788	969	1487	2068	930	2958	3427
168	2322	2279	902	2107	2043	1606	2894	922	3304	2445	2232	1938	1058	1598	2250	996	3218	3691
182	2516	2478	995	2277	2243	1714	3176	980	3582	2644	2412	2084	1151	1685	2445	1055	3494	3958
196	2724	2683	1093	2448	2462	1814	3488	1029	3886	2850	2594	2222	1239	1773	2622	1100	3741	4259
210	2927	2880	1208	2608	2717	1938	3821	1092	4232	3062	2785	2363	1351	1859	2847	1153	4037	4546
224	3125	3087	1310	2780	2942	2064	4122	1162	4520	3261	2963	2503	1455	1962	3054	1208	4309	4828
238	3356	3324	1430	2958	3206	2188	4467	1244	4836	3496	3161	2662	1562	2094	3265	1292	4186	5112
252	3588	3557	1544	3140	3452	2298	4789	1289	5132	3711	3348	2816	1674	2212	3473	1337	4855	5386
266	3801	3780	1666	3320	3694	2467	1599	1336	5424	3926	3520	2955	1780	2343	3683	1412	5116	5640
280	5701	5167	1833	3434	3990	2689	5488	1398	5770	4900	4696	3305	1908	2462	3920	1489	5383	5864
294	6147	6100	1994	3710	4299	2866	5911	1480	6178	5157	4632	3420	1960	2582	3870	1582	5433	5954
297	Ultimate Load																	

COMPRESSION TEST DATA

JC24IF-513 SPECIMEN

Strain Readings (μ)

Load (KIPS)	1	2	3	4	5	6	7	8	9	10	11	12	13	14	15	16	17	18
0	0	0	0	0	0	0	0	0	0	0	0	0	0	0	0	0	0	0
28	304	285	101	217	207	175	244	89	447	403	433	330	214	300	393	233	544	818
56	713	682	256	550	518	474	680	291	1037	784	824	654	400	603	733	456	1007	1430
84	1092	1053	403	876	820	766	1093	482	1568	1174	1190	963	570	893	1052	661	1439	1963
112	1485	1446	555	1222	1137	1071	1528	676	2114	1521	1572	1286	742	1196	1379	860	1884	2496
140	1884	1839	702	1567	1451	1369	1963	849	2645	1899	1957	1611	913	1496	1712	1045	2338	3029
154	2107	2055	785	1759	1631	1537	2211	943	2961	2112	2178	1795	1010	1660	1903	1148	2593	3337
168	2314	2229	855	1906	1788	1655	2438	1002	3276	2271	2361	1916	1083	1756	2054	1210	2798	3629
182	2537	2432	938	2088	1967	1815	2685	1095	3576	2463	2562	2074	1175	1878	2248	1316	3047	3909
196	2741	2620	1012	2259	2131	1955	2940	1197	3890	2669	2762	2241	1278	2005	2461	1415	3315	4192
210	2929	2807	1093	2430	2318	2092	3191	1281	4170	2863	2951	2409	1375	2127	2662	1499	3568	4464
224	3146	3018	1175	2608	2514	2192	3458	1390	4469	3071	3160	2576	1474	2257	2871	1585	3835	4746
238	3360	3236	1266	2798	2727	2283	3750	1462	4783	3305	3379	2751	1583	2355	3100	1676	4120	5041
252	3592	3462	1355	2969	2929	2380	4026	1563	5069	3539	3581	2959	1677	2488	3297	1762	4373	5305
266	3828	3675	1448	3152	3185	2531	4310	1610	5355	3789	3802	3179	1775	2653	3495	1859	4628	5576
280	4113	3963	1562	3410	3405	2720	4611	1699	5666	4091	4077	3411	1877	2837	3701	1976	4900	5841
294	4348	5108	1646	5240	3678	3284	4965	2002	6005	5366	4580	3729	1933	3207	3882	2063	5149	6030
302	Ultimate Load																	

APPENDIX B

SUBCOMPONENT JOINT ANALYSES

- A4EJ Multirow Joint Solutions
For Each Configuration

2-ROW TENSION JOINT

ULTIMATE JOINT STRENGTH (LBS) = 69808.8
 TEMPERATURE DIFFERENTIAL (OPERATING - STRESS-FREE) (DEG. F) = 0.0
 FASTENER(S) MOST SEVERELY LOADED IN STEP NUMBER 2
 MEMBER(S) "ONE" MOST SEVERELY LOADED IN STEP NUMBER 2
 MEMBER(S) "TWO" MOST SEVERELY LOADED IN STEP NUMBER 2
 TENSILE LOADING

N	BLTLOD (LBS)	SHRSTR (LBS)	DLTDIF (INCH)	DELTAL (INCH)	DELTA2 (INCH)	TLDONE (LBS)	STRAN1 (IN/IN)	SGMNT1 (PSI)	TLDTWO (LBS)	STRAN2 (IN/IN)	SGMNT2 (PSI)	SGBRG1 (PSI)	SGBRG2 (PSI)
1			0.1670	0.0000	0.1670	69809.	0.0042	39026.	0.	0.0000	0.		
1						69809.	0.0042	50851.	0.	0.0000	0.		
2	34931.	37300.	0.1579	0.0090	0.1670	34878.	0.0021	25407.	34931.	0.0017	21170.	83968.	69861.
2							0.0021	25407.		0.0017	21170.		
3	34878.	37300.	0.1572	0.0132	0.1704	0.	0.0000	0.	69809.	0.0035	42308.	83842.	69756.
3							0.0000	0.		0.0035	32469.		
4			0.1647	0.0132	0.1780	0.	0.0000	0.	69809.	0.0035	32469.		

2-ROW COMPRESSION JOINT

ULTIMATE JOINT STRENGTH (LBS) = -64936.7
 TEMPERATURE DIFFERENTIAL (OPERATING - STRESS-FREE) (DEG. F) = 0.0
 FASTENER(S) MOST SEVERELY LOADED IN STEP NUMBER 2
 MEMBER(S) "ONE" MOST SEVERELY LOADED IN STEP NUMBER 2
 MEMBER(S) "TWO" MOST SEVERELY LOADED IN STEP NUMBER 3
 COMPRESSIVE LOADING

N	BLTLOD (LBS)	SHRSTR (LBS)	DLTDIF (INCH)	DELTA1 (INCH)	DELTA2 (INCH)	TLDONE (LBS)	STRAN1 (IN/IN)	SGMNT1 (PSI)	TLDIWO (LBS)	STRAN2 (IN/IN)	SGMNT2 (PSI)	SGBRG1 (PSI)	SGBRG2 (PSI)
1			-.1338	0.0000	-.1338	-64937.	-.0039	-36302.	0.	0.0000	0.		
1						-64937.	-.0039	-47302.	0.	0.0000	0.		
2	-32493.	37300.	-.1254	-.0084	-.1338	-32444.	-.0020	-23633.	-32493.	-.0016	-19693.	-78108.	-64985.
2							-.0020	-23633.		-.0016	-19693.		
3	-32444.	37300.	-.1248	-.0123	-.1371	0.	.0000	0.	-64937.	-.0032	-39356.	-77990.	-64888.
3							.0000	0.		-.0032	-30203.		
4			-.1318	-.0123	-.1441	0.	0.0000	0.	-64937.	-.0032	-30203.		

4-ROW TENSION JOINT

ULTIMATE JOINT STRENGTH (LBS) = 77881.5
 TEMPERATURE DIFFERENTIAL (OPERATING - STRESS-FREE) (DEG. F) = 0.0
 FASTENER(S) MOST SEVERELY LOADED IN STEP NUMBER 7
 MEMBER(S) "ONE" MOST SEVERELY LOADED IN STEP NUMBER 3
 MEMBER(S) "TWO" MOST SEVERELY LOADED IN STEP NUMBER 5
 TENSILE LOADING

N	BLTLOD (LBS)	SHRSR (LBS)	DLTDIF (INCH)	DELTA1 (INCH)	DELTA2 (INCH)	TL DONE (LBS)	STRAN1 (IN/IN)	SGMNT1 (PSI)	TTDIWO (LBS)	STRAN2 (IN/IN)	SGMNT2 (PSI)	SGRRG1 (PSI)	SGRRG2 (PSI)
1			0.1551	0.0000	0.1551	77881.	0.0047	43538.	0.	0.0000	0.		
1						77881.	0.0047	43538.	0.	0.0000	0.		
2			0.1522	0.0029	0.1551	77881.	0.0047	43538.	0.	0.0000	0.		
2						77881.	0.0047	52737.	0.	0.0000	0.		
3	10040.	20980.	0.1499	0.0053	0.1551	67841.	0.0041	45938.	10040.	0.0016	18014.	32180.	85267.
3							0.0041	37926.		0.0016	14872.		
4			0.1480	0.0083	0.1563	67841.	0.0041	37926.	10040.	0.0011	10565.		
4						67841.	0.0041	45938.	10040.	0.0011	12797.		
5	19720.	20980.	0.1458	0.0114	0.1572	48121.	0.0029	32585.	29760.	0.0026	29415.	63206.	92258.
5							0.0029	26901.		0.0026	24284.		
6			0.1456	0.0136	0.1591	48121.	0.0029	26901.	29760.	0.0021	19803.		
6						48121.	0.0029	32585.	29760.	0.0021	23986.		
7	20980.	20980.	0.1450	0.0157	0.1607	27141.	0.0016	18378.	50740.	0.0031	34524.	67244.	67569.
7							0.0016	15173.		0.0031	28503.		
8			0.1464	0.0174	0.1638	27141.	0.0016	15173.	50740.	0.0025	23600.		
8						27141.	0.0016	19049.	50740.	0.0025	29629.		
9	27141.	28560.	0.1469	0.0182	0.1651	0.	0.0000	0.	77881.	0.0039	45478.	74563.	62036.
9							0.0000	0.		0.0039	36224.		
10			0.1513	0.0182	0.1695	0.	0.0000	0.	77881.	0.0039	36224.		

4-ROW COMPRESSION JOINT

ULTIMATE JOINT STRENGTH (LBS) = -77160.2
 TEMPERATURE DIFFERENTIAL (OPERATING - STRESS-FREE) (DEG. F) = 0.0
 FASTENER(S) MOST SEVERELY LOADED IN STEP NUMBER 9
 MEMBER(S) "ONE" MOST SEVERELY LOADED IN STEP NUMBER 6
 MEMBER(S) "TWO" MOST SEVERELY LOADED IN STEP NUMBER 6
 COMPRESSIVE LOADING

N	BULTOD (LBS)	SHRSTR (LBS)	DLTDIF (INCH)	DELTA1 (INCH)	DELTA2 (INCH)	TLDONE (LBS)	STRAN1 (IN/IN)	SGMNT1 (PSI)	TLDTWO (LBS)	STRAN2 (IN/IN)	SGMNT2 (PSI)	SGBRG1 (PSI)	SGBRG2 (PSI)
1			-1.537	0.0000	-1.537	-77160.	-.0047	-43660.	0.	0.0000	0.		
1						-77160.	-.0047	-43660.	0.	0.0000	0.		
2			-1.508	-.0029	-1.537	-77160.	-.0047	-43660.	0.	0.0000	0.		
2						-77160.	-.0047	-52884.	0.	0.0000	0.		
3	-9520.	20980.	-.1485	-.0053	-1.537	-67640.	-.0041	-46359.	-9520.	-.0015	-17081.	-30884.	-80850.
3							-.0041	-38273.		-.0015	-14102.		
4			-.1483	-.0055	-1.538	-67640.	-.0041	-38273.	-9520.	-.0013	-11714.		
4						-67640.	-.0041	-38273.	-9520.	-.0013	-11714.		
5			-.1463	-.0084	-1.547	-67640.	-.0041	-38273.	-9520.	-.0009	-8751.		
5						-67640.	-.0041	-46359.	-9520.	-.0009	-10600.		
6	-19645.	20980.	-.1439	-.0115	-1.554	-47995.	-.0029	-32895.	-29165.	-.0026	-28827.	-63731.	-91907.
6							-.0029	-27157.		-.0026	-23799.		
7			-.1439	-.0116	-1.555	-47995.	-.0029	-26831.	-29165.	-.0023	-21396.		
7						-47995.	-.0029	-26831.	-29165.	-.0023	-21396.		
8			-.1435	-.0136	-1.571	-47995.	-.0029	-27157.	-29165.	-.0019	-17756.		
8						-47995.	-.0029	-32895.	-29165.	-.0019	-21507.		
9	-20980.	20980.	-.1428	-.0158	-1.586	-27015.	-.0016	-18515.	-50145.	-.0030	-34119.	-68062.	-67569.
9							-.0016	-15286.		-.0030	-28168.		
10			-.1428	-.0159	-1.587	-27015.	-.0016	-15286.	-50145.	-.0027	-25518.		
10						-27015.	-.0016	-15286.	-50145.	-.0027	-25518.		
11			-.1439	-.0175	-1.613	-27015.	-.0016	-15286.	-50145.	-.0025	-23703.		
11						-27015.	-.0016	-19191.	-50145.	-.0025	-29758.		
12	-27015.	28560.	-.1443	-.0183	-1.626	0.	0.0000	0.	-77160.	-.0039	-45790.	-75120.	-62752.
12							0.0000	0.		-.0039	-36472.		
13			-.1487	-.0183	-1.670	0.	0.0000	0.	-77160.	-.0039	-36472.		

2-ROW, 3-COLUMN TENSION JOINT

ULTIMATE JOINT STRENGTH (LBS) = 345501.6
 TEMPERATURE DIFFERENTIAL (OPERATING - STRESS-FREE) (DEG. F) = 0.0
 FASTENER(S) MOST SEVERELY LOADED IN STEP NUMBER 2
 MEMBER(S) "ONE" MOST SEVERELY LOADED IN STEP NUMBER 2
 MEMBER(S) "TWO" MOST SEVERELY LOADED IN STEP NUMBER 2
 TENSILE LOADING

N	BLTLOD (LBS)	SHRSTR (LBS)	DLTDIF (INCH)	DELTA1 (INCH)	DELTA2 (INCH)	TLDONE (LBS)	STRAN1 (IN/IN)	SGMNT1 (PSI)	TLDIWO (LBS)	STRAN2 (IN/IN)	SGMNT2 (PSI)	SGERG1 (PSI)	SGERG2 (PSI)
1			0.0444	0.0000	0.0444	345502.	0.0041	38451.	0.	0.0000	0.		
1						345502.	0.0041	41946.	0.	0.0000	0.		
2	176108.	84000.	0.0351	0.0093	0.0444	169393.	0.0020	20565.	176108.	0.0016	16035.	78396.	58797.
2							0.0020	20565.		0.0016	16035.		
3	169390.	84000.	0.0338	0.0154	0.0492	3.	0.0000	0.	345498.	0.0031	31459.	75405.	56554.
3							0.0000	0.		0.0031	28838.		
4			0.0408	0.0154	0.0561	0.	0.0000	0.	345498.	0.0031	28838.		

2-ROW, 3-COLUMN COMPRESSION JOINT

ULTIMATE JOINT STRENGTH (LBS) = -383921.6
 TEMPERATURE DIFFERENTIAL (OPERATING - STRESS-FREE) (DEG. F) = 0.0
 FASTENER(S) MOST SEVERELY LOADED IN STEP NUMBER 2
 MEMBER(S) "ONE" MOST SEVERELY LOADED IN STEP NUMBER 1
 MEMBER(S) "TWO" MOST SEVERELY LOADED IN STEP NUMBER 3
 COMPRESSIVE LOADING

N	BLTLOD (LBS)	SHRSTR (LBS)	DLTDF (INCH)	DELTA1 (INCH)	DELTA2 (INCH)	TLDONE (LBS)	STRAN1 (IN/IN)	SCMNT1 (PSI)	TLDIWO (LBS)	STRAN2 (IN/IN)	SCMNT2 (PSI)	SGBRG1 (PSI)	SGBRG2 (PSI)
1			-0.0699	0.0000	-0.0699	-383922.	-0.0046	-42726.	0.	0.0000	0.		
1						-383922.	-0.0046	-46611.	0.	0.0000	0.		
2	-192406.	84000.	-0.0595	-0.0103	-0.0699	-191516.	-0.0023	-23251.	-192406.	-0.0017	-17519.	-85651.	-64238.
2							-0.0023	-23251.		-0.0017	-17519.		
3	-191516.	84000.	-0.0578	-0.0172	-0.0750	0.	.0000	0.	-383921.	-0.0034	-34958.	-85255.	-63941.
3							.0000	0.		-0.0034	-32045.		
4			-0.0656	-0.0172	-0.0828	0.	0.0000	0.	-383921.	-0.0034	-32045.		

4-ROW, 3-COLUMN TENSION JOINT

ULTIMATE JOINT STRENGTH (LBS) = 286055.1
 TEMPERATURE DIFFERENTIAL (OPERATING - STRESS-FREE) (DEG. F) = 0.0
 FASTENER(S) MOST SEVERELY LOADED IN STEP NUMBER 3
 MEMBER(S) "ONE" MOST SEVERELY LOADED IN STEP NUMBER 3
 MEMBER(S) "TWO" MOST SEVERELY LOADED IN STEP NUMBER 3
 TENSILE LOADING

N	BLTLOD (LBS)	SHRSTR (LBS)	DLTDIF (INCH)	DELTA1 (INCH)	DELTA2 (INCH)	TLDONE (LBS)	STRAN1 (IN/IN)	SGMNT1 (PSI)	TLDIWO (LBS)	STRAN2 (IN/IN)	SGMNT2 (PSI)	SGBRG1 (PSI)	SGBRG2 (PSI)
1			0.0385	0.0000	0.0385	286055.	0.0051	47752.		0.0000	0.		
1						286055.	0.0051	47752.		0.0000	0.		
2			0.0346	0.0039	0.0385	286055.	0.0051	47752.		0.0000	0.		
2						286055.	0.0051	52093.		0.0000	0.		
3	45160.	37300.	0.0308	0.0077	0.0385	240895.	0.0043	43869.	45160.	0.0017	17178.	30155.	62985.
3							0.0043	40213.		0.0017	15746.		
4			0.0295	0.0099	0.0393	240895.	0.0043	40213.	45160.	0.0016	14530.		
4						240895.	0.0043	40213.	45160.	0.0016	14530.		
5			0.0281	0.0120	0.0401	240895.	0.0043	40213.	45160.	0.0013	11797.		
5						240895.	0.0043	43869.	45160.	0.0013	12870.		
6	79006.	37300.	0.0250	0.0164	0.0414	161889.	0.0029	29482.	124166.	0.0028	28361.	52755.	66169.
6							0.0029	27025.		0.0028	25998.		
7			0.0250	0.0178	0.0428	161889.	0.0029	27025.	124166.	0.0027	24754.		
7						161889.	0.0029	27025.	124166.	0.0027	24754.		
8			0.0248	0.0193	0.0441	161889.	0.0029	27025.	124166.	0.0023	21692.		
8						161889.	0.0029	29482.	124166.	0.0023	23664.		
9	65434.	37300.	0.0243	0.0222	0.0464	96455.	0.0017	17565.	189600.	0.0029	29165.	43693.	36906.
9							0.0017	16102.		0.0029	26734.		
10			0.0246	0.0226	0.0472	96455.	0.0017	16102.	189600.	0.0028	26224.		
10						96455.	0.0017	16102.	189600.	0.0028	26224.		
11			0.0263	0.0254	0.0517	96455.	0.0017	16102.	189600.	0.0026	23738.		
11						96455.	0.0017	17974.	189600.	0.0026	26498.		
12	96455.	58300.	0.0268	0.0265	0.0533		0.0000	0.	286055.	0.0039	39979.	51525.	38644.
12							0.0000	0.		0.0039	35814.		
13			0.0341	0.0265	0.0605		0.0000	0.	286055.	0.0039	35814.		

4-ROW, 3-COLUMN COMPRESSION JOINT

ULTIMATE JOINT STRENGTH (LBS) = -343930.0

TEMPERATURE DIFFERENTIAL (OPERATING - STRESS-FREE) (DEG. F) = 0.0


FASTENER(S) MOST SEVERELY LOADED IN STEP NUMBER 3

MEMBER(S) "ONE" MOST SEVERELY LOADED IN STEP NUMBER 6

MEMBER(S) "TWO" MOST SEVERELY LOADED IN STEP NUMBER 3

COMPRESSIVE LOADING

N	BLTLOD (LBS)	SHRSTR (LBS)	DLTIDF (INCH)	DELTA1 (INCH)	DELTA2 (INCH)	TLDONE (LBS)	STRAN1 (IN/IN)	SGMNT1 (PSI)	TLDIWO (LBS)	STRAN2 (IN/IN)	SGMNT2 (PSI)	SGBRG1 (PSI)	SGBRG2 (PSI)
1			-0.0656	0.0000	-0.0656	-343930.	-0.0062	-57414.	0.	0.0000	0.		
1						-343930.	-0.0062	-57414.	0.	0.0000	0.		
2			-0.0610	-0.0046	-0.0656	-343930.	-0.0062	-57414.	0.	0.0000	0.		
2						-343930.	-0.0062	-62633.	0.	0.0000	0.		
3	-51300.	37300.	-0.0564	-0.0093	-0.0656	-292630.	-0.0053	-53291.	-51300.	-0.0019	-19513.	-34255.	-71548.
3						-292630.	-0.0053	-48850.	-51300.	-0.0019	-17887.		
4			-0.0547	-0.0119	-0.0666	-292630.	-0.0053	-48850.	-51300.	-0.0018	-16506.		
4						-292630.	-0.0053	-48850.	-51300.	-0.0018	-16506.		
5			-0.0530	-0.0145	-0.0675	-292630.	-0.0053	-48850.	-51300.	-0.0014	-13401.		
5						-292630.	-0.0053	-53291.	-51300.	-0.0014	-14620.		
6	-85156.	37300.	-0.0491	-0.0198	-0.0689	-207474.	-0.0037	-37783.	-136456.	-0.0031	-31169.	-56862.	-71320.
6						-207474.	-0.0037	-34634.	-136456.	-0.0031	-28571.		
7			-0.0488	-0.0216	-0.0704	-207474.	-0.0037	-34634.	-136456.	-0.0029	-27204.		
7						-207474.	-0.0037	-34634.	-136456.	-0.0029	-27204.		
8			-0.0484	-0.0235	-0.0719	-207474.	-0.0037	-34634.	-136456.	-0.0026	-23839.		
8						-207474.	-0.0037	-37783.	-136456.	-0.0026	-26006.		
9	-85647.	37300.	-0.0473	-0.0272	-0.0745	-121827.	-0.0022	-22186.	-222103.	-0.0034	-34164.	-57189.	-48306.
9						-121827.	-0.0022	-20337.	-222103.	-0.0034	-31317.		
10			-0.0475	-0.0278	-0.0753	-121827.	-0.0022	-20337.	-222103.	-0.0033	-30720.		
10						-121827.	-0.0022	-20337.	-222103.	-0.0033	-30720.		
11			-0.0494	-0.0313	-0.0807	-121827.	-0.0022	-20337.	-222103.	-0.0030	-27807.		
11						-121827.	-0.0022	-22702.	-222103.	-0.0030	-31041.		
12	-121827.	58300.	-0.0499	-0.0327	-0.0825	0.	0.0000	0.	-343930.	-0.0046	-48067.	-65079.	-48809.
12						0.	0.0000	0.	-343930.	-0.0046	-43060.		
13			-0.0585	-0.0327	-0.0912	0.	0.0000	0.	-343930.	-0.0046	-43060.		

1. Report No. NASA CR-3711		2. Government Accession No.		3. Recipient's Catalog No.	
4. Title and Subtitle CRITICAL COMPOSITE JOINT SUBCOMPONENTS - ANALYSIS AND TEST RESULTS				5. Report Date September 1983	
				6. Performing Organization Code	
7. Author(s) B. L. Bunin				8. Performing Organization Report No. ACEE-26-TR-3074	
9. Performing Organization Name and Address Douglas Aircraft Company McDonnell Douglas Corporation 3855 Lakewood Boulevard Long Beach, CA 90846				10. Work Unit No.	
				11. Contract or Grant No. NAS1-16857	
				13. Type of Report and Period Covered <u>Contractor Report</u>	
12. Sponsoring Agency Name and Address National Aeronautics and Space Administration Washington, DC 20546				14. Sponsoring Agency Code	
15. Supplementary Notes NASA Langley Technical Monitor: Andrew J. Chapman					
16. Abstract This program has been conducted to develop the technology for critical structural joints of a composite wing structure meeting design requirements for a 1990 commercial transport aircraft. A prime objective of the program was to demonstrate the ability to reliably predict the strength of large bolted composite joints. Load sharing between bolts in multirow joints was computed by a nonlinear analysis program (A4EJ) which was used both to assess the efficiency of different joint design concepts and to predict the strengths of large test articles representing a section from a wing root chord-wise splice. In most cases, the predictions were accurate to within a few percent of the test results. A highlight of these tests was the consistent ability to achieve gross-section failure strains on the order of 0.005 which represents a considerable improvement over the state of the art. The improvement was attained largely as the result of the better understanding of the load sharing in multirow joints provided by the analysis. The typical load intensity on the structural joints was about 40 to 45 thousand pounds per inch in laminates having interspersed 37 1/2-percent 0-degree plies, 50-percent ± 45 -degrees plies and 12 1/2-percent 90-degrees plies. The composite material was Toray 300 fiber and Ciba-Geigy 914 resin, in the form of 0.010-inch thick unidirectional tape.					
17. Key Words (Suggested by Author(s)) Advanced Composite Structures Structural Joints Structural Analysis Weight Reduction			18. Distribution Statement 		
19. Security Classif. (of this report) UNCLASSIFIED		20. Security Classif. (of this page) UNCLASSIFIED		21. No. of Pages 158	
				22. Price	